Cancer In-vitro Diagnostics Using Upconversion Nanoprobe

By

Hao He

Institute for Biomedical Materials & Devices,

School of Mathematical and Physical Sciences, Faculty of Science

Supervisors:

Prof. Dayong Jin & Dr. Christopher B. Howard

This thesis is presented for the degree of Doctor of Philosophy

October 2019

Certificate of Original Authorship

I, Hao He, declare that this thesis, submitted in fulfilment of the requirements for the award of Doctor of Philosophy, in the School of Mathematical and Physical Sciences, Faculty of Science, University of Technology Sydney.

This thesis is wholly my own work unless otherwise reference or acknowledged. In addition, I certify that all information sources and literatures used are indicated in the thesis.

This document has not been submitted for qualifications at any other academic institution.

This research is supported by an Australian Government Research Training Program.

Signature: Production Note:
Signature removed prior to publication.

Date: 03/10/2019

Acknowledgements

Completing my PhD study means a significant milestone in my life. Many people have given me help and encouragement over the past four years. Here I will express my sincere appreciation to them.

Firstly, I would like to thank my principle supervisor, distinguished Prof. Dayong Jin. I appreciate everything he has done to support me in the research training, and academic presentation and writing, especially providing me the opportunity to explore the nanomaterial world. Under his supervision, I learned how to solve problems and overcome challenges in a logical way. I also learnt from him how to communicate and collaborate with other researchers. His attitude to life will continue to inspire me.

I would also thank my co-supervisor: Dr. Christopher B. Howard. He provided me the opportunity to study in the Australian Institute for Bioengineering and Nanotechnology, University of Queensland and provided his professional advice on my project. I appreciate his efforts.

Besides my supervisors, I would like to thank my collaborators for contributing significantly to my PhD projects. Thanks to Dr. Shihui Wen and Ms Jiayan Liao for providing me with upconversion nanoparticles at a high constant quality, Dr. Fan Wang, Dr Zhiguang Zhou and Mr Baolei Liu for building up the optical systems, Dr Martina Jones and Ms Neetika Arora for teaching me the phage display technique, and Dr. Gungun Lin and Dr. Jiajia Zhou for improving the illustrations and writing in my publications.

Thanks to all my friends, A/Prof. Wei Ren, Dr. Ming Guan, Mr. Chao Mi, Ms. Yingzhu Zhou, Ms. Yinghui Chen. They provided my life in Australia with laughs and fun.

To my family, particularly my parents and wife, thanks for your love and support.

Finally, I would like to acknowledge the China Scholarship Council, the Faculty of Science, UTS, and Australian Research Council Integrated Device for End-User Analysis

at Low Levels Research Hub. They supported my tuition fees, my living expenses, and top-up scholarship.

Format of Thesis

This is a thesis by compilation with six chapters.

Chapter 1 is an introduction chapter, including a comprehensive literature review.

Chapters 2-5 are result chapters, including two published first author papers, one published co-author paper and two unpublished works.

Chapter 6 is a conclusion and perspective chapter.

List of Publications

Research papers:

[1] **Hao He**, Christopher B. Howard*, Yinghui Chen, Shihui Wen, Gungun Lin, Jiajia Zhou, Kristofer J. Thurecht and Dayong Jin*. Bispecific Antibody-Functionalized Upconversion Nanoprobe. Analytical Chemistry. 2018, 90 (5): 3024-3029.

[2] **Hao He**, Baolei Liu, Shihui Wen, Jiayan Liao, Gungun Lin, Jiajia Zhou, and Dayong Jin*. Quantitative Lateral Flow Strip Sensor Using Highly Doped Upconversion Nanoparticles. Analytical chemistry. 2018, 90 (21): 12356-12360.

[3] Fan Wang*, Shihui Wen, **Hao He**, Baoming Wang, Zhiguang Zhou, Olga Shimoni, and Dayong Jin*. Microscopic inspection and tracking of single upconversion nanoparticles in living cells. Light: Science & Applications. 2018, 7 (4): 18007.

[4] Yingzhu Zhou, Yinghui Chen, **Hao He**, Jiayan Liao, Hien TT Duong, Maryam Parviz*, and Dayong Jin*. A homogeneous DNA assay by recovering inhibited emission of rare earth ions-doped upconversion nanoparticles. Journal of Rare Earths. 2019, 37 (1): 11-18.

[5] Wei Ren, Yingzhu Zhou, Shihui Wen, **Hao He**, Gungun Lin, Deming Liu, and Dayong Jin*. DNA-mediated anisotropic silica coating of upconversion nanoparticles. Chemical Communications. 2018, 54 (52): 7183-7186.

Papers [1] - [5] are closely related to my PhD program.

Statement of Contribution of Authors

[1] **Hao He**, Christopher B. Howard*, Yinghui Chen, Shihui Wen, Gungun Lin, Jiajia Zhou, Kristofer J. Thurecht and Dayong Jin*. Bispecific Antibody-Functionalized Upconversion Nanoprobe. Analytical Chemistry. 2018, 90 (5): 3024-3029.

	H.H	C.H	Y.C	S.W	G.L	J.Z	K.T	D.J
Experiment Design	●	●						●
Sample Preparation	●	●		●				
Data Collection	●		●					
Analysis	●							●
Manuscript	●	●			●	●	●	●

The concept of this paper was developed by my supervisor Christopher B. Howard, and he prepared all the bispecific antibodies. I designed the experiments and conducted the majority of experimental work, including modification of UCNPs, characterization of upconversion nanoprobe, ELISA-like assay, cell labelling, data analysis, and manuscript writing.

[2] **Hao He**, Baolei Liu, Shihui Wen, Jiayan Liao, Gungun Lin, Jiajia Zhou, and Dayong Jin*. Quantitative Lateral Flow Strip Sensor Using Highly Doped Upconversion Nanoparticles. Analytical chemistry. 2018, 90 (21): 12356-12360.

	H.H	B.L	S.W	J.L	G.L	J.Z	D.J
Experiment Design	●						●
Sample Preparation	●		●	●			
Data Collection	●	●					
Analysis	●						●
Manuscript	●				●	●	●

This project has been primarily carried out by myself, which reflects my independence in conducting research from concept development, experimental design, sample preparations, data collections and analysis, to the final stage of publication preparation.

[3] Fan Wang*, Shihui Wen, **Hao He**, Baoming Wang, Zhiguang Zhou, Olga Shimoni, and Dayong Jin*. Microscopic inspection and tracking of single upconversion nanoparticles in living cells. Light: Science & Applications. 2018, 7 (4): 18007.

	F.W	S.W	H.H	B.W	Z.Z	O.S	D.J
Experiment Design	●	●	●			●	●
Sample Preparation	●	●	●	●			
Data Collection	●	●	●	●	●		
Analysis	●	●	●	●	●		●
Manuscript	●					●	●

This co-authored paper that I designed and did most of the cell experiments has inspired me. I used the system in this paper and developed it into an in-vitro detection platform.

List of Acronyms (in alphabetic order)

ABTS	2,2'-azino-bis(3-ethylbenzo-thiazoline-6-sulfonic acid) diammonium salt
AGRF	Australia genome research facility
APTES	(3-aminopropyl) triethoxysilane
AuNPs	Gold nanoparticles
BSA	Bovine serum albumin
BsAb	Bispecific antibody
CDs	Carbon dots
CT	Computed tomography
CTAB	Cetyl trimethyl ammonium bromide
DNA	Deoxyribonucleic acid
DSNPs	Downshifting nanoparticles
ECL	Electrochemiluminescence
EDC	1-ethyl-3-(3-dimethylaminopropyl) carbodiimide
ELISA	Enzyme-linked immunosorbent assay
EphA2	Ephrin type-A receptor 2
ESA	Excited state absorption
ETU	Energy transfer upconversion
FISH	Fluorescent in situ-hybridization
FRET	Förster resonance energy transfer
GOx	Glucose oxidase
GQDs	Graphene quantum dots
HRP	Horseradish peroxide

ITO	Indium tin oxide
IVD	In-vitro diagnostics
LFS	Lateral flow strip
LOD	Limit of detection
LRET	Luminescence resonance energy transfer
LSPR	Localized surface plasmon resonance
MGNP	Magnetic glycol-nanoparticle
mPEG	Methoxy polyethylene glycol
MRI	Magnetic resonance imaging
MRS	Magnetic relaxation switch
NGS	Next Generation Sequencing
NHS	N-hydroxysuccinimide
NIR	Near-infrared
NSE	Neuron specific enolase
OA	Oleic acid
PAA	Polyacrylic acid
PAMAM	Poly(amidoamine)
PBB15	Polybrominated biphenyl
PCR	Polymerase chain reaction
PEG	Polyethylene glycol
PET	Positron emission tomography
PMHC18	Poly(maleic anhydride-alt-1-octadecene)
POC	Point of Care

PSA	Prostate specific antigen
PVP	Polyvinylpyrrolidone
QDs	Quantum dots
RENPs	Rare earth doped nanoparticles
RNA	Ribonucleic acid
scFv	Single-chain variable fragment
SDS	Sodium dodecyl sulfate
SERS	Surface enhanced Raman spectroscopy
SMCC	Succinimidyl-4-(N-maleimidomethyl) cyclohexane-1-carboxylate
SPR	Surface plasmon resonance
TBA	Thrombin binding aptamer
TEOS	Tetraethyl orthosilicate
THF	Tetrahydrofuran
TMB	3,3’,5,5’-Tetramethylbenzidine
UCNPs	Upconversion nanoparticles
ULISA	Upconversion-linked immunosorbent assay

Abstract

Developing sensitive, specific and fast assays to detect and quantify cancer biomarkers at low concentration permit early stage diagnosis of cancer and to improve the survival rate. Many kinds of nanomaterials have been applied to break the limitations of conventional bioassays so as to offer high sensitivity, simplicity and at lower cost. The current development of nanoparticle based in-vitro diagnostics tests, such as paper-based testing strips using gold nanoparticles, remain as being indicative rather than being quantitative. To fill the gap between lab based quantitative assays and techniques for point of care testing, smartphones will play an essential role. This takes the advantage of build-in optics and electronics suitable for data acquisition, quantification and communication. But this still requires the biochemistry methods to be more stable, selective and quantitative, particularly suitable for small volume of samples after minimum level of preparations.

This thesis explores a new class of fluorescent probes and detection methods to bridge this gap. The new probes are rare earth doped upconversion nanoparticles (UCNPs) with high fluorescent intensity and negligible background noise. To improve the stability and selectivity of UCNPs, two techniques have been explored. Phage display has been employed to select antibodies that can bind to UCNPs surface forming more stable and biocompatible upconversion nanoprobe; bispecific antibodies are used to avoid chemical reaction in the bioconjugation step and deactivation of antibody bioconjugated to UCNPs so that the upconversion nanoprobes can have higher binding efficiency to the cancer biomarker. To meet the requirements of simple and quantitative point of care testing, highly rare earth doped UCNPs with hundreds to thousands of emitters have been introduced to essentially amplify the signal strength so that smartphone can read and quantify the prostate cancer biomarkers resulted in a paper based strip sensor; single nanoparticle image system has been applied to reach a single molecule level sensitivity for detecting prostate cancer biomarkers in sub-microliter samples.

Key words: in-vitro diagnosis, cancer detection, upconversion nanoparticles, phage display, bispecific antibody, lateral flow strip, single-molecule detection.

Table of Contents

Chapter 1 Introduction

This thesis describes an experimental study aimed at developing nanomaterial-based in-vitro diagnostic assays for early-stage cancer detection, which is currently facing challenges using conventional approaches. Using upconversion nanoparticles (UCNPs) with distinct advantages such as high fluorescence intensity, multi-colors, and eliminating background interference arising from auto-fluorescence, upconversion nanoprobes were designed combined with phage display and bispecific antibody techniques. Moreover, two different in-vitro diagnosis assays under different application situations are developed for prostate cancer in-vitro detection.

This introduction chapter serves to provide a clear description of the motivation behind the study. It firstly emphasized the significance of early-stage cancer detection, followed by a brief view of current cancer in-vitro diagnostic assays. Finally, advances of using different nanomaterials including gold nanoparticle, quantum dot, magnetic nanoparticle and UCNPs in this area and the surface functionalization of these nanomaterials are discussed in details.

These have been used to design and conduct experiments for the present study.

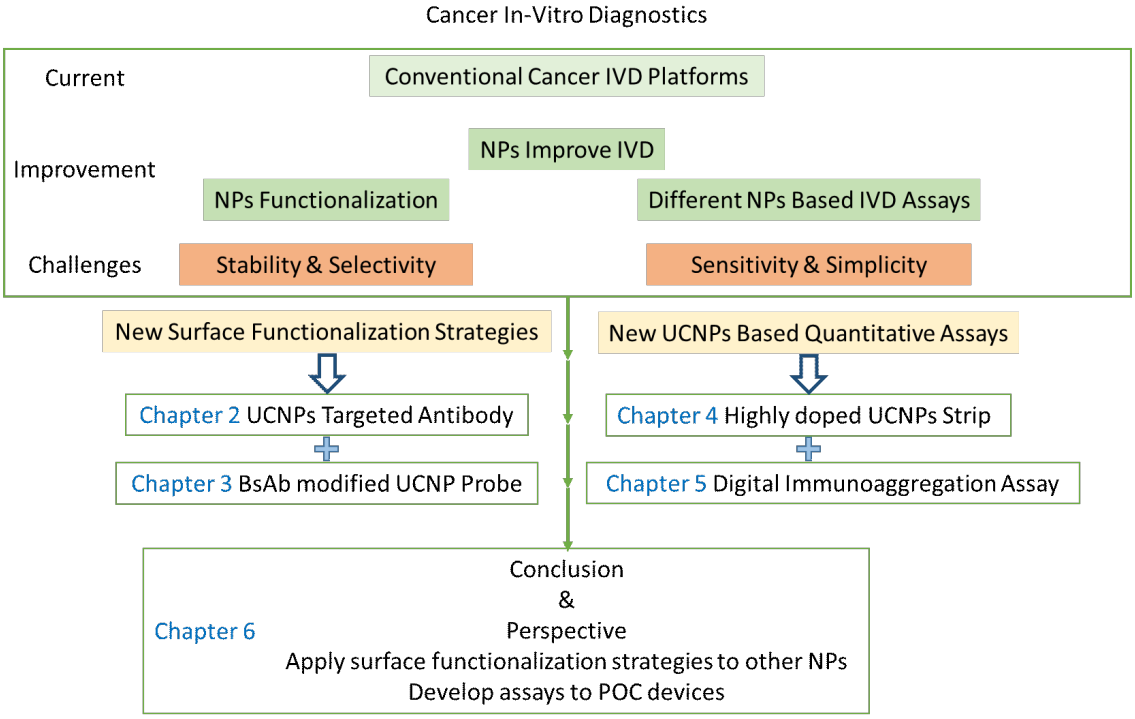

This flow chart outlines the structure of the thesis consist of the significance of applications of nanoparticles in in-vitro diagnosis, its challenges, and proposed solutions for the two bottlenecks.

1.1 Cancer and early detection

Cancer is a group of diseases involving abnormal cell growth with the potential to invade or spread to other parts of the body. Typically, cells grow and multiply in a controlled way; however, if something causes gene mutation to happen inside the cells, this control can be lost. Cancer is the term used to describe collections of these cells, growing and potentially spreading within the body. As cancer cells can arise from almost any type of tissue cell, there are about 100 kinds of cancer types. Cancer cells that do not spread beyond the immediate area in which they arise are said to be benign, i.e. they are not dangerous. If these cells spread into surrounding areas, or to different parts of the body, they are known as malignant - commonly referred to as cancer. [1]

Cancer is an important issue around the world and the No.2 killer in Australia. An estimated 144,713 new cancer patients will be confirmed in Australia this year, with that number set to rise to 150,000 by 2020, and more than 48,000 cancer patients will pass away. These numbers are getting larger due mainly to population growth and aging. [2]

Development of better treatment methods is not the only way; the mortality rate from cancer is often significantly reduced by early diagnostics. For example, prostate cancer is the first common cancer diagnosed in men in Australia and the third most common cancer killer. The patients diagnosed with prostate cancer that has spread to other parts of the body have only 30% 5-year survival rate. In contrast, the number improves significantly in patients who start treatment in the early stages to nearly 100% and 98% of these patients are alive even after ten years. [3]

Today, most clinical methods to detect cancer rely on imaging technologies or the morphological screening of cells from tissues. Imaging techniques, such as ultrasound, X-ray, computed tomography (CT), magnetic resonance imaging (MRI) and positron emission tomography (PET), are limited to their low sensitivity and poor performance in distinguishing cancer stages. While histopathology, taking a biopsy of suspected tumour tissue, is usually used to determine the malignancy of targeted tissues and needs to work with CT or MRI these imaging methods. [4] Therefore, the development of

assays for early detection of cancer, especially in-vitro detection methods, is in urgent need.

1.2 Cancer biomarkers

A biomarker is an objectively measured characteristic that describes a normal or abnormal biological state in an organism by analyzing biomolecules such as DNA, RNA, protein, peptide, and biomolecule chemical modifications. These biomarkers can be used to detect early-stage cancer outside of the patient's body. They are produced by the cancer cells themselves or by other cells in response to cancer. They can be found in bodily fluids such as blood and urine. [4]

1.2.1 Proteins

Proteins are large biomolecules, or macromolecules, consisting of one or more long chains of amino acid residues. They perform a vast array of functions within organisms, including catalyzing metabolic reactions, gene replication, responding to stimuli, providing structure to cells and organisms, and transporting molecules from one location to another[5].

However, in cancer cells, some specific proteins which cannot be found in healthy tissues and some normal proteins will be over-expressed. For example, CA-125 found in the blood can be used to detect ovarian cancer, and the overexpression of prostate specific antigen (PSA) can be used to detect prostate cancer. Most of the conventional cancer protein biomarkers are listed in Table 1-1.[4]

Table 1-1. Cancer protein biomarkers and their related cancer types.

Protein	Cancer Type
Alpha-fetoprotein (AFP)	Liver cancer and germ cell tumors
Beta-2-microglobulin (B2M)	Multiple myeloma, chronic lymphocytic leukemia, and some lymphomas
Beta-human chorionic gonadotropin (Beta-hCG)	Choriocarcinoma and germ cell tumors

C-kit/CD117	Gastrointestinal stromal tumor and mucosal melanoma
CA15-3/CA27.29	Breast cancer
CA19-9	Pancreatic cancer, gallbladder cancer, bile duct cancer, and gastric cancer
CA-125	Ovarian cancer
Calcitonin	Medullary thyroid cancer
Carcinoembryonic antigen (CEA)	Colorectal cancer and some other cancers
CD20	Non-Hodgkin lymphoma
Chromogranin A (CgA)	Neuroendocrine tumors
Cytokeratin fragment 21-1	Lung cancer
Estrogen receptor (ER)/progesterone receptor (PR)	Breast cancer
Fibrin/fibrinogen	Bladder cancer
HE4	Ovarian cancer
Immunoglobulins	Multiple myeloma and Waldenström macroglobulinemia
Lactate dehydrogenase	Germ cell tumors, lymphoma, leukemia, melanoma, and neuroblastoma
Neuron-specific enolase (NSE)	Small cell lung cancer and neuroblastoma
Nuclear matrix protein 22	Bladder cancer
Programmed death ligand 1 (PD-L1)	Non-small cell lung cancer
Prostate-specific antigen (PSA)	Prostate cancer
Thyroglobulin	Thyroid cancer
Urokinase plasminogen activator (uPA) and plasminogen activator inhibitor (PAI-1)	Breast cancer

1.2.2 Nuclear acids

Deoxyribonucleic acid (DNA) carries genetic information and passes it on from one generation to the next.[6] Ribonucleic acid (RNA) contains information that has been copied from DNA. Body cells make several different types of RNA molecules that are necessary for the synthesis of protein molecules. For example, mRNA, or messenger RNA molecules, serve as templates for the synthesis of proteins from amino acid building blocks, while tRNA, or transfer RNA molecules, bring the amino acid residues to the ribosome. Inside the ribosome – an organelle where the protein is being synthesized – tRNA "reads" the mRNA template in a process called translation.[7]

Compare to healthy cells, we can find gene mutations, gene rearrangements, extra copies of genes, and missing genes in cancer cells. These special gene sequences can be used for cancer diagnostics. For example, the BRCA1 and BRCA2 gene mutations can be used to detect ovarian cancer. Most of the common cancer-related gene mutations are listed in Table 1-2.[4]

Table 1-2. Cancer gene mutations and their related cancer types.

Gene Mutation	Cancer Type
BRCA1 and BRCA2 gene mutations	Ovarian cancer
BCR-ABL fusion gene (Philadelphia chromosome)	Chronic myeloid leukemia, acute lymphoblastic leukemia, and acute myelogenous leukemia
BRAF V600 mutations	Cutaneous melanoma and colorectal cancer
Chromosomes 3, 7, 17, and 9p21	Bladder cancer
EGFR gene mutation analysis	Non-small cell lung cancer
HER2/neu gene amplification	Breast cancer, gastric cancer, and gastroesophageal junction adenocarcinoma
KRAS gene mutation analysis	Colorectal cancer and non-small cell lung cancer

1.3 Current cancer in-vitro diagnostics assays

To detect these cancer biomarkers, tests done on samples such as blood or tissue derived from the human body are needed. This results in a booming development in cancer in-vitro diagnostics (IVD) research and commercial products.

1.3.1 Immunoassay

To detect the protein cancer biomarkers, immunoassays based on the antibody-antigen interaction are normally used and can be presented in different formats.

1.3.1.1 Enzyme-linked immunosorbent assay (ELISA)

ELISA is a commonly used analytical biochemistry assay, first described by Engvall and Perlmann in 1972. The assay uses a solid-phase enzyme immunoassay to detect the presence of the analyte in a liquid sample using antibodies directed against the protein to be measured. ELISA has been widely used as a diagnostic tool in cancer IVD to detect different kinds of protein biomarkers.[8]

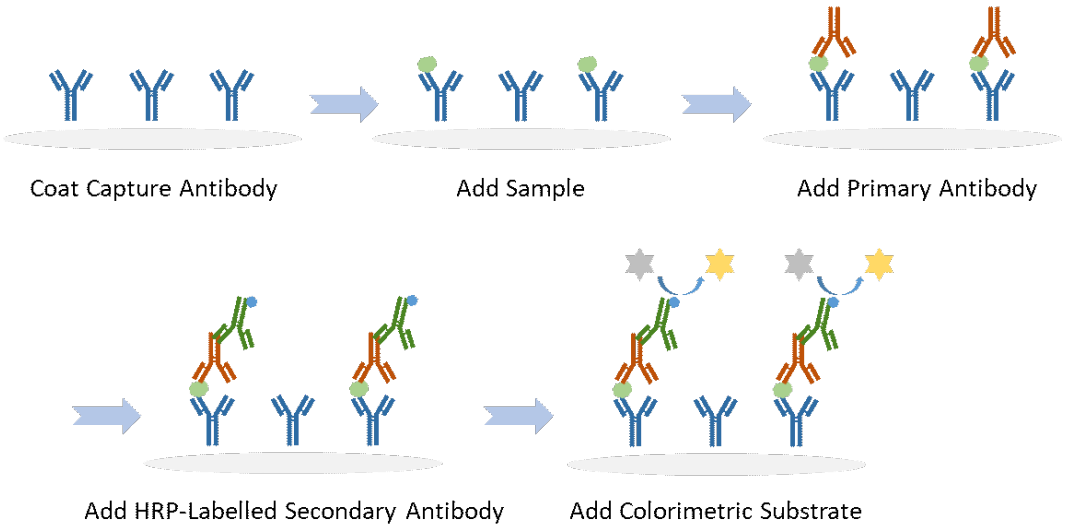

Figure 1-1. Schematic illustration of a sandwich structure ELISA test.

1.3.1.2 Protein Microarray

Protein microarray (or protein chip) is a high-throughput method used to track the interactions and activities of proteins and to determine their function on a large scale. It can be used to detect a large number of cancer biomarkers at on time. Its mechanism is similar to ELISA using immunoassay. Fluorescent dyes are used instead of enzyme here for faster detection.[9]

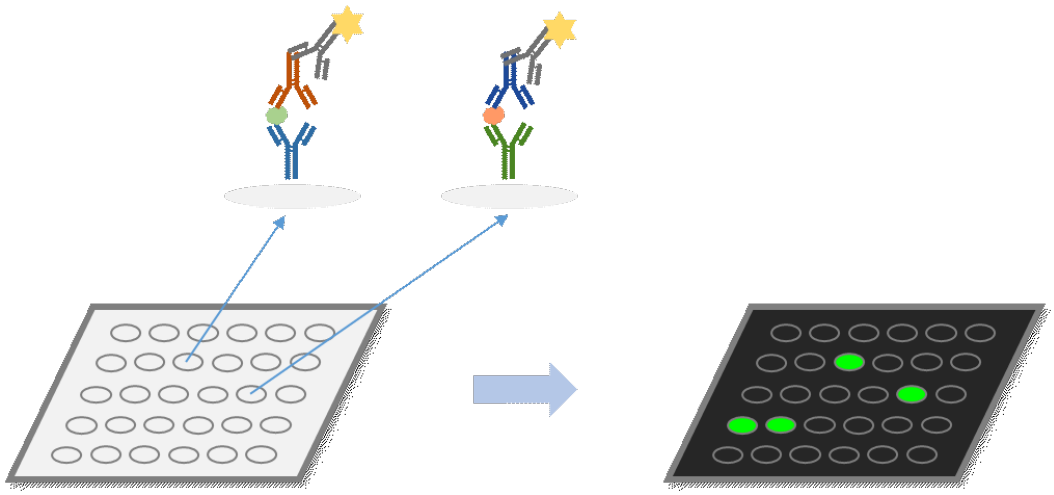

Figure 1-2. Schematic illustration of protein microarray.

1.3.2 Molecular diagnostics

Detection of disease-related nuclear acids is called molecular diagnostics, and its market is broadly divided into polymerase chain reaction (PCR), next generation sequencing (NGS), microarray and fluorescent in situ-hybridization (FISH).

1.3.2.1 Polymerase chain reaction (PCR)

PCR is a method widely used in molecular biology to make many copies of a specific DNA segment. Using PCR, copies of DNA sequences are exponentially amplified to generate thousands to millions of more copies of that particular DNA segment. PCR is now a common and often indispensable technique used in medical laboratory and clinical laboratory research for a wide variety of applications.[10]

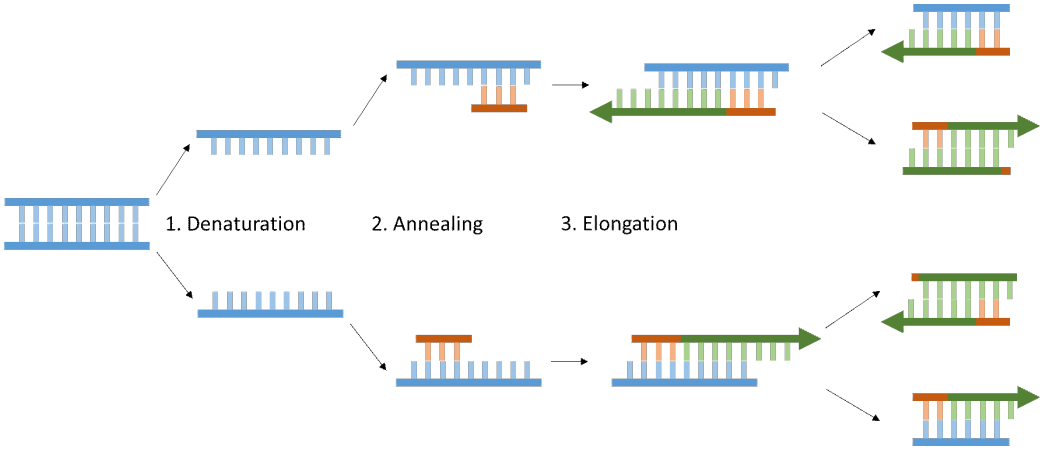

Figure 1-3. Schematic illustration of PCR.

A real-time PCR (rtPCR), also known as quantitative PCR (qPCR), is a laboratory technique of molecular biology based on the PCR. It monitors the amplification of a targeted DNA molecule during the PCR, i.e., in real-time, and not at its end, as in conventional PCR. rtPCR can be used quantitatively and semi-quantitatively, i.e., above/below a certain amount of DNA molecules. Two conventional methods for the detection of PCR products in real-time PCR are (1) non-specific fluorescent dyes that intercalate with any double-stranded DNA, and (2) sequence-specific DNA probes consisting of oligonucleotides that are labeled with a fluorescent reporter which permits detection only after hybridization of the probe with its complementary sequence.[11]

1.3.2.2 Next Generation Sequencing (NGS)

DNA sequencing is the process of determining the nucleic acid sequence – the order of nucleotides in DNA. The high demand for low-cost sequencing has driven the development of high-throughput or next-generation sequencing technologies that parallelize the sequencing process, producing thousands or millions of sequences concurrently. Advances in genetic analysis tools for molecular diagnostics are revolutionizing the practice of medicine, improving prenatal and reproductive care, enabling earlier disease detection, and advancing the treatment of heritable disease.[12]

1.3.2.3 DNA Microarray

DNA microarray (or DNA chip) is a collection of different DNA probes attached to a solid surface. These DNA probes can be a short section of a gene or other DNA element that are used to hybridize a DNA/RNA sample under high-stringency conditions. Probe-target hybridization is usually detected and quantified by fluorescence or chemiluminescence-based detection to determine the relative abundance of DNA/RNA sequences in the samples. The DNA microarray can be used to screen cancer-related mutant DNA or RNA sequences.[13]

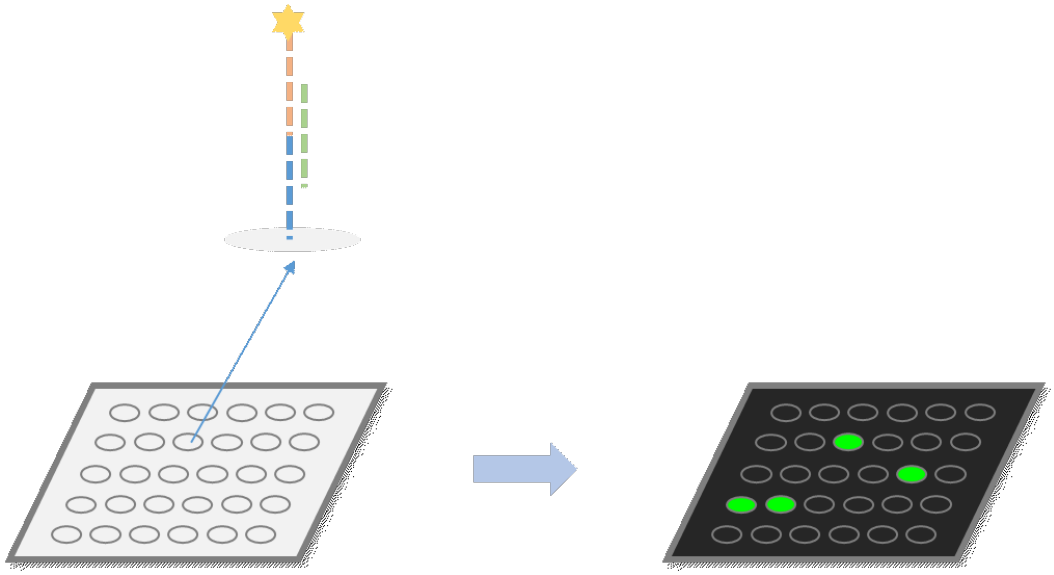

Figure 1-4. Schematic illustration of DNA microarray.

1.3.2.4 Fluorescence in situ hybridization (FISH)

FISH is a molecular cytogenetic technique that uses fluorescent probes that bind to only those parts of a nucleic acid sequence with a high degree of sequence complementarity. It was developed by biomedical researchers in the early 1980s to detect and localize the presence or absence of specific DNA sequences. In medicine, FISH can be used to form a diagnosis, to evaluate prognosis, or to evaluate remission of a disease, such as cancer.[14]

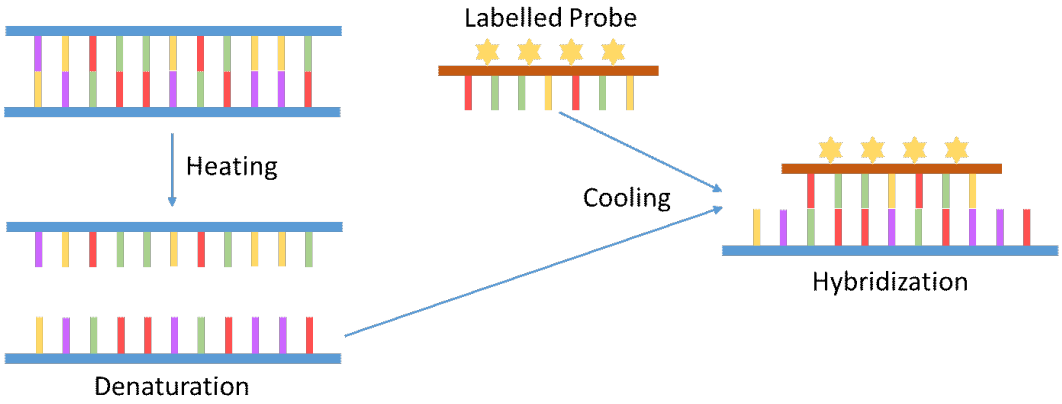

Figure 1-5. Schematic illustration of FISH.

1.3.3 Summary of cancer IVD platforms

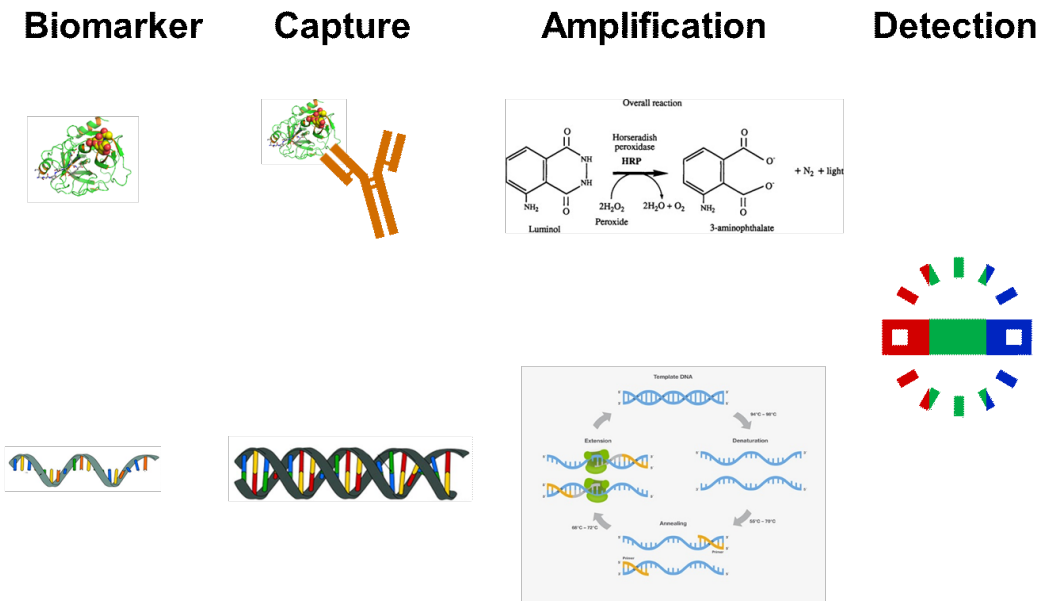

Figure 1-6. Schematic illustration of the process of cancer IVD platforms.

To in-vitro detect the low abundance of cancer biomarkers, either protein or nuclear acids, current immunoassays based on antibody-antigen interaction and DNA or RNA hybridization can afford enough specificity to capture the right target biomarkers. However, the balance between sensitivity and simplicity is hard to achieve. To make the detection assays sensitive enough to detect trace cancer biomarkers, complicated and time-consuming amplification steps cannot be avoided. Moreover, the commonly used

organic dyes for the final optical signal reading are not satisfactory due to their poor fluorescent properties.

1.4 Nanoparticle in IVD

Due to the complexity of the sample and low concentration of cancer-related molecules, to develop fast, reliable, specific and cost-effective detection of a few molecules or even single molecule in a complex, non-amplified and unlabelled biological sample is urgent. The fast development of nanotechnology, nanoparticles have made significant contributions to the development of new detection assays.

Nanoparticles have unique physical and chemical properties such as the large surface area to volume ratio, multi-properties, surface tailorability, and multifunctionality. These advantages offer new possibilities for the detection of biological samples. The large surface areas provide enough space for loading more different capture molecules (antibodies, DNAs, enzymes or peptides), resulting in an excellent performance for detecting a very low concentration of targets and making single molecule detection possible. Moreover, their optical, magnetic, and electrical properties bring opportunities to detect analytes in complex biological environments.

To date, many different kinds of nanomaterials, such as gold nanoparticles (AuNPs), quantum dots (QDs), carbon dots (CDs), magnetic nanoparticles (MNPs) and rare-earth doped nanoparticles (RENPs) have been applied in creating high-performance IVD assays that can detect different targeted biomarkers at nanomolar, pico-molar and even femtomolar levels. These advantages would help to open a new era of early diagnostics applications. [15]–[26]

1.4.1 Gold nanoparticles (AuNPs)

In 1971, colloidal gold nanoparticles were first reported as labeling markers for detecting *Salmonella* antigens in electron microscopy.[27] Since then, AuNPs have been extensively applied into many different IVD assays, due to their several advantages, including easy-to-synthesize, flexible surface properties, controllable size/shape, and unique optical and electrical attributes. Moreover, their better

biocompatibility and biosafety make them more suitable in biological applications. These distinct properties bring many AuNPs based IVD assays for the detection of different biomarkers ranging from small molecules to proteins. [16], [23], [24], [28]–[44]

1.4.1.1 AuNPs based fluorescent assays

Fluorescence is the emission of light by a substance that has absorbed light or other electromagnetic radiation. Its application in analytical chemistry procedure can offer an ultra-high sensitivity that can reach a single-molecule level. Moreover, fluorescence in several wavelengths can be detected by the detector to detect multiple analytes in complex samples.

In recent years, nanomaterials-based fluorescent assays have attracted more attention due to their better photostability, brighter emission, and unique properties of nano-size. Among these nanomaterials, AuNPs are an excellent candidate and have been reported in many IVD assays in two different types. They can be used directly as fluorophores or as one part in an energy transfer system.

(1) AuNPs as fluorophores

It was first reported that gold has photoluminescence in the visible spectral range in 1969 by A. Mooradian.[45] After that, there have been many research works talking about the fluorescence in AuNPs with a size smaller than 3 nm. AuNPs can emit light in a broad region. The visible emission most likely arises from transitions between electrons in conduction-band states below the Fermi level and holes in the d bands generated by excitation light, while the NIR emission comes from the interaction of the surface ligands with AuNPs. Moreover, the emission of AuNPs depends on size and composition. The fluorescent mechanism of AuNPs results in low quantum yield ratio that limits their applications. However, their excellent biocompatibility still attracts efforts in applications in biological labeling and sensors.

Yu Tao et al. developed a bovine serum albumin (BSA) stabilized AuNCs fluorescent sensor for detecting dopamine. After adding dopamine, the photo-induced electron

transfer from the attached dopamine to the BSA-AuNPs results in a dramatic decrease of the fluorescence intensity. This assay can reach a limit of detection at 10 nM for dopamine.[46]

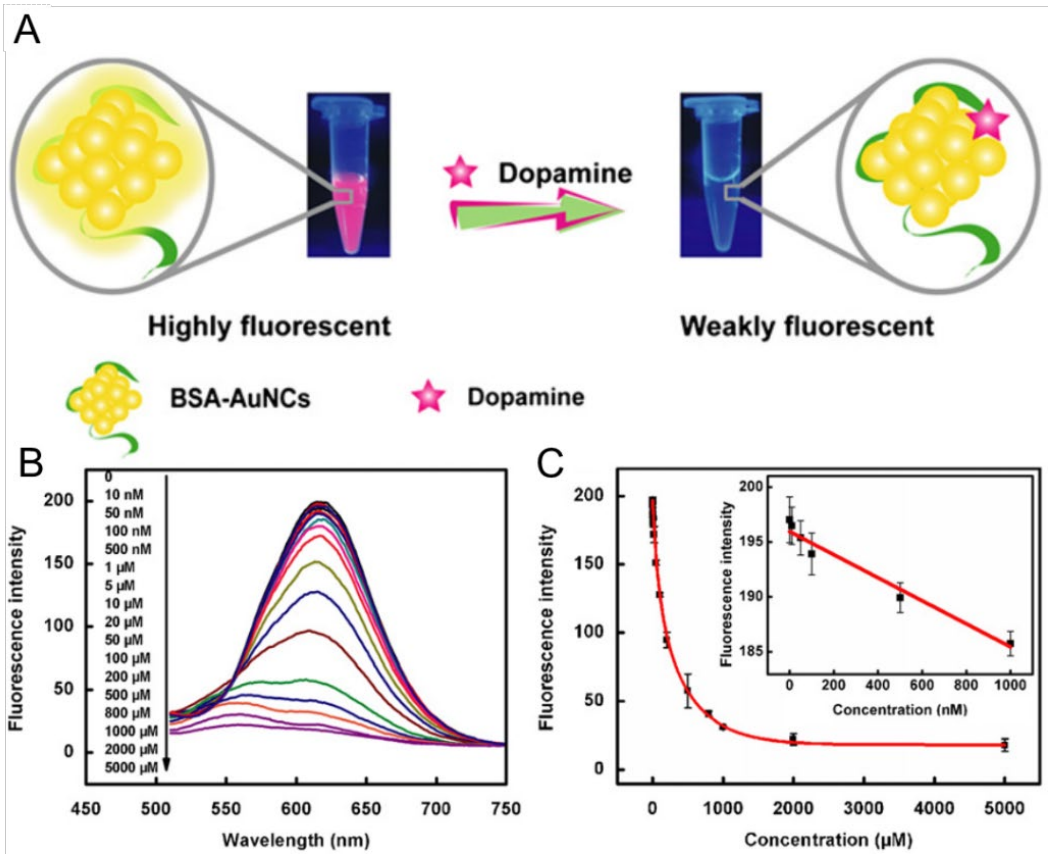

Figure 1-7. (A) Schematic illustration of the fluorescence response of the BSA stabilized AuNPs to DA. (B) Fluorescence emission spectra of the BSA stabilized AuNPs in the presence of increasing dopamine concentrations (0 - 5000 μM). (C) Plots of the fluorescence intensity at 615 nm as a function of the dopamine concentration (0 - 5000 μM). The error bars represent the standard deviation of three measurements. Inset: the linear plot. Reproduced from Ref. [46]

AuNPs have also been reported for cancer in-vitro diagnostics. Juan Peng et al. used porously structured $CaCO_3$ to load AuNPs resulted in $CaCO_3$/AuNPs hybrid fluorescent probe for detecting the cancer biomarker neuron specific enolase (NSE). This fluorescent immunoassay can reach a limit of detection at 2.0 pg/mL. [47]

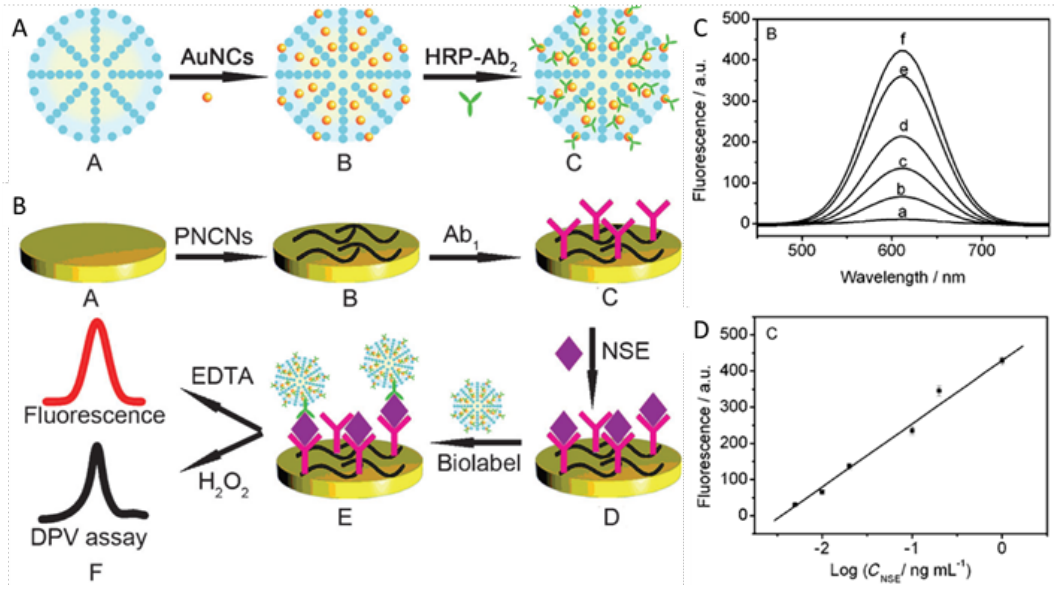

Figure 1-8. (A) Schematic illustration of fabrication process of CaCO3/AuNCs probe. (B) Process of sandwich immunoassay. (C) Fluorescence intensity at target NSE concentrations of 0.005, 0.01, 0.02, 0.1, 0.2, and 1.0 ng/mL (curves a–g, respectively). (D) Linear relationship between fluorescence intensity and the logarithm of the target NSE concentration. Reproduced from Ref. [47]

(2) AuNPs based energy transfer system

Förster resonance energy transfer (FRET), one classical energy transfer system named after the German scientist Theodor Förster, is a mechanism describing energy transfer between two light-sensitive fluorophores. [48] A donor fluorophore, initially in its electronic excited state, may transfer energy to an acceptor fluorophore through a nonradiative dipole-dipole coupling. The efficiency of this energy transfer is inversely proportional to the sixth power of the distance between donor and acceptor, making FRET extremely sensitive to small changes in distance. [49]

AuNPs have been used as a highly efficient energy acceptor mainly because of their continuous electron-hole pair excitations. When one AuNP as an acceptor and another one fluorophore as a donor get close to each other, the energy of the fluorophore can transfer to the AuNP surface via dipole-surface interactions. The continuum of the electron-hole pair excitations on AuNPs surfaces increases the possibility of the dipole-

surface interactions, results in higher energy transfer efficiency. This makes them excellent candidates in different FRET systems for detecting different kinds of analytes ranging from small molecules to proteins. Moreover, many different fluorophores, such as organic dyes and fluorescent nanomaterials, have been used with AuNPs to form the FRET pairs to develop highly sensitive fluorescent assays.

Recently, my colleagues and I developed a fluorescence turn-on assay based on AuNPs and upconversion nanoparticles (UCNPs). The two nanoparticles were brought together by a hairpin structure through the formation of double-stranded DNA, with quenched upconversion fluorescence. In the presence of analytes, the molecular beacon opens to push AuNPs away from UCNPs, with a distance longer than the efficient quenching distance, so that the inhibited upconversion emission will be restored. We demonstrated that this assay provides a homogeneous, facile, simple, and highly selective HIV-1 based DNA detection system with restore efficiency up to 85% and the detection limit of 5 nM. [37]

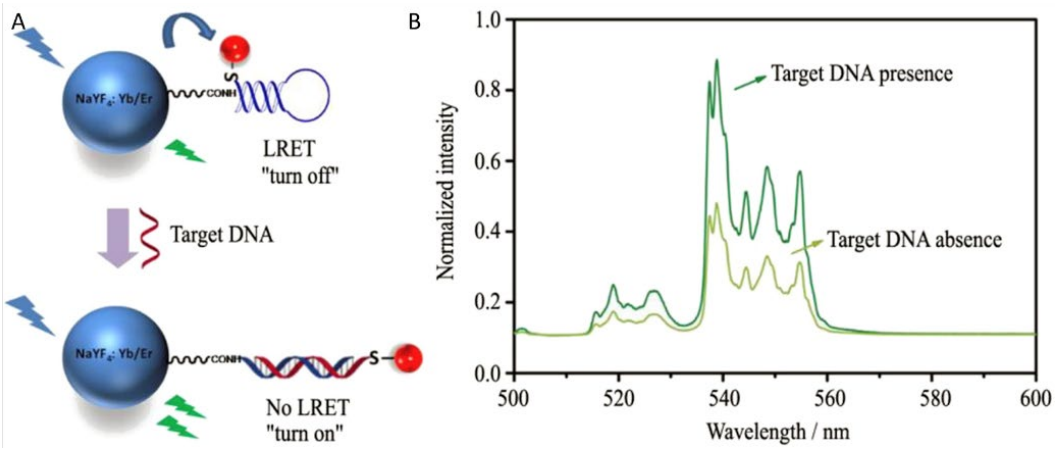

Figure 1-9. (A) Schematic illustration of AuNPs-UCNPs FRET assay. (B) The normalized fluorescence intensity of AuNPs-UCNPs system before and after adding target DNA. Reproduced from Ref. [37]

1.4.1.2 AuNPs based localized surface plasmon resonance (LSPR) assays

Surface plasmon resonance (SPR) is the resonant oscillation of conduction electrons at the interface between negative and positive permittivity material stimulated by incident light. LSPR is the result of the confinement of SPR in a nanoparticle of a size

comparable to or smaller than the wavelength of light used to excite the plasmon. LSPR has two significant effects: electric fields near the nanoparticle's surface are greatly enhanced, and the nanoparticle's optical absorption has a maximum at the plasmon resonant frequency. This phenomenon can be affected by the nanoparticles' size, shape, surface, and local environment so that we can apply it to detect different biomarkers.

AuNPs are the most commonly used nanoparticles in LSPR sensing systems. Because their plasmon absorption bands are generally located in the visible wavelength. Moreover, with their excellent stability and biosafety, a lot of AuNPs based LSPR sensors have been developed. After analytes bind on the AuNPs surface, the dielectric environments around AuNPs will change, resulted in a significant LSPR peak shift that can be used to detect the concentration of analytes. This LSPR peak shift can be read using the spectrometer.

Longhua Guo et al. developed a LSPR peak shifts based assay for the detection of proteins. Gold nanorods (AuNRs) are used in this study. After modification of thrombin binding aptamer (TBA), the AuNRs capture thrombin and the binding causes a measurable LSPR peak shift. Then an anti-thrombin antibody binds to the captured thrombin and can exhibit a nearly 150% amplification in the LSPR signal. This assay can reach a limit of detection of 1.6 pM for thrombin. [50]

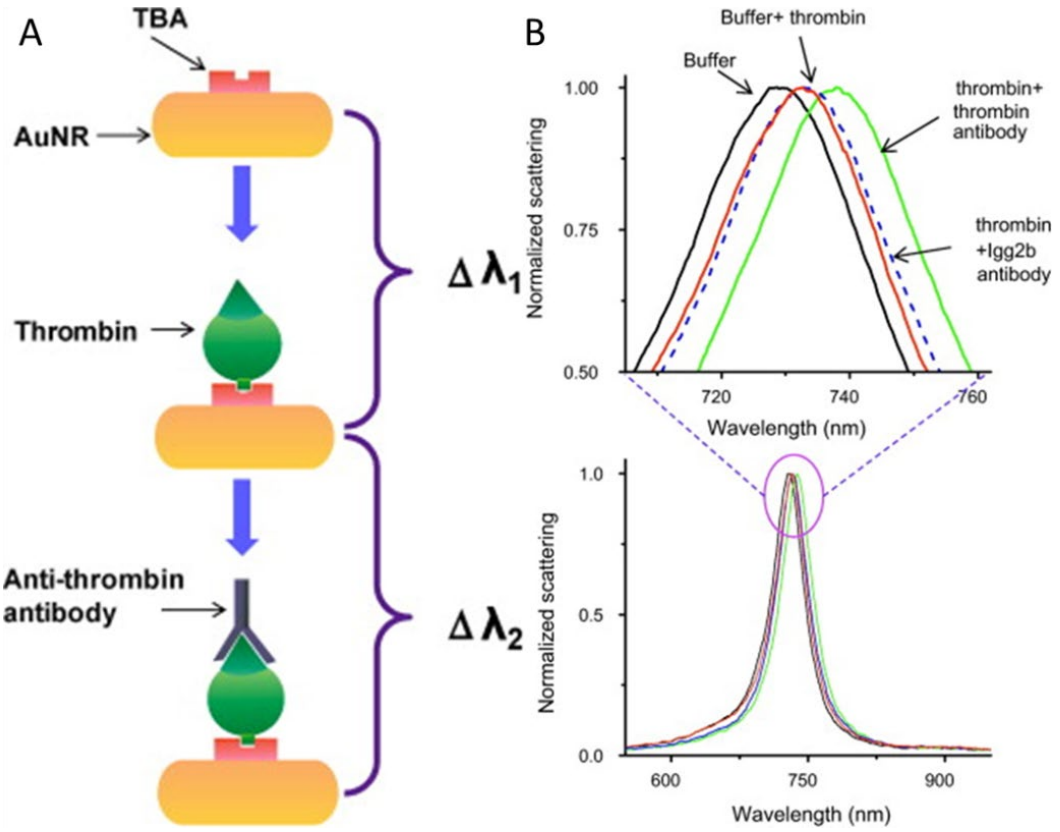

Figure 1-10. (A) Schematic diagram of an assay based on AuNRs LSPR shift. (B) The steady-state LSPR spectra of TBA-modified AuNRs by the sequential incubation with different molecules. Reproduced from Ref. [50]

The other way to detect this LSPR phenomenon is colorimetric analysis. This is based on the aggregation or dispersion of AuNPs. The remarkable red shift of LSPR often causes a distinctive colour change of the AuNPs solutions from red to blue or purple, which can be checked by the naked eye. AuNPs are a perfect candidate for colorimetric assays due to their ultrahigh extinction coefficients. This property allows the detection limit for AuNP-based colorimetric assays to be as low as the nanomolar level, much lower than the assays using organic molecules.

1.4.1.3 AuNPs based electrochemical assays

Electrochemical sensors are devices that give information about the composition of a system in real time by coupling a chemically selective layer (the recognition element) to an electrochemical transducer. They are widely used in IVD assays because they are simple-to-use, low cost, portable, and stable. Like previously introduced assays,

nanomaterials also help electrochemical sensors to reach a better performance. Gold is one of the best materials used in electrochemical sensors due to its excellent conductivity and catalytic property. Moreover, the high surface area of AuNPs brings further advantages to these sensors.

AuNPs have been applied in different electrode fabrications as a part of the electrode substrate or signal transduction probe. For example, Ja-an Annie Ho et al. developed an AuNPs based electrochemical immunosensor to detect the human lung cancer-associated antigen. In this electrochemical immunoassay, AuNPs acts as signal probes that provide a more sensitive approach for detecting the cancer biomarker, α-Enolase (ENO1), with a detection limit as low as 11.9 fg. [51]

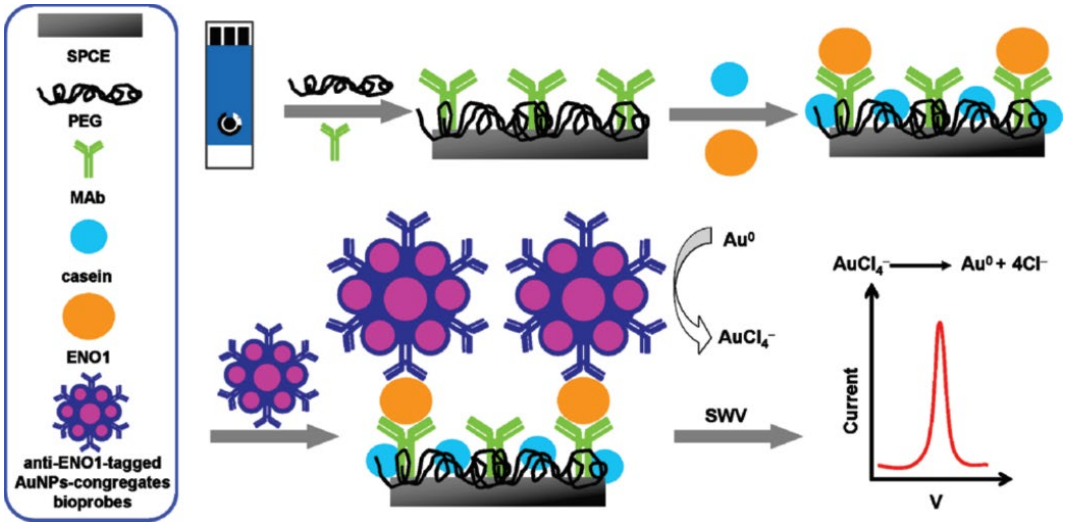

Figure 1-11. Scheme of the electrochemical immunosensor for the detection of ENO1. Reproduced from Ref. [51]

1.4.1.4 AuNPs based surface enhanced Raman spectroscopy (SERS) assays

Raman spectroscopy is a spectroscopic technique used to observe vibrational, rotational, and other low-frequency modes in a system. The Raman spectrum can provide the chemical information of analytes in complex samples. However, the weak Raman signal limits the detection sensitivity. Later, researchers found that the Raman scattering can be enhanced by molecules adsorbed on rough metal surfaces or by nanostructures and the enhancement factor can reach up to 10^{14}. This phenomenon is called SERS. SERS

helps to expand the applications of Raman spectroscopy into many fields such as sensing, material, and medical science. AuNPs are considered as a good candidate not only because they have good stability and biosafety that we have mentioned for so many times, but also because they can scatter visible light and has good photostability. The AuNPs based SERS assays have been widely used to detect chemical or biological samples, such as small molecules, DNAs, proteins, bacteria, and cells.

AuNPs can serve as the substrates of SERS by coating AuNPs on a solid surface to build plasmonic sensors. Ramón A. Alvarez-Puebla et al. used three-dimensional organized AuNRs as SERS substrates for the rapid detection of scrambled prions in serum and blood. The nearly perfect three-dimensional organization of nanorods render these systems excellent surface enhanced Raman scattering spectroscopy substrates with uniform electric field enhancement, leading to reproducibly high enhancement factor in the desirable spectral range. [52]

1.4.2 Quantum dots (QDs)

QDs are one kind of well-established fluorescent nanomaterials that have been widely applied into different areas from electronics to biological areas. They are semiconductor nanoparticles that possess unique optical and electrical behaviours that are highly composition and size dependent. These unique properties bring many QDs based assays for the detection of different analytes. [53]–[62]

1.4.2.1 QDs based fluorescent assays

An exciton will be created in semiconductors after the absorption of a photon with energy above the semiconductor band gap energy. If the semiconductor nanoparticle has a diameter smaller than its exciton Bohr radius, the electrons and holes are confined, leading to a so-called quantum confinement effect where energy levels are quantized, with values directly dependent on the nanocrystal size. As the size of the quantum dots decreases (typically smaller than 10nm), the quantum confinement effects become more dominant.

Quantum dot photoluminescence occurs when the excited electron relaxes to the ground state and recombines with the hole, releasing electromagnetic energy with a narrow and symmetric energy band within the UV to the near-infrared regime. With broad excitation spectra and narrow and symmetric emission spectra, quantum dots have a very large wavelength difference between their respective absorption and emission peaks. Meanwhile, quantum dots made up of different materials, or different sized quantum dots of the same material, have distinct emission wavelengths. Other QD optical properties interesting to biological applications include their high quantum yield, better photostability compared with conventional standard fluorophores, high molar extinction coefficients that are 10 to 100 times of that of conventional organic dyes, as well as exceptional resistance to photo- and chemical degradation. So far, many QDs based assays have been developed for detection of different analytes such as proteins or DNA/RNA.

(1) QDs as fluorophores

The most common method is the direct labeling of targeted analytes. Unlike organic dyes, the QDs can be excited using a single wavelength light source and show different emissions by different sizes. This makes that QD-based detection assays have been developed well beyond single-colour assays to simultaneous multiplex assays. By conjugating different antibodies to different colour QDs, each analyte can be captured by the corresponding QD probe and quantified by different colours.

Chifang Peng et al. developed a multiplexed fluoroimmunoassay based on cadmium telluride QDs for simultaneous detection of five chemical residues. Five different QDs with different emission peaks were used, and five antibodies were conjugated with the corresponding QDs to establish the indirect competition fluorescent-linked immunosorbent assay. This multiplexed assay can detect five chemical drug residues: dexamethasone (DEX), medroxyprogesterone acetate (MPA), gentamicin (GM), ceftiofur (CEF) and clonazepam (CZP) with limits of detection of 0.13 μg/kg, 0.16 μg/kg, 0.07 μg/kg, 0.06 μg/kg and 0.14 μg/kg respectively in one well of a microplate. [61]

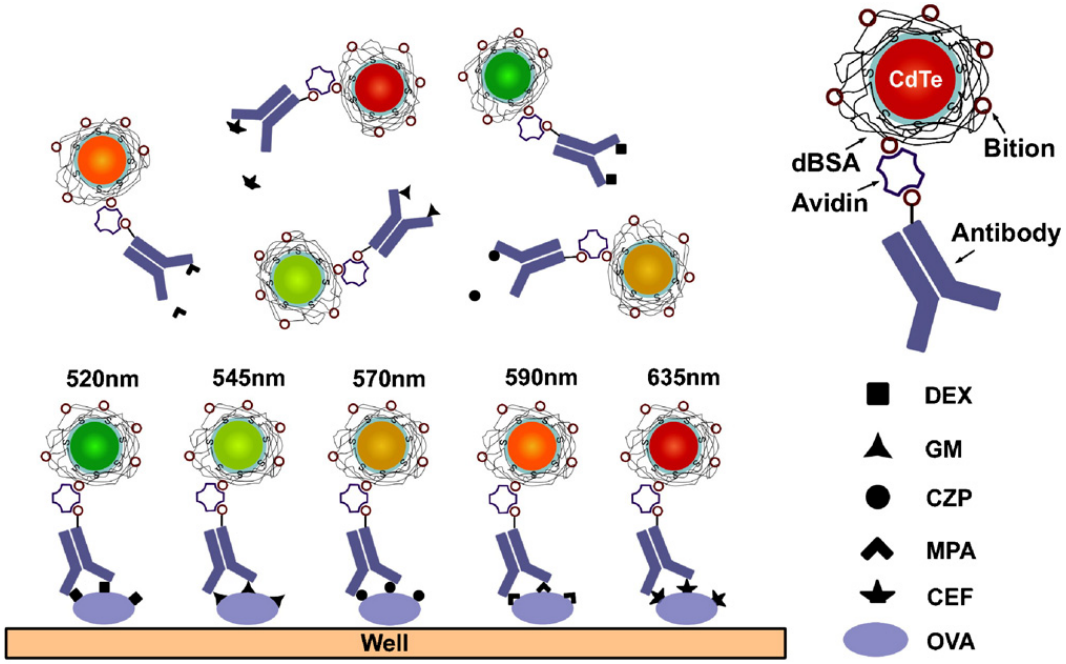

Figure 1-12. Scheme of the QDs based multiplexed indirect competition fluorescent-linked immunosorbent assay. Reproduced from Ref. [61]

(2) QDs based energy transfer system

As QDs show excellent fluorescence properties, they can also be well applied in energy transfer systems. However, unlike AuNPs that generally work as acceptors, QDs are designed to be donors that their energy is transferred via resonance to other fluorophores nearby without emission of light by QDs. The FRET mechanism brings another dimension to QDs based fluorescent assays.

Armen Shamirian et al. developed a ratiometric FRET sensing assay based on a QD donor and a dithiol-linked organic dye acceptor for detection of aqueous H_2S in vitro. H_2S can cleave the disulphide bridge between the two fluorophores, resulting in termination of FRET as the dye is pushed away from the QD. This results in recovered QD emission and dye quenching. The resulting ratiometric response can be correlated quantitatively to the concentration of bisulfide and was found to have a detection limit as low as 1.36 ± 0.03 μM. Furthermore, the assay does not need to wash steps to achieve target detection. [63]

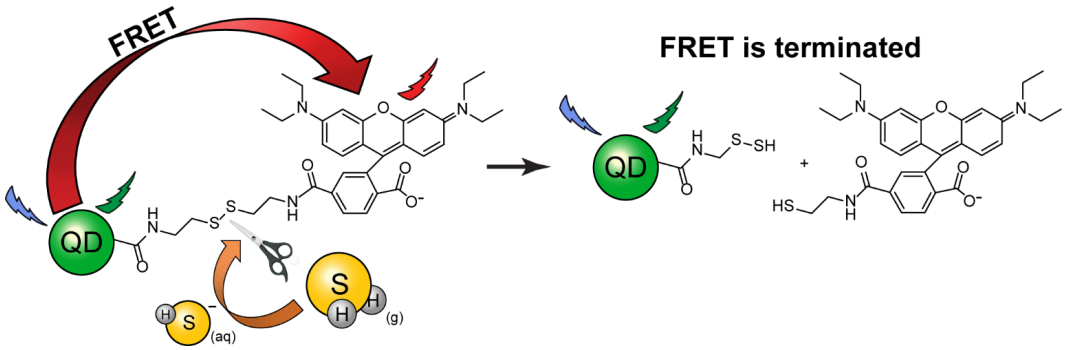

Figure 1-13. Scheme of the ratiometric FRET sensor based on a QD donor and a dithiol-linked organic dye acceptor. Reproduce from Ref. [63]

1.4.2.1 QDs based electrochemical assays

Assays utilizing the unique electrical properties of QDs also attracts increasing interest.

Electrochemiluminescence (ECL) is a kind of luminescence produced during electrochemical reactions in solutions. The energy from QDs can also be transferred to other molecules through the ECL way. Xuan Liu et al. first reported the anodic ELC of QDs in aqueous system and applied this phenomenon for detection of catechol derivatives. The system consists of an indium tin oxide (ITO) electrode and water-soluble QDs dissolved in aqueous solution. Both dissolved oxygen and the semiconductor surface play important roles in the anodic ECL process, which lead to the formation of electron-injected anion radicals $QD^{-\bullet}$. The direct electron-hole recombination of $QD^{-\bullet}$ with hole-injected cation radicals $QD^{+\bullet}$ that are produced from the oxidation of QDs forms the excited QDs, leading to ECL emission. The electrooxidation products of catechol derivatives such as DA and L-adrenalin, which follows the Stern-Volmer equation with relatively large quenching constants, producing a sensitive analytical method for anodic ECL detection of dopamine (DA) and L-adrenalin can quench the ECL emission. The quenching process is demonstrated to be an ECL energy-transfer process from the excited QDs to quencher and could be developed for ECL detection of quenchers and quencher-related analytes. [60]

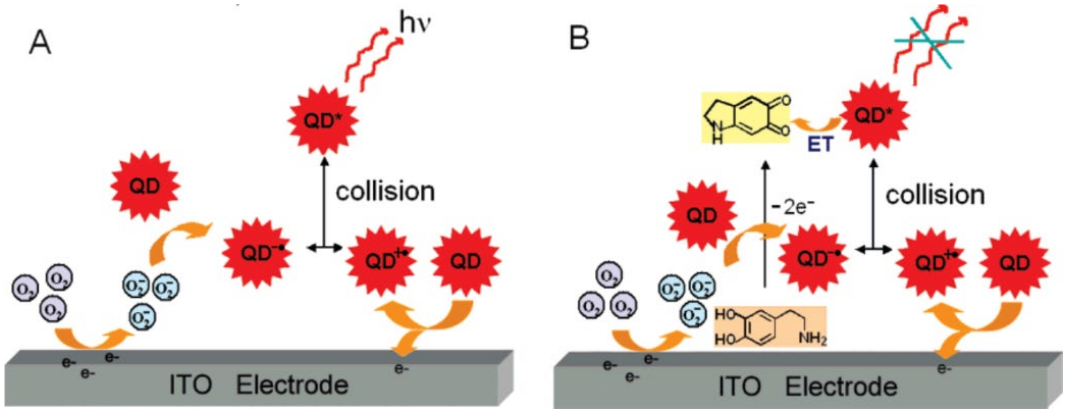

Figure 1-14. Anodic ECL mechanism of QDs (A) and its quenching procedure by oxidation product of DA (B). Reproduced from Ref. [60]

1.4.3 Carbon dots (CDs)

CDs are a kind of carbon material with a size of less than 10 nm and have unique properties that are quite different from bulk carbon. CDs have fluorescence property that is similar to that of semiconductor QDs. They are strongly fluorescent, non-blinking, and have size-dependent emission. CDs become strong competitors to semiconductor QDs because of their properties of the composition. They are water soluble, biocompatible, neglectable toxic, and can be easily synthesized at a low cost. These favourable properties enable CDs of great potential for biological applications. [47], [64]–[75]

1.4.3.1 CDs based fluorescent assays

(1) CDs as fluorophores

Similar to other fluorescent nanomaterials, CDs can be used directly as fluorophores in IVD assays. Moreover, as CDs also have fluorescence aggregation-caused quenching effect, it is easy to design on-off sensors for different targets by controlling the aggregation of CDs. For example, Nan Ma et al. developed a CDs based on-off sensor for detection of mucin 1 (MUC1). Anti-MUC1 antibodies and MUC1 aptamer were modified on CDs surface separately. After adding MUC1 to the solution with the two kinds of CDs based MUC1 probes, the immunoreactions will cause the aggregation of CDs probes resulted in fluorescence quenching. The fluorescence intensity change had a

linear correlation with the concentration of MUC1 in the range from 5 to 100 nM. The sensor can reach a limit of detection at 2 nM. This on-off assay was cost-effective and convenient. [64]

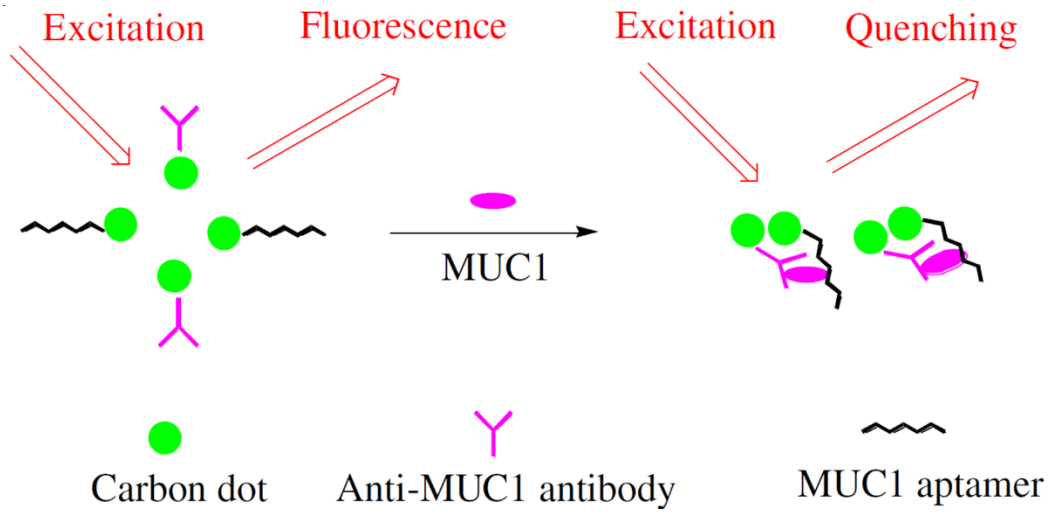

Figure 1-15. Schematic representation of the CDs based immunoaggregation assay for detection of MUC1. Reproduced from Ref. [64]

(2) CDs based energy transfer system

Due to the quite wide range and adjustable absorption and emission spectrum of CDs, they can be used as either donor or acceptor in the FRET system.

Hailong Li et al. developed a fluorescent sensing platform for nucleic acid detection using CDs as energy acceptor and organic dye as an energy donor in this system. Without the target DNA molecules, the dye-labeled single-stranded DNA probe was attached on the CDs surface via π-π interaction, and the emission energy of the dye is transfer to the CDs resulted in dye quenching. After adding the target DNA, the probe DNA escaped from the CDs surface and hybridized with the target DNA, forming a double-stranded DNA. The fluorescence of the dye recovered. [68]

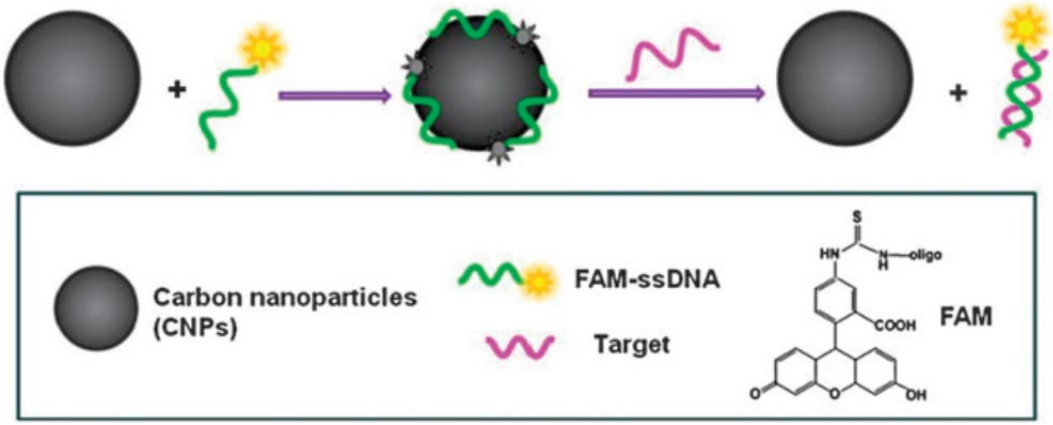

Figure 1-16. Schematic illustrating the fluorescent sensing platform for nucleic acid detection based on CDs. Reproduced from Ref. [68]

Dan Bu et al. designed an immunosensor for polybrominated biphenyl (PBB15) detection using CDs as an energy donor and AuNPs as an energy acceptor in this system. CDs were conjugated with PBB15 antigen and AuNPs were conjugated with the anti-PBB15 antibody. These two probes bind together, and the energy transferred from CDs to AuNPs resulted in the quenching of CDs fluorescence. After adding PBB15 to the solution, the competitive immunoreaction leads to the separation of the two probes and recovery of the CDs fluorescence. Fluorescence intensity was proportional to PBB15 concentration in the range of 0.05-4 μg/mL, with a limit of detection at 0.039 μg/mL. [69]

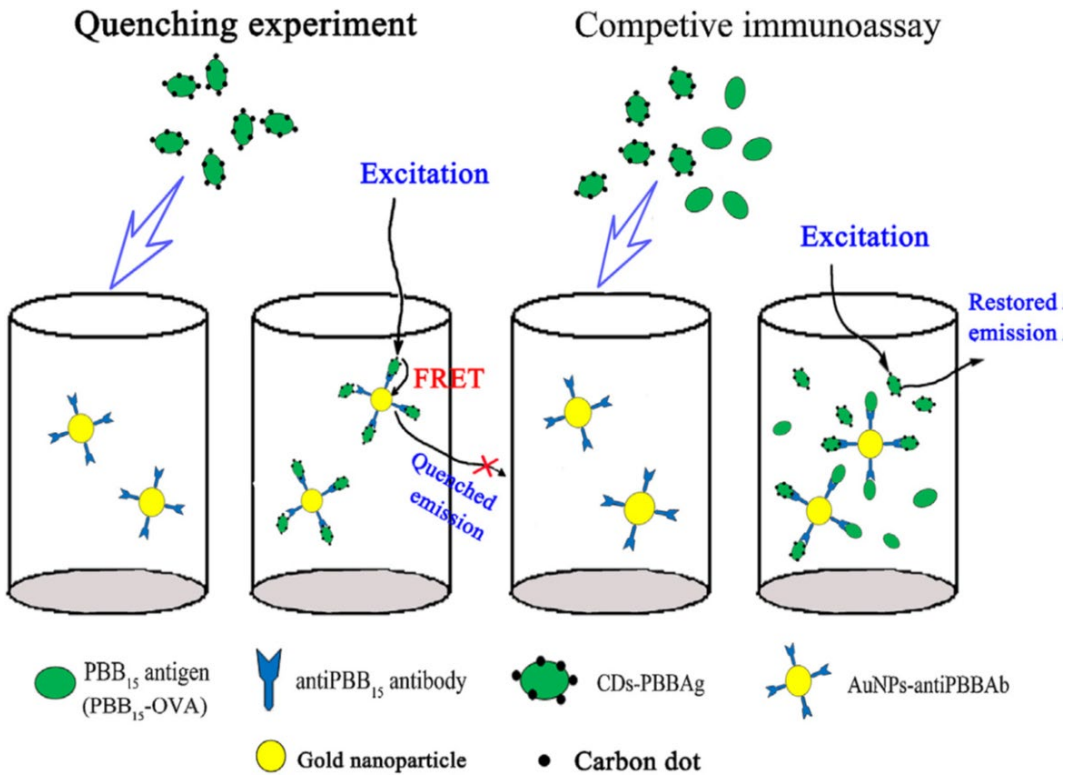

Figure 1-17. Schematic illustration of the immunosensor for PBB15 detection based on FRET between CDs and AuNPs. Reproduced from Ref. [69]

1.4.3.2 CDs based electrochemical assay

(1) CDs based ECL assay

As we introduced in quantum dots section, semiconductor nanoparticles are well known to exhibit ECL, and it comes as no surprise that CDs have aroused interest for ECL studies. The suggested ECL mechanism involves the formation of excited-state CD (R*) by electron-transfer annihilation of negatively charged ($R^{-\bullet}$) and positively charged ($R^{+\bullet}$) species. $RC^{+\bullet}$ is the more stable of the two species, as indicated by the higher intensity of the cathodic ECL. Moreover, this ELC property brings CDs more opportunities for detection of different analytes.

Lingling Li et al. developed a novel sensor for Cd^{2+} detection based on the ECL of graphene quantum dots(GQDs), one kind of CDs. The ECL intensity can be quench by $Cd^{2+,}$ and the intensity decrease ratio was proportional to the concentration of Cd^{2+}. This

ECL sensor based on CDs can detect Cd^{2+} over the range from 20 nM to 150 nm with a limit of detection at 13 nm. [76]

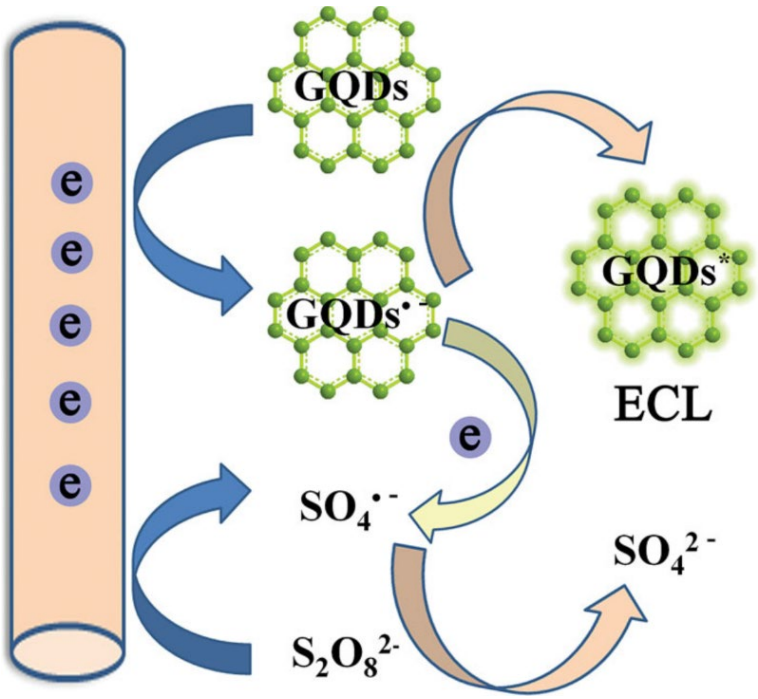

Figure 1-18. Schematic illustration of the ECL mechanism of GQDs. Reproduced from Ref. [76]

(2) CDs based electrocatalytic assays

CDs also have a high electrocatalytic activity that can be used in electrochemical sensors.

Xiangling Shao et al. developed an electrochemical sensor for the detection of Cu^{2+} based on CDs. N-(2-aminoethyl)-N,N′,N′-tris(pyridine-2-yl-methyl)ethane-1,2-diamine (TPEA) that coordinate with Cu^{2+} with high specificity to form a stable complex was conjugated on CDs surface to improve the selectivity. The electrode assembled with CDs-TPEA hybridized nanocomposites shows high selectivity toward Cu^{2+}. By taking advantage of CDs, a dynamic linear range from 1 μM to 60 μM is first achieved with a detection limit of ~100 nM in aCSF solution. [70]

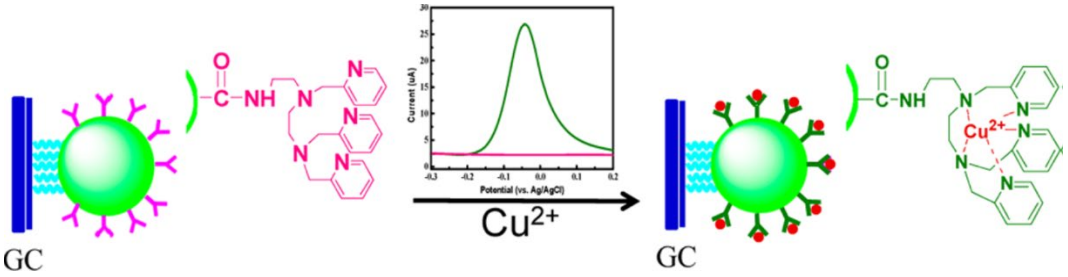

Figure 1-19. Schematic illustration of the electrochemical sensor based on CDs. Reproduced from Ref. [70]

1.4.4 Magnetic nanoparticles (MNPs)

Different from AuNPs and QDs that normally work as reporters or transducers in IVD assays, MNPs are often used as capturers to separate complex biological samples because of their unique property superparamagnetism. [77]–[83] The movement of magnetic nanoparticles can be controlled by an external magnetic field. Due to their other abilities of enzyme mimetic activity and magnetic resonance contrast enhancement, they were also reported as catalysts or transducers in some IVD assays. [84], [85]

1.4.4.1 Magnetic capturer

It is advantageous to use MNPs for capturing different analytes from small molecules to cells not only because of their unique property superparamagnetism. The high surface to volume ratio offers more contact surface area for attaching capture molecules such as antibodies and nuclear acids to recognize targets.

Kheireddine El-Boubbou et al. reported a magnetic glycol-nanoparticle (MGNP) based system to detect *E. coli* in the medium. As many bacteria use mammalian cell membrane carbohydrates as anchors for attachments, the researchers modified magnetic nanoparticles with carbohydrates to have the binding affinities to the bacteria. As results, this system can short the detection time into less than 5 min and remove up to 88% of the target bacteria. [83]

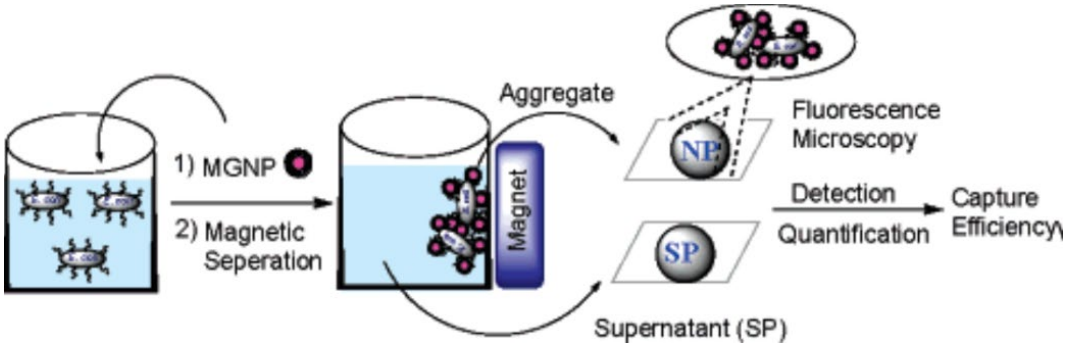

Figure 1-20. Schematic demonstration of pathogen detection by MGNPs. Reproduced from Ref. [83]

1.4.4.2 MNPs as catalysts

Artificial enzyme mimetic is a current research interest because natural enzymes bear some serious disadvantages, such as their catalytic activity can be easily inhibited and they can be digested by proteases. Fe_3O_4 magnetic nanoparticles have been found that they can exhibit an intrinsic enzyme mimetic activity similar to that found in natural peroxidases. This phenomenon opens up great opportunities to design MNPs as catalysts for detection of some analytes.

Hui Wei et al. reported the applications of Fe_3O_4 MNPs as peroxidase mimetics in H_2O_2 and glucose detection. The MNPs provide a colorimetric detection assay by catalyzing the oxidation of a peroxidase substrate 2,2'-azino-bis(3-ethylbenzo-thiazoline-6-sulfonic acid) diammonium salt (ABTS) by H_2O_2 and oxidation of glucose by glucose oxidase (GOx) to the oxidized coloured products. The colorimetric assay showed good sensitivities with H_2O_2 and glucose detection with a linear range from 5×10^{-6} to 1×10^{-4} mol/L and 5×10^{-5} to 1×10^{-3} mol/L respectively. [85]

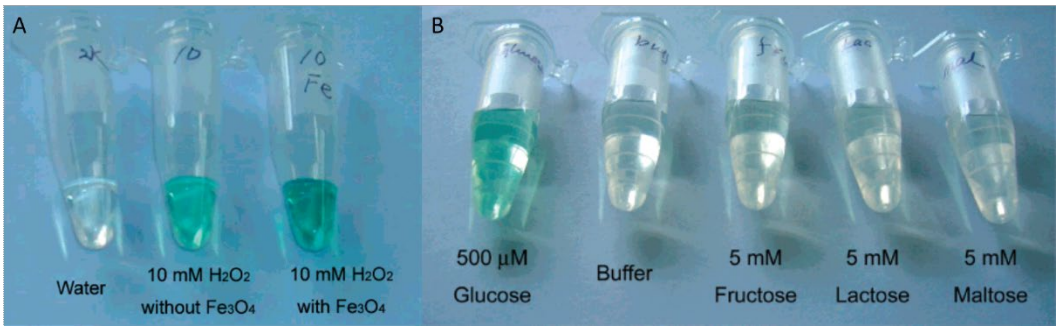

Figure 1-21. Photos of MNPs based colorimetric assay for detection of (A) H_2O_2 and (B) glucose. Reproduced from Ref. [85]

1.4.4.3 Magnetic nanoparticles based magnetic resonance assays

Typically, single nanoparticle and nanoparticles cluster have different optical and magnetic properties. After assembling, the MNPs become more efficient at dephasing the spins of surrounding water protons and decreasing spin-spin relaxation time (T_2 relaxation time, δT_2), so that the MNPs can act as magnetic relaxation switch (MRS). This unique magnetic phenomenon gives MNPs the ability to detect different analytes.

J. Manuel Perez et al. reported a virus detection assay based on this phenomenon. The MNPs were conjugated with anti-virus antibodies and could aggregate together in the presence of specific viral particles. The resulted supramolecular structure had enhanced magnetic properties. The magnetic relaxation changes allowed for the detection of the virus with high sensitivity and specificity in complex solutions. The assay can detect adenovirus-5 and herpes simplex virus-1 with a limit of detection of 5 viral particles/10 µL. [84]

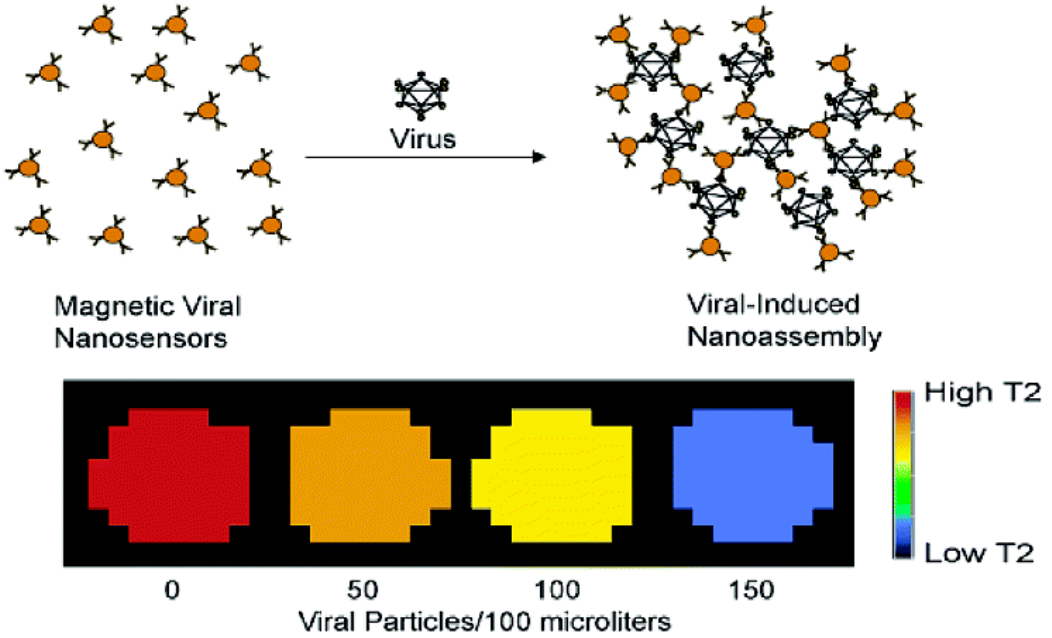

Figure 1-22. Scheme of MNPs based immunoassenmbly assay for detection of virus. Reproduced from Ref. [84]

1.4.5 Rare earth doped nanoparticles (RENPs)

Just as QDs and CDs are regarded as vigorous reinforcements of the organic dye family, RENPs, as another phosphors branch, also possess unique optical characteristics. Rare earth elements are composed of a set of 17 chemical elements, including 15 lanthanides, scandium (Sc), and yttrium (Y). Sc and Y are considered to be rare earth elements because they tend to occur in the same core deposits as lanthanides and exhibit identical chemical properties. Lanthanides are mostly stable in the trivalent form (Ln^{3+}), and their unique optical properties arise from electronic transitions within the 4f shell or from 4f–5d shell. Their 4f inner shell is (partially) filled with electrons, and the Ln^{3+} ions have the electronic configuration $4f^n\ 5s^2\ 5p^6$ where n varies from 0 to 14. The 4f electrons are shielded by the completely filled $5s^2$ and $5p^6$ orbitals resulting in weak electron-phonon coupling and the f-f transitions are in principle parity forbidden. Consequently, their absorption and emission feature narrow f-f transition bands with low transition probabilities and substantially long lifetimes. [86]

Conventional rare earth bulk phosphors play a vital role in lighting sources and solid-state lasers. Now, growing endeavours are devoted to their nano-size synthesis for new

applications. This is not only because of the increased surface area to volume ratio, It has also been reported that the RENPs inherit the unique characteristics: (1) RENPs have a much longer fluorescence lifetime than QDs and organic species, up to millisecond magnitude, which makes it possible to substantially diminish the spontaneous background fluorescence of the biological specimen via time-gated detection; (2) the luminescence of Ln ions does not involve valence electron transitions, which may be conducive to the stability of compounds against photo-oxidation; (3) multicolour luminescence can be easily realized by varying the Ln dopant and host matrix. The atomic like emission lines of Ln ions are entirely isolated without overlap. Moreover, unlike the size-dependent emission of QDs, the fluorescence wavelength of Ln ions is not sensitive to particle size. Rigorous synthesis is thus avoided while the spectral purity of the products is ensured. [86]

Many synthesized RENPs consisted of one rare earth element or combinations of more than one rare earth elements, to produce a wide range of spectral characteristics. They can be tuned to emit from the UV to the near-infrared (NIR) region by the process of upconversion or downshifting depending on the composition of nanoparticles.

1.4.6.1 Upconversion nanoparticles (UCNPs)

UCNPs are fluorescent lanthanide-doped nanoparticles, which possess upconversion characteristics. Upconversion occurs when two or more photons of lower energy are absorbed, followed by the emission of a photon of higher energy. [87]

The two most common processes by which upconversion can occur in lanthanide-doped nanoparticles are excited state absorption (ESA) and energy transfer upconversion (ETU). [88]

A single ion in the lattice sequentially absorbs two photons and emits a photon of higher energy as it returns to the ground state. ESA is most common when dopant concentrations are low and energy-transfer is not probable. Since ESA is a process where two photons must be absorbed in a single lattice site, coherent pumping and high

intensity are much more important (but not necessarily required) than for ETU. Because of its single-ion nature, ESA does not depend on the lanthanide ion concentration.

Two-ion processes are usually dominated by ETU. This is characterized by the successive transfer of energy from singly excited ions (sensitizers/donors) to the ion which eventually emits (activators/acceptors). This process is commonly portrayed as the optical excitation of the activator followed by further excitation to the final fluorescing state due to an energy transfer from a sensitizer. While this depiction is valid, the more strongly contributing process is the sequential excitation of the activator by two or more different sensitizer ions.

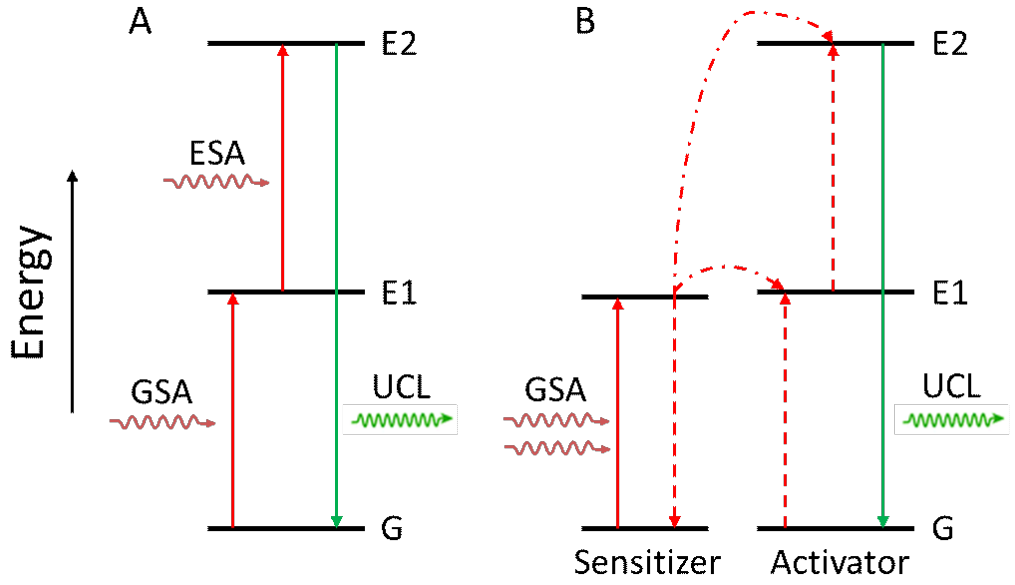

Figure 1-23. Schematic illustration of the mechanism of upconversion luminescence: (A) GSA and (B) ETU.

The presence of multiple metastable states in lanthanide ions makes them good candidates for upconversion. Initially, these nanomaterials were being used in solid state lasers and other optical applications. However, their unique characteristic of absorbing NIR light and emitting in the visible region paved the way for their exploration in biological applications. Upconversion is very well suited for biological applications because NIR light does not excite any biological molecules, and hence, there is almost zero background autofluorescence, which significantly decreases the background noise in different IVD assays. UCNPs show excellent photostability, chemical stability, and

thermal stability. Good photostability ensures long-term storing of these nanoparticles, which is not possible in conventional organic fluorescent labels, which photobleach very quickly. They also do not exhibit the phenomenon of “on-off” photoblinking, which is prevalent in quantum dots and causes the loss of information about the process under study when it is in an “off” state. UCNPs can also be tuned to emit various colours depending on the type of crystal lattice, lanthanide dopant ions, and their respective concentration. These multicolour UCNPs have potential application in multiplex detection assays, where different analytes can be labeled with different colours.

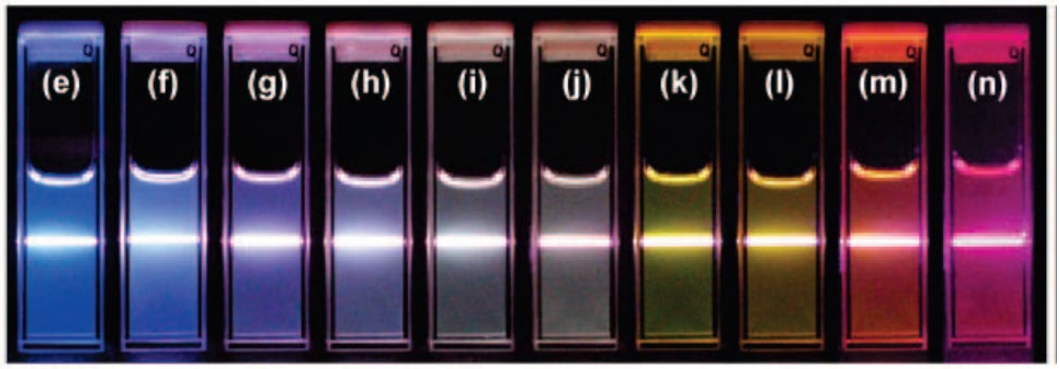

Figure 1-24. Upconversion NaYF4 nanoparticles doped with different concentrations of Yb3+, Er3+, and Tm3+ showing multicolour emissions. Reproduced from Ref. [89]

The unique mechanism of upconversion luminescence makes UCNPs one kind of outstand fluorescent nanoprobe in biological applications, especially the in-vitro detection assays. Like other fluorescent nanoprobes, UCNPs can be used as fluorophore to label target directly or as a donor in the energy transfer system. [90]–[99]

(1) UCNPs as fluorophore

Antonín Hlaváček et al. developed an upconversion-linked immunosorbent assay (ULISA) by replacing the conventionally used enzyme in the ELISA assay to UCNPs label. This optimized ULISA reached a limit of detection at 0.05 ng/mL for diclofenac (DCF). This number is close to the conventional, and it does not need an enzyme-mediated signal amplification step. [99]

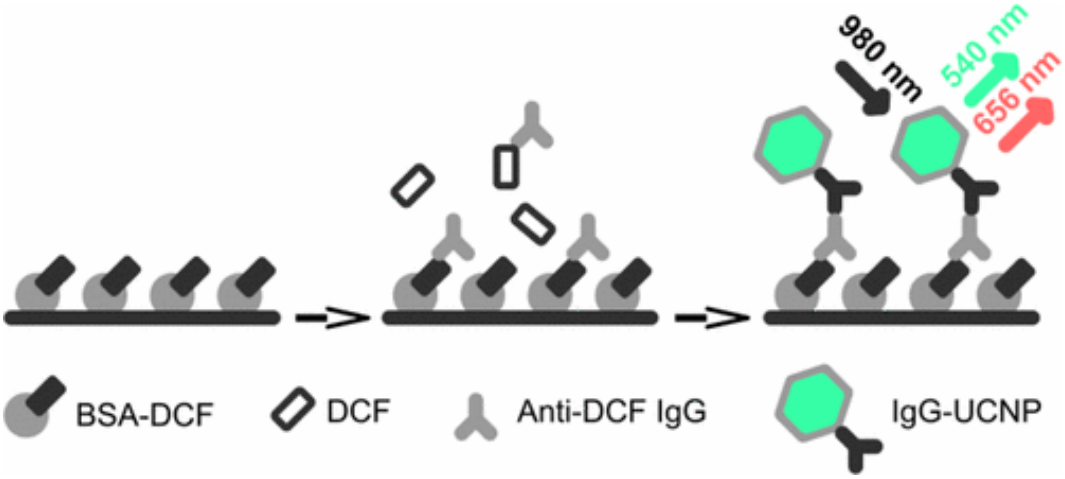

Figure 1-25. Scheme of the indirect competitive ULISA for the detection of DCF. A microtiter plate is coated with a bovine serum albumin-DCF conjugate (BSA-DCF). Dilution series of DCF are prepared in the microtiter plate followed by the addition of anti-diclofenac mouse antibody. The attachment of anti-diclofenac antibody is then detected by an anti-mouse IgG-UCNP secondary antibody conjugate. The upconversion luminescence is recorded under 980 nm laser excitation. Reproduced from Ref. [99]

(2) UCNPs in energy transfer system

Yinghui Chen et al. reported an Exonuclease III-assisted upconversion resonance energy transfer in a wash-free suspension DNA assay. In the presence of target DNA, the Exo III recycles the target DNA by selectively digesting the dye-tagged sequence-matched probe DNA strand only, so that the amount of free dye removed from the probe DNA is proportional to the number of target DNAs. Remaining intact probe DNAs are then bound onto upconversion nanoparticles (energy donor), which allows for upconversion luminescence resonance energy transfer (LRET) that can be used to quantify the difference between the free dye and tagged dye (energy acceptor). Using this approach, an ultra-high sensitivity assay with a detection limit of 15 pM of DNA has been achieved. [97]

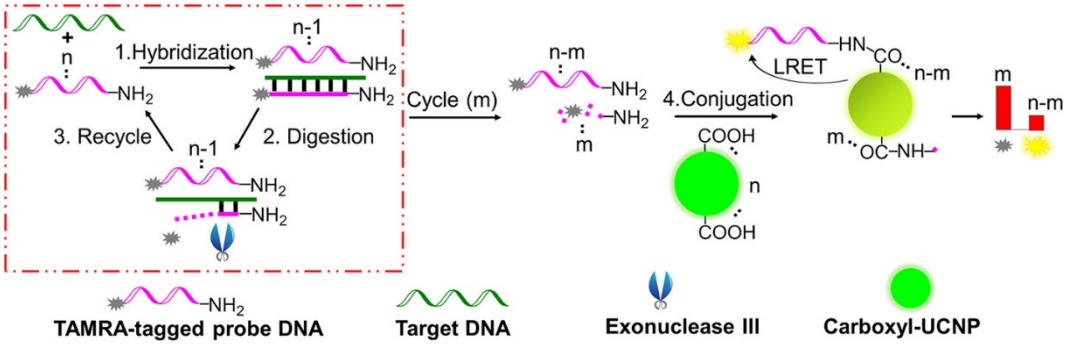

Figure 1-26. Scheme illustrating the use of Exonuclease III-assisted upconversion resonance energy transfer in a wash-free suspension DNA assay. Reproduced from Ref. [97]

1.4.6.2 Downshifting nanoparticles (DSNPs)

DSNPs are a class of lanthanide-doped nanoparticles that fluoresce by a mechanism similar to conventional fluorophores such as quantum dots. DCNPs absorb high-energy photons and emit low-energy photons. They can absorb UV light and emit in the visible and infrared region. DSNPs also exhibit quantum cutting phenomenon, a single high-energy photon is absorbed to produce two photons of lower energy. Even though there are only fifteen lanthanides, various factors such as the combinations in which they are used, the phonon energy of the host crystal lattice, the oxidation state of the lanthanide ions, and the concentration ratio of dopant ions to the host play a major role to bring DSNPs multiple emission peaks. [86] DSNPs have been applied in different IVD assays. [100]–[105]

Lianyu Lu et al. used Eu doped nanoparticles as a nanoprobe and reported a novel assay to sensitive and specific detection of low-abundance miRNA via a unique strategy of nanoprobe dissolution-enhanced fluorescence amplification. Using this strategy, miRNA-21 was detected with a limit of detection at 1.38 fM. High selectivity of the newly developed biosensor was demonstrated by the good discrimination against a target with a single-base mismatch. [100]

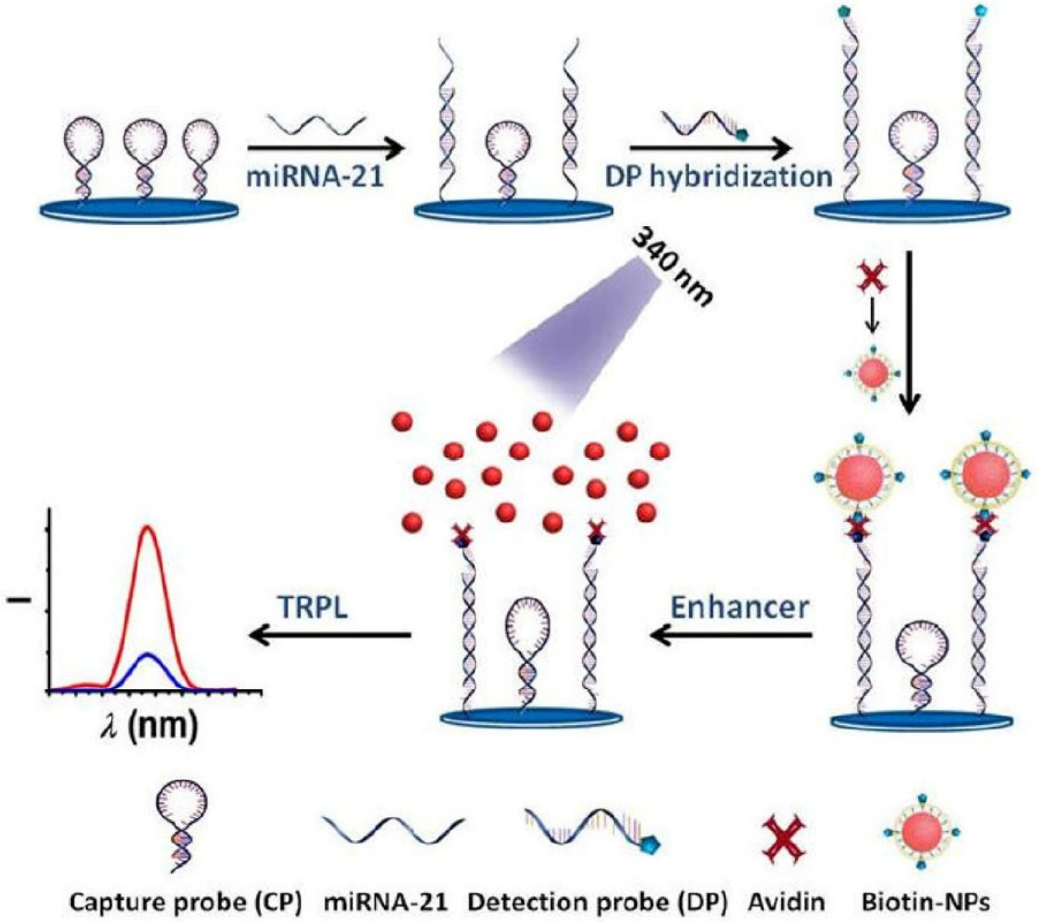

Figure 1-27. Schematic illustration of the luminescent bioassay of miRNA based on amplification of fluorescence of lanthanide nanoprobes. Reproduced from Ref. [100]

Although a wide variety of DSNPs has been developed, they are not promising for biological applications due to its inherent disadvantages similar to other biological probes. They have been mainly used in the electronics industry for lamps, optical amplifiers and the construction of lasers. [86]

1.4.6.3 RENPs with magnetic resonance

Though RENPs become popular mostly because of their fluorescent properties, especially the upconversion luminescence, they can also present magnetic resonance contrast enhancement that also attracts attention in bioapplications. [106]

Gadolinium (Gd) is one of the fifteen lanthanides. Except for fluorescent properties like most of the rare earth elements, it also has a magnetic property. Gadolinium is

paramagnetic at room temperature, with a ferromagnetic Curie point of 20 °C. Paramagnetic ions enhance nuclear relaxation rates, making gadolinium useful for magnetic resonance imaging (MRI). MRI has garnered particular interest as a platform for pathology applications due to its ability to monitor histological changes concomitant with changes. Gadolinium compounds can provide the requisite sensitivity to detect molecular signatures within disease pathologies by significantly enhancing the magnetic resonance contrast. [107]

Elizabeth Kehr et al. used gadolinium-enhanced MRI for in-vitro detection and quantification of fibrosis in human myocardium. They compared this novel in-vitro gadolinium-enhanced MRI with histologically determined myocardial collagen volume fraction, the current gold standard for quantification of myocardial fibrosis. Moreover, there was a significant positive correlation between the results of the two methods. These findings indicate an expanded potential for gadolinium enhanced MRI as a novel, non-invasive alternative to histological evaluation. [32]

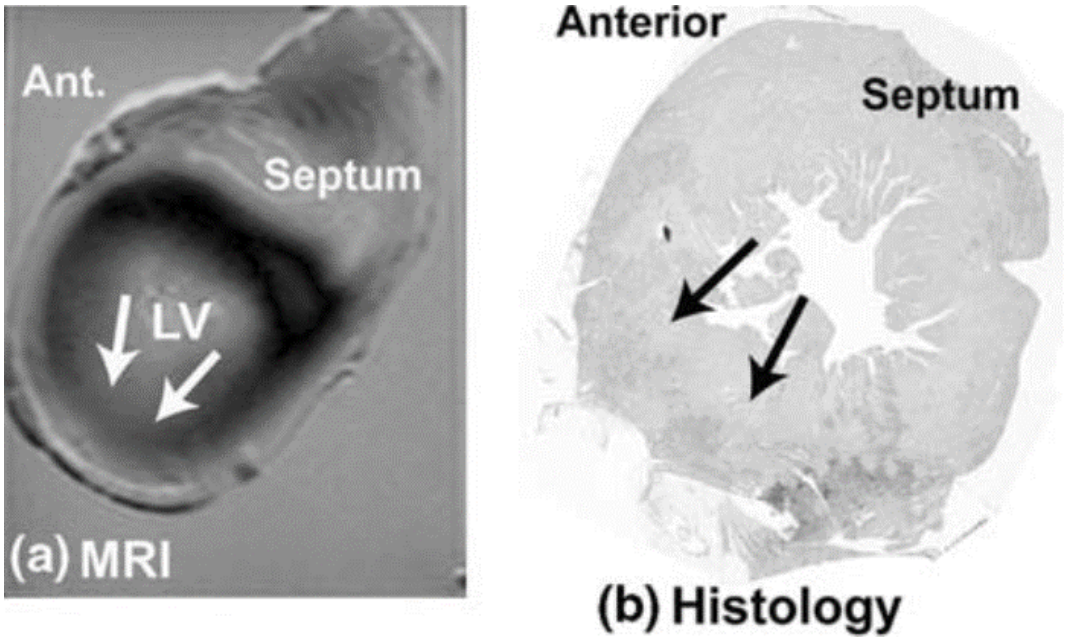

Figure 1-28. (A) Post-mortem T1-weighted MRI image of a heart slice (patient with cardiomegaly, and extensive atherosclerosis) after 24 h incubation in gadolinium solution. The inversion time of 300 ms resulted in a contrast, such that tissue with higher gadolinium distribution volume appears. (B) Histological image of the same

myocardial slice stained with picrosirius red showing extensive fibrosis in posterior-lateral areas, matching those with increased signal intensity on the MRI image brighter. [32]

1.4.6 Nanoparticles based Point of Care Assays

These nanoparticles based IVD assays can detect and quantify different analytes with high sensitive and specificity. However, these methods are not simple, and most of them can only be done under lab environment. Moreover, some of these methods need complex sample preparation steps with a large volume of samples.

POC assays are characteristic of portability and automatization, and the analysis of the readout results does not require complex training. Therefore, these formats are promising tools for rapid diagnosis and on-site assessment of diseases. This is helpful for early stage cancer screening and monitoring after treatment.

Due to AuNPs' unique colorimetric property, AuNPs-based lateral flow strip assays offer high sensitivity and simplicity. Like the most commonly used pregnancy strip, these AuNPs based paper strip assays give a "yes or no" diagnosis result visualized by the naked eye. They also play vital roles in various medical diagnostics, such as screening for infectious diseases and measurement of biomarkers in blood.

Figure 1-29. Paper based lateral flow strips using AuNPs.

However, these strips remain as being indicative rather than being quantitative and cannot provide enough information for the cancer diagnosis.

1.5 Nanoparticle surface functionalization

After synthesis, these nanoparticles cannot be directly used in bioapplications, biomolecules such as antibodies or DNA need to be modified on their surface. This surface functionalization normally consists of two steps: surface modification and bioconjugation.

1.5.1 Surface modification

Not like AuNPs and CDs that are normally water-soluble after synthesis, a large portion of nanoparticles such as MNPs, QDs, and UCNPs are synthesized in high-boiling organic solvents. High-temperature synthesis in organic phase offers several advantages over aqueous synthesis. Firstly, high temperature allows the impurities of nanoparticles to be annealed out to obtain good crystallite structure. Furthermore, a long chain of organic ligands enables steric stabilization of nanoparticles and allows a higher concentration of nanoparticles to be produced. Moreover, the temperature can be used to manipulate the morphology and size of the nanoparticles through controlling the growth kinetics of crystals. As results, the synthesized nanoparticles are with a hydrophobic layer and have no functional groups for linking biomolecules. Therefore, post-synthesis surface modification is necessary to transfer nanoparticles to hydrophilic and biocompatible, and functional groups are needed for further bioconjugation.

The most commonly used surface modification methods include silica coating, ligand exchange, ligand oxidization, ligand interaction. [108]

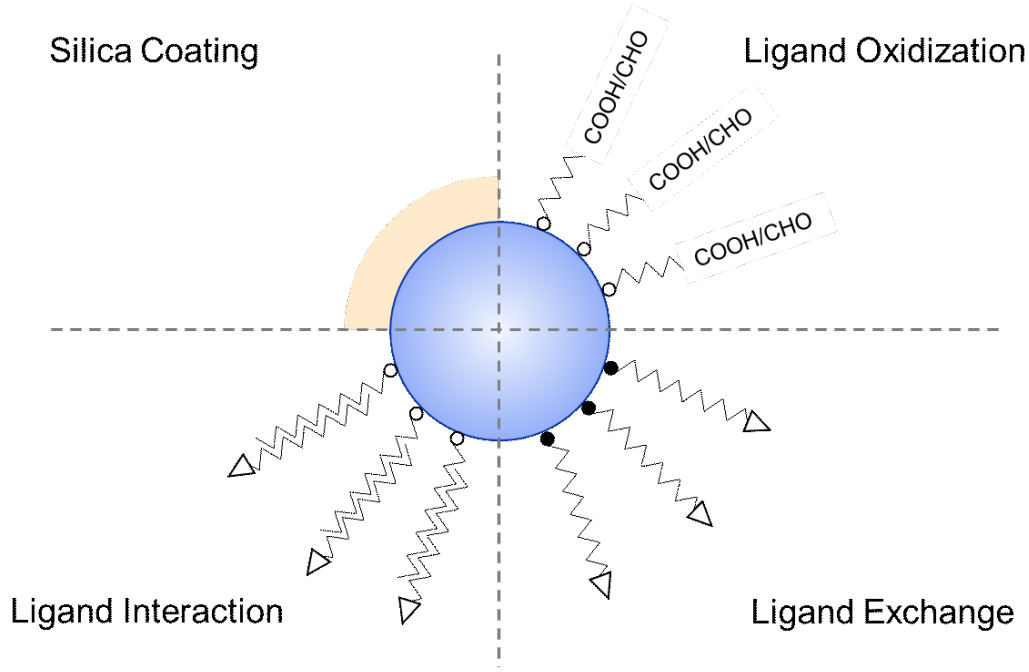

Figure 1-30. Schematic illustration of four kinds of surface modification methods.

1.5.1.1 Silica coating

Deposition of a silica shell on nanomaterials is a traditional and useful technique to generate hydrophilic nanoparticles that are well dispersible in aqueous buffers. [31], [109]–[115] The biocompatible silica shell with high transparency brings several advantages for biological applications. [116]–[119] Furthermore, the silica shell is easy to be modified with different functional groups for further bioconjugation steps. [30], [120], [121]

To coat as-synthesized hydrophobic nanoparticles with a silica shell, a microemulsion method is typically used. [122]–[124] Firstly, a detergent, such as CO-520, is used to form micelles in a nonpolar solvent. These reverse micelles are served as reactors for the nanoparticles and silica source, tetraethyl orthosilicate (TEOS). After adding ammonia, TEOS starts to hydrolyze to form silanol. The silanol condenses to form a solid layer on the nanoparticles' surface. The size and shape of the micelles are controlled by the amount of detergent and both the micelles and amount of TEOS contribute to the final thickness of the silica shell.

Silica coating based on TEOS results in lack of functional group for further bioconjugation. Therefore, a silanization reaction is normally performed after or during the silica coating step. [30], [120], [121] (3-aminopropyl) triethoxysilane (APTES), an amino siloxane, is often used to functionalize silica-coated nanoparticles with amine groups. It can be added for growing an amine-modified silica shell on the original silica shell or during the microemulsion process. Then the amine groups can be conjugated with biomolecules via carbodiimide chemistry, such as the 1-ethyl-3-(3-dimethylaminopropyl) carbodiimide (EDC) method.

Although the flexible coating of a silica shell provides advantages for nanoparticles, there are some limitations. The silica shell can increase the size of the final nanoprobe with deceased fluorescence intensity. Moreover, the uniformity is not easy to control, more than one nanoparticle can be enclosed in a silica shell, resulted in a much bigger particle. [125]–[127] Furthermore, the silica shell can bring more non-specific binding biomolecules. [128]

1.5.1.2 Ligand oxidization

The common used nanoparticle surfactant-oleic acid has a double bond between C9 and C10, and this double bond can be oxidized to azelaic acid and nonanoic acid. The azalaic acid left on the nanoparticle surface brings the property of hydrophilic and enables further conjugation. [129]–[135]

Lemieux–von Rudloff reagent is often used to perform the oxidization and consists of permanganate (MnO^{4-}) in catalytic amounts and periodate (IO^{4-}) in stoichiometric amounts. [131]–[133] MnO^{4-} first oxidizes the double bond and is then reoxidized by IO^{4-}. After oxidization, azelaic acid coated nanoparticles can disperse in aqueous solutions and be further conjugated with biomolecules. Moreover, this surface modification method does not change the size, shape, or crystal phase of nanoparticles. However, MnO_2 can form during the reaction, and it is hard to be separated from the nanoparticles leading to the decrease of luminescence intensity. [130]

Ozone can also be used to oxidize the double bond. [134], [135] The ozonolysis can generate azelaic acid or aldehyde on the nanoparticles' surface. The intermediate after first oxidization by ozone can be further reduced to aldehydes by adding dimethyl sulfide or oxidized to carboxylic acids by adding another oxidant. The aldehydes and azelaic acid provide more choices in the further bioconjugation step. Although the ozonolysis can remove the effect from MnO_2, the complicated processing limits the application of this oxidization surface modification method.

1.5.1.3 Ligand interaction

Although the original surfactants of nanoparticles are hydrophobic and cannot be directly used for further bioconjugation reactions, they can be used as attachment sites for another layer of amphiphilic molecules through ligand interaction. The hydrophobic alkyl chains of both the original surfactants and the amphiphilic molecules bind together through van-der-Waals interactions.

Modified polymers and detergents are normally chosen as the amphiphilic molecules in this method. These polymers consist of both hydrophobic parts such as alkyl chains and hydrophilic parts such as polyethylene glycol (PEG). [34], [136]–[138] For example, by conjugation of hydrophobic poly(maleic anhydride-alt-1-octadecene) (PMHC18) and hydrophilic amine-functionalized PEG, the resulted polymer can bind to the oleic acid on UCNPs surfaces and generate nanoparticles with stable aqueous dispersions. [138] Detergents such as sodium dodecyl sulfate (SDS) and cationic cetyl trimethyl ammonium bromide (CTAB) [139]–[141] can be used for the ligand interaction. Phospholipids are a major component of cell membranes and can also be used as biological surfactants that form a hydrophilic and biocompatible layer on nanoparticles' surface by ligand interaction. [33], [142], [143] These amphiphilic molecules can be easily modified with functional groups for further conjugation.

However, amphiphilic molecules are easy to form micelles and cause aggregations during the reactions.

1.5.1.4 Ligand exchange

To replace the hydrophobic surfactants of nanoparticles with hydrophilic ligands is becoming a popular surface modification method now. The hydrophilic ligands used in the ligand exchange method often consist of binding parts that have stronger binding affinity to the nanoparticles' surface and functional groups for further bioconjugation. Ligands with multidentate are preferred compared to ligands with monodentate as they can form a stronger binding, including small molecules, polymers, and biomolecules.

Small molecules with high affinity head functional group are preferred candidates for generating hydrophilic nanoparticles because the after-modified nanoparticles have a smaller hydrodynamic radius, which promotes less fluorescent intensity loss and better biocompatibility. [144] Commonly used small molecules are alkylthiol terminated molecules that can strongly bind to the surface of AuNPs or QDs, [59], [145]–[148] citrate acid, hexanedioic acid, 1-hydroxyethane-1,1-diphosphonic acid and dopamine that can replace the oleic acid on UCNPs surface. [149]–[153]

Compared to the small molecules, polymers can have more groups for the coordination binding and form a more solid layer on the nanoparticles' surface and can be equipped with other properties by synthesizing other copolymers. Polyacrylic acid (PAA), polyvinylpyrrolidone (PVP) and poly(amidoamine) (PAMAM) are common used polymers for the ligand exchange modification. [154]–[157] These polydentate polymers can attach to the positively charged ions on UCNPs surface using multi-carboxylic, pyrrolidine, or amine groups. Moreover, the remaining uncoordinated carboxylic, pyrrolidine, or amine groups enable following bioconjugation processing.

Biomolecules such as glucose, DNA, and peptide can also be used as the new ligands. [158]–[161] For example, DNA can easily replace the oleic acid on UCNPs surface resulted in water solvable and biocompatible UCNPs.

A suitable solvent is also important in the ligand exchange reactions, and it depends on the solvability of the new ligands and the original surfactants. Compared with using two different polar solvents to dissolve hydrophobic nanoparticles and new ligands separately, using one bipolar solvent such as tetrahydrofuran (THF) performs better and

is more popular. [162], [163] Nanoparticles and new ligands can be mixed in one solvent leading to high exchange yield ratio.

1.5.2 Bioconjugation

The surface modification brings nanoparticles to water-soluble and stable in solution. Then these nanoparticles are required to conjugated with biomolecules for the final bioapplications.

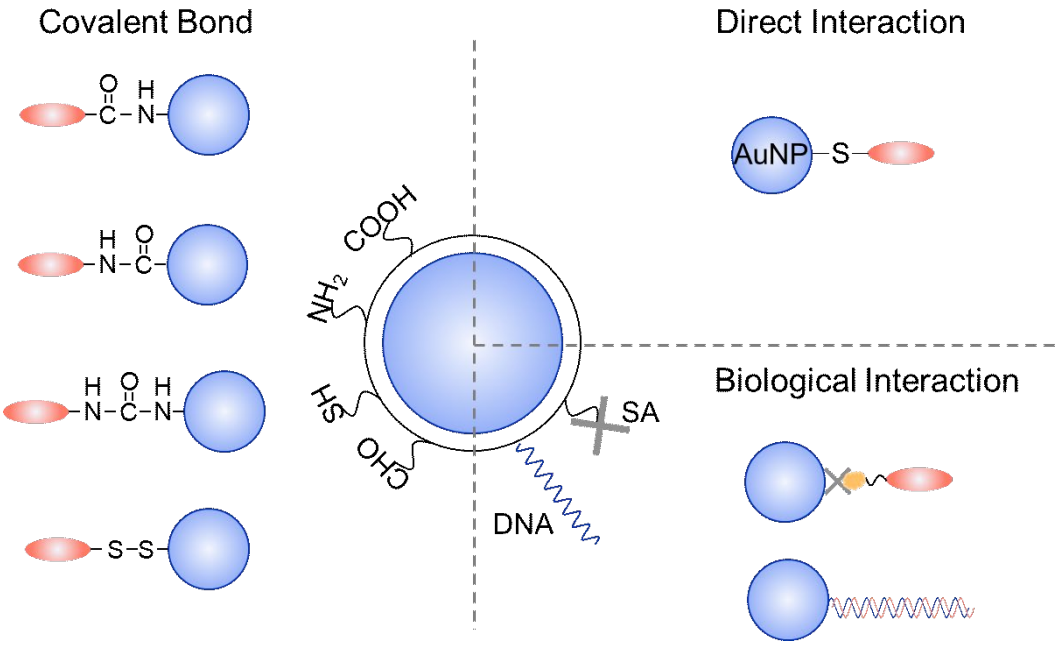

Figure 1-31. Schematic illustration of different bioconjugation methods.

1.5.2.2 Covalent coupling

Covalent coupling is the most commonly used method to conjugate biomolecules with NPs. The functional groups modified on nanoparticles' surface can react with paired groups in biomolecules through different strategies.

Carboxylic group-amine group coupling. The most commonly coupling pair is the carboxylic group and the amine group. The linkage between these two groups is usually mediated by zero-length crosslinking agents-carbodiimides. They are called zero-length reagents because in forming these bonds, no additional chemical structure is introduced between the conjugating molecules. N-substituted carbodiimides can react with

carboxylic acids to form highly reactive, o-acylisourea derivatives that are extremely short-lived. This active species then can react with a nucleophile such as a primary amine to form an amide bond. This reaction efficiency can be enhanced by adding n-hydroxysuccinimide (NHS) or sulfo-NHS to form a succinimide ester intermediate. This method has been used to conjugate proteins, amine-terminated DNA, etc. to carboxylic groups modified NPs.

Amine group-thiol group coupling. Succinimidyl-4-(N-maleimidomethyl)cyclohexane-1-carboxylate (SMCC) is a heterobifunctional reagent with significant utility in crosslinking proteins. SMCC reacts with amine-containing molecules to form stable amide bonds. Its maleimide end then may be conjugated to a sulfhydryl-containing compound to create a thioether linkage. Sulfo-SMCC is a water-soluble analog of SMCC and more commonly used for conjugate proteins to amine modified NPs.

However, this approach is not only time-consuming, but also less efficient in keeping the antibodies active and maintaining correct presentation to analytes. This is because the covalent coupling is not site-specific and often leads to blocking of the antibody binding area.

1.5.2.2 Direct interaction

The direct interaction of biomolecules and nanoparticles refers to the specific attachment of certain biomolecules to nanoparticles with relative strong non-covalent interaction.

Biomolecules with special functional groups can directly bind to some NPs. Peptides and proteins with cytosine amino have a thiol group that can coordinate to AuNPs. DNA terminated with thiol group can also be modified to AuNPs through this way.

However, due to the limitation of these unique interactions, this method cannot be applied to all the NPs.

1.5.2.3 Biological interaction

Some biological interactions can also be used to conjugate biomolecules with NPs.

The streptavidin-biotin complex is the strongest known non-covalent interaction (K_d = 10^{-15} M) between a protein and ligand. The bond formation is very rapid, and once formed, is unaffected by extremes of pH, temperature, organic solvents, and other denaturing agents. After modified with streptavidin, the nanoparticles can be easily conjugated with the biotin modified antibodies or DNA. DNA hybridization is another biological interaction that can be used for the bioconjugation.

However, using these methods, covalent bond reactions are still needed to modify antibodies with these biomolecules.

1.6 Thesis outline

The following result chapters 2-5 have been designed to explore new strategies of applying nanomaterials into cancer IVD focusing on two major problems: UCNPs surface functionalization (chapter 2 & chapter 3) and simple and quantitative cancer IVD assay (chapter 4 & chapter 5).

Chapter 2 is about a new kind of UCNPs surface modification strategy using phage display technique. This work focuses on finding some proteins that can bind to the UCNPs surface with high affinity. Because the conventional UCNPs surface modification methods restrict the applications of UCNPs with issues of agglomeration, non-specific binding and low biocompatibility, we want to find a new peptide based ligand that can be modified on UCNPs surface resulted in stable and biocompatible UCNPs probes for further biological applications. We have selected two single-chain variable fragments that have strong binding affinity to UCNPs surface, and further experiments need to be done to demonstrate the performance of these two new ligands on UCNPs surface modification. This chapter shows a possible way to modify nanomaterials surface.

Chapter 3 reports the published results (Analytical Chemistry 2018) for developing a facile and high-yield UCNPs bioconjugation approach based on a bispecific antibody (BsAb), free of chemical reaction steps. One end of the BsAb is designed to recognize

methoxy polyethylene glycol (mPEG) coated UCNPs, and the other end of the BsAb is to recognize the cancer antigen biomarker. Through simple vortexing, BsAb-UCNP nanoprobes form within 30 min and show higher (up to 54%) association to the target than the traditional UCNP nanoprobes in the ELISA-like assay. We further demonstrate its successful binding to the cancer cells with high efficiency and specificity for background-free fluorescence imaging under near-infrared excitation. This chapter broadens the applications of UCNPs and suggests a general approach broadly suitable for functionalizing a range of nanoparticles to specifically target biomolecules.

Chapter 4 presents published results (Analytical Chemistry 2018) for point of care prostate cancer detection assay using UCNPs. We design a compact device to create a focused illumination spot with high irradiance, which activates a range of highly doped 50 nm UCNPs to produce orders of magnitude more brighter emissions. The device employs a very low-cost laser diode, simplified excitation, and collection optics, and permits a mobile phone camera to record the results. Using highly erbium ions (Er^{3+}) and thulium ions (Tm^{3+}) doped UCNPs as two independent reporters on two-color lateral flow strips, new records of the limit of detection, 89 pg/mL and 400 pg/mL, have been achieved for the ultra-sensitive detection of PSA and EphA2 biomarkers, respectively without crosstalk. The technique and device presented in this chapter suggest a broad scope of low-cost, rapid, and quantitative lateral flow assays in early detection of bio-analytes.

Chapter 5 applies UCNPs and single nanoparticle image system to develop a single-molecule level detection assay for prostate cancer. After mixing 0.5 μL of PSA sample with polyclone antibodies modified UCNP probes and spreading the solution on a cover glass, we use a wide-field microscope with a 980 nm laser light source to image every single UCNP and aggregated immunocomplexes consisting of PSA and UCNPs. We calculate the number of UCNPs in each immunocomplex using fluorescence intensity. The distribution of single UCNP and immunocomplexes consisting of different numbers of UCNPs fits the Poisson distribution and is related to the concentration of PSA. Our digital immune-aggregation assay reaches a limit of detection of 1.0 pg/mL PSA in 0.5

μL of sample and covers a dynamic range of three orders of magnitude. This chapter further broadens the applications of UCNPs for trace target molecules detection.

Finally, Chapter 6 summarized the key research outcomes and outputs of the thesis and discusses the further prospects for cancer IVD using nanomaterials.

Reference

[1] Cancer Council, “What is cancer?” [Online]. Available: https://www.cancer.org.au/about-cancer/what-is-cancer/. [Accessed: 01-Jun-2019].

[2] Australian Institute of Health and Welfare, *Cancer in Australia: in brief 2019*. 2019.

[3] Cancer Council, “Prostate cancer.” [Online]. Available: https://www.cancer.org.au/about-cancer/types-of-cancer/prostate-cancer/. [Accessed: 01-Jun-2019].

[4] N. C. Institute, “Cancer diagnosis.” [Online]. Available: https://www.cancer.gov/about-cancer/diagnosis-staging/diagnosis. [Accessed: 01-Jun-2019].

[5] Wikipedia, “Protein.” [Online]. Available: https://en.wikipedia.org/wiki/Protein. [Accessed: 01-Jun-2019].

[6] Wikipedia, “DNA.” [Online]. Available: https://en.wikipedia.org/wiki/DNA. [Accessed: 01-Jun-2019].

[7] Wikipedia, “RNA.” [Online]. Available: https://en.wikipedia.org/wiki/RNA. [Accessed: 01-Jun-2019].

[8] Wikipedia, “ELISA.” [Online]. Available: https://en.wikipedia.org/wiki/ELISA. [Accessed: 01-Jun-2019].

[9] Wikipedia, “Protein microarray.” [Online]. Available: https://en.wikipedia.org/wiki/Protein_microarray.

[10] Wikipedia, “PCR.” [Online]. Available: https://en.wikipedia.org/wiki/Polymerase_chain_reaction. [Accessed: 01-Jun-2019].

[11] Wikipedia, “Real-Time PCR.” [Online]. Available: https://en.wikipedia.org/wiki/Real-time_polymerase_chain_reaction. [Accessed: 01-Jun-2019].

[12] Wikipedia, “DNA sequencing.” [Online]. Available: https://en.wikipedia.org/wiki/DNA_sequencing. [Accessed: 01-Jun-2019].

[13] Wikipedia, “DNA microarray.” [Online]. Available: https://en.wikipedia.org/wiki/DNA_microarray. [Accessed: 01-Jun-2019].

[14] Wikipedia, “Fluorescence in situ hybridization.” [Online]. Available: https://en.wikipedia.org/wiki/Fluorescence_in_situ_hybridization. [Accessed: 01-Jun-2019].

[15] W. Zhou, X. Gao, D. Liu, and X. Chen, “Gold nanoparticles for in vitro diagnostics,” *Chem. Rev.*, vol. 115, no. 19, pp. 10575–10636, 2015.

[16] Y. Xing and J. Rao, “Quantum dot bioconjugates for in vitro diagnostics & in vivo imaging,” *Cancer Biomarkers*, vol. 4, no. 6, pp. 307–319, 2008.

[17] B. A. Kairdolf, X. Qian, and S. Nie, “Bioconjugated nanoparticles for biosensing, in vivo imaging, and medical diagnostics,” *Anal. Chem.*, vol. 89, no. 2, pp. 1015–1031, 2017.

[18] S. K. Sahoo, R. Misra, and S. Parveen, “Nanoparticles: a boon to drug delivery, therapeutics, diagnostics and imaging,” in *Nanomedicine in Cancer*, Pan Stanford, 2017, pp. 73–124.

[19] H. M. E. Azzazy and M. M. H. Mansour, “In vitro diagnostic prospects of nanoparticles,” *Clin. Chim. Acta*, vol. 403, no. 1–2, pp. 1–8, 2009.

[20] I. H. El-Sayed, X. Huang, and M. A. El-Sayed, “Surface plasmon resonance scattering and absorption of anti-EGFR antibody conjugated gold nanoparticles in cancer diagnostics: applications in oral cancer,” *Nano Lett.*, vol. 5, no. 5, pp. 829–834, 2005.

[21] E. Boisselier and D. Astruc, “Gold nanoparticles in nanomedicine: preparations, imaging, diagnostics, therapies and toxicity,” *Chem. Soc. Rev.*, vol. 38, no. 6, pp. 1759–1782, 2009.

[22] R. Ladj, A. Bitar, M. Eissa, Y. Mugnier, R. Le Dantec, H. Fessi, and A. Elaissari, “Individual inorganic nanoparticles: preparation, functionalization and in vitro biomedical diagnostic applications,” *J. Mater. Chem. B*, vol. 1, no. 10, pp. 1381–1396, 2013.

[23] S. D. Caruthers, S. A. Wickline, and G. M. Lanza, “Nanotechnological applications in medicine,” *Curr. Opin. Biotechnol.*, vol. 18, no. 1, pp. 26–30, 2007.

[24] X. Huang, P. K. Jain, I. H. El-Sayed, and M. A. El-Sayed, “Gold nanoparticles: interesting optical properties and recent applications in cancer diagnostics and therapy,” 2007.

[25] P. Fortina, L. J. Kricka, D. J. Graves, J. Park, T. Hyslop, F. Tam, N. Halas, S. Surrey, and S. A. Waldman, “Applications of nanoparticles to diagnostics and therapeutics in colorectal cancer,” *Trends Biotechnol.*, vol. 25, no. 4, pp. 145–152, 2007.

[26] Z. Gao, H. Ye, D. Tang, J. Tao, S. Habibi, A. Minerick, D. Tang, and X. Xia, “Platinum-decorated gold nanoparticles with dual functionalities for ultrasensitive colorimetric in vitro diagnostics,” *Nano Lett.*, vol. 17, no. 9, pp. 5572–5579, 2017.

[27] W. Page Faulk and G. Malcolm Taylor, “An immunocolloid method for the electron microscope,” *Immunochemistry*, vol. 8, no. 11, pp. 1081–1083, Nov. 1971.

[28] J. E. Dover, G. M. Hwang, E. H. Mullen, B. C. Prorok, and S.-J. Suh, “Recent advances in peptide probe-based biosensors for detection of infectious agents,” *J. Microbiol. Methods*, vol. 78, no. 1, pp. 10–19, 2009.

[29] E. M. Barnett, X. U. Zhang, D. Maxwell, Q. Chang, and D. Piwnica-Worms, "Single-cell imaging of retinal ganglion cell apoptosis with a cell-penetrating, activatable peptide probe in an in vivo glaucoma model," *Proc. Natl. Acad. Sci.*, vol. 106, no. 23, pp. 9391–9396, 2009.

[30] M. Wang, C.-C. Mi, W.-X. Wang, C.-H. Liu, Y.-F. Wu, Z.-R. Xu, C.-B. Mao, and S.-K. Xu, "Immunolabeling and NIR-excited fluorescent imaging of HeLa cells by using NaYF4: Yb, Er upconversion nanoparticles," *ACS Nano*, vol. 3, no. 6, pp. 1580–1586, 2009.

[31] D. Giaume, M. Poggi, D. Casanova, G. Mialon, K. Lahlil, A. Alexandrou, T. Gacoin, and J.-P. Boilot, "Organic Functionalization of Luminescent Oxide Nanoparticles toward Their Application As Biological Probes," *Langmuir*, vol. 24, no. 19, pp. 11018–11026, Oct. 2008.

[32] E. Kehr, M. Sono, S. S. Chugh, and M. Jerosch-Herold, "Gadolinium-enhanced magnetic resonance imaging for detection and quantification of fibrosis in human myocardium in vitro," *Int. J. Cardiovasc. Imaging*, vol. 24, no. 1, pp. 61–68, 2008.

[33] A. Wagner, M. Platzgummer, G. Kreismayr, H. Quendler, G. Stiegler, B. Ferko, G. Vecera, K. Vorauer-Uhl, and H. Katinger, "GMP production of liposomes—a new industrial approach," *J. Liposome Res.*, vol. 16, no. 3, pp. 311–319, 2006.

[34] C. Luccardini, C. Tribet, F. Vial, V. Marchi-Artzner, and M. Dahan, "Size, charge, and interactions with giant lipid vesicles of quantum dots coated with an amphiphilic macromolecule," *Langmuir*, vol. 22, no. 5, pp. 2304–2310, 2006.

[35] K. E. Conrath, M. Lauwereys, L. Wyns, and S. Muyldermans, "Camel single-domain antibodies as modular building units in Bispecific and bivalent antibody constructs," *J Biol Chem*, vol. 276, 2001.

[36] M. P. A. Laitinen and M. Vuento, "Affinity immunosensor for milk progesterone: identification of critical parameters," *Biosens. Bioelectron.*, vol. 11, no. 12, pp. 1207–1214, 1996.

[37] Y. Zhou, Y. Chen, H. He, J. Liao, H. T. T. Duong, M. Parviz, and D. Jin, "A homogeneous DNA assay by recovering inhibited emission of rare earth ions-doped upconversion nanoparticles," *J. Rare Earths*, vol. 37, no. 1, pp. 11–18, 2019.

[38] M. J. Ruedas-rama and E. A. H. Hall, "Analytical Nanosphere Sensors Using Quantum Dot - Enzyme Conjugates for Urea and Creatinine," *Anal. Chem.*, vol. 82, no. 21, pp. 9043–9049, 2010.

[39] D. M. Rissin, C. W. Kan, T. G. Campbell, S. C. Howes, D. R. Fournier, L. Song, T. Piech, P. P. Patel, L. Chang, A. J. Rivnak, E. P. Ferrell, J. D. Randall, G. K. Provuncher, D. R. Walt, and D. C. Duffy, "Single-molecule enzyme-linked immunosorbent assay detects serum proteins at subfemtomolar concentrations," *Nat. Biotechnol.*, vol. 28, no. 6, pp. 595–599, 2010.

[40] D. H. Choi, S. K. Lee, Y. K. Oh, B. W. Bae, S. D. Lee, S. Kim, Y.-B. Shin, and M.-G. Kim, "A dual gold nanoparticle conjugate-based lateral flow assay (LFA) method for the analysis of troponin I," *Biosens. Bioelectron.*, vol. 25, no. 8, pp. 1999–2002, 2010.

[41] M. Jäger, A. Schoberth, P. Ruf, J. Hess, and H. Lindhofer, "The trifunctional antibody ertumaxomab destroys tumor cells that express low levels of human epidermal growth factor receptor 2," *Cancer Res*, vol. 69, 2009.

[42] F. Hirschhaeuser, T. Leidig, B. Rodday, C. Lindemann, and W. Mueller-Klieser, "Test system for trifunctional antibodies in 3D MCTS culture," *J Biomol Screen*, vol. 14, 2009.

[43] W. J. McBride, R. M. Sharkey, H. Karacay, C. A. D'Souza, E. A. Rossi, and P. Laverman, "A novel method of 18F radiolabeling for PET," *J Nucl Med*, vol. 50, 2009.

[44] H. Frauenfelder, G. Chen, J. Berendzen, P. W. Fenimore, H. Jansson, B. H. McMahon, I. R. Stroe, J. Swenson, and R. D. Young, "A unified model of protein

dynamics," *Proc. Natl. Acad. Sci.*, vol. 106, no. 13, pp. 5129–5134, 2009.

[45] A. Mooradian, "Photoluminescence of Metals," *Phys. Rev. Lett.*, vol. 22, no. 5, pp. 185–187, Feb. 1969.

[46] Y. Tao, Y. Lin, J. Ren, and X. Qu, "A dual fluorometric and colorimetric sensor for dopamine based on BSA-stabilized Au nanoclusters," *Biosens. Bioelectron.*, vol. 42, no. 1, pp. 41–46, 2013.

[47] J. Peng, L. N. Feng, K. Zhang, X. H. Li, L. P. Jiang, and J. J. Zhu, "Calcium carbonate-gold nanocluster hybrid spheres: Synthesis and versatile application in immunoassays," *Chem. - A Eur. J.*, vol. 18, no. 17, pp. 5261–5268, 2012.

[48] L. Stryer and R. P. Haugland, "Energy transfer: a spectroscopic ruler," *Proc. Natl. Acad. Sci. U. S. A.*, vol. 58, no. 2, pp. 719–726, Aug. 1967.

[49] L. Stryer, "Fluorescence Energy Transfer as a Spectroscopic Ruler," *Annu. Rev. Biochem.*, vol. 47, no. 1, pp. 819–846, 1978.

[50] L. Guo and D.-H. Kim, "LSPR biomolecular assay with high sensitivity induced by aptamer–antigen–antibody sandwich complex," *Biosens. Bioelectron.*, vol. 31, no. 1, pp. 567–570, 2012.

[51] J. A. Ho, H.-C. Chang, N.-Y. Shih, L.-C. Wu, Y.-F. Chang, C.-C. Chen, and C. Chou, "Diagnostic Detection of Human Lung Cancer-Associated Antigen Using a Gold Nanoparticle-Based Electrochemical Immunosensor," *Anal. Chem.*, vol. 82, no. 14, pp. 5944–5950, Jul. 2010.

[52] R. A. Alvarez-Puebla, A. Agarwal, P. Manna, B. P. Khanal, P. Aldeanueva-Potel, E. Carbó-Argibay, N. Pazos-Pérez, L. Vigderman, E. R. Zubarev, N. A. Kotov, and L. M. Liz-Marzán, "Gold nanorods 3D-supercrystals as surface enhanced Raman scattering spectroscopy substrates for the rapid detection of scrambled prions," *Proc. Natl. Acad. Sci.*, vol. 108, no. 20, p. 8157 LP-8161, May 2011.

[53] J. Owen and L. Brus, "Chemical Synthesis and Luminescence Applications of

Colloidal Semiconductor Quantum Dots," *J. Am. Chem. Soc.*, vol. 139, no. 32, pp. 10939–10943, Aug. 2017.

[54] M. Gong, Q. Liu, B. Cook, B. Kattel, T. Wang, W.-L. Chan, D. Ewing, M. Casper, A. Stramel, and J. Z. Wu, "All-Printable ZnO Quantum Dots/Graphene van der Waals Heterostructures for Ultrasensitive Detection of Ultraviolet Light," *ACS Nano*, vol. 11, no. 4, pp. 4114–4123, Apr. 2017.

[55] M. Massey, M. Wu, E. M. Conroy, and W. R. Algar, "Mind your P's and Q's: the coming of age of semiconducting polymer dots and semiconductor quantum dots in biological applications," *Curr. Opin. Biotechnol.*, vol. 34, pp. 30–40, 2015.

[56] J. Zhou, Y. Yang, and C. Zhang, "Toward Biocompatible Semiconductor Quantum Dots: From Biosynthesis and Bioconjugation to Biomedical Application," *Chem. Rev.*, vol. 115, no. 21, pp. 11669–11717, Nov. 2015.

[57] Z. Lu, X. Chen, and W. Hu, "A fluorescence aptasensor based on semiconductor quantum dots and MoS2 nanosheets for ochratoxin A detection," *Sensors Actuators B Chem.*, vol. 246, pp. 61–67, 2017.

[58] W. Gu, Y. Yan, C. Zhang, C. Ding, and Y. Xian, "One-Step Synthesis of Water-Soluble MoS2 Quantum Dots via a Hydrothermal Method as a Fluorescent Probe for Hyaluronidase Detection," *ACS Appl. Mater. Interfaces*, vol. 8, no. 18, pp. 11272–11279, May 2016.

[59] D. M. Willard, L. L. Carillo, J. Jung, and A. Van Orden, "CdSe− ZnS quantum dots as resonance energy transfer donors in a model protein− protein binding assay," *Nano Lett.*, vol. 1, no. 9, pp. 469–474, 2001.

[60] X. Liu, H. Jiang, J. Lei, and H. Ju, "Anodic electrochemiluminescence of CdTe quantum dots and its energy transfer for detection of catechol derivatives," *Anal. Chem.*, vol. 79, no. 21, pp. 8055–8060, 2007.

[61] C. Peng, Z. Li, Y. Zhu, W. Chen, Y. Yuan, L. Liu, Q. Li, D. Xu, R. Qiao, L.

Wang, S. Zhu, Z. Jin, and C. Xu, “Simultaneous and sensitive determination of multiplex chemical residues based on multicolor quantum dot probes,” *Biosens. Bioelectron.*, vol. 24, no. 12, pp. 3657–3662, 2009.

[62] T. R. Pisanic Ii, Y. Zhang, and T. H. Wang, “Quantum dots in diagnostics and detection: principles and paradigms,” *Analyst*, vol. 139, no. 12, pp. 2968–2981, 2014.

[63] A. Shamirian, H. Samareh Afsari, D. Wu, L. W. Miller, and P. T. Snee, “Ratiometric QD-FRET Sensing of Aqueous H2S in Vitro,” *Anal. Chem.*, vol. 88, no. 11, pp. 6050–6056, Jun. 2016.

[64] N. Ma, W. Jiang, T. Li, Z. Zhang, H. Qi, and M. Yang, “Fluorescence aggregation assay for the protein biomarker mucin 1 using carbon dot-labeled antibodies and aptamers,” *Microchim. Acta*, vol. 182, no. 1–2, pp. 443–447, 2015.

[65] X. Miao, X. Yan, D. Qu, D. Li, F. F. Tao, and Z. Sun, “Red Emissive Sulfur, Nitrogen Codoped Carbon Dots and Their Application in Ion Detection and Theraonostics,” *ACS Appl. Mater. Interfaces*, vol. 9, no. 22, pp. 18549–18556, Jun. 2017.

[66] T. N. J. I. Edison, R. Atchudan, J.-J. Shim, S. Kalimuthu, B.-C. Ahn, and Y. R. Lee, “Turn-off fluorescence sensor for the detection of ferric ion in water using green synthesized N-doped carbon dots and its bio-imaging,” *J. Photochem. Photobiol. B Biol.*, vol. 158, pp. 235–242, 2016.

[67] L. Li, B. Yu, and T. You, “Nitrogen and sulfur co-doped carbon dots for highly selective and sensitive detection of Hg (II) ions,” *Biosens. Bioelectron.*, vol. 74, pp. 263–269, 2015.

[68] H. Li, Y. Zhang, L. Wang, J. Tian, and X. Sun, “Nucleic acid detection using carbon nanoparticles as a fluorescent sensing platform,” *Chem. Commun.*, vol. 47, no. 3, pp. 961–963, 2011.

[69] D. Bu, H. Zhuang, G. Yang, and X. Ping, “An immunosensor designed for

polybrominated biphenyl detection based on fluorescence resonance energy transfer (FRET) between carbon dots and gold nanoparticles," *Sensors Actuators, B Chem.*, vol. 195, pp. 540–548, 2014.

[70] X. Shao, H. Gu, Z. Wang, X. Chai, Y. Tian, and G. Shi, "Highly selective electrochemical strategy for monitoring of cerebral Cu2+ based on a carbon dot-TPEA hybridized surface," *Anal. Chem.*, vol. 85, no. 1, pp. 418–425, 2013.

[71] N. Ben Messaoud, M. E. Ghica, C. Dridi, M. Ben Ali, and C. M. A. Brett, "Electrochemical sensor based on multiwalled carbon nanotube and gold nanoparticle modified electrode for the sensitive detection of bisphenol A," *Sensors Actuators B Chem.*, vol. 253, pp. 513–522, 2017.

[72] M. J. Tan, Z.-Y. Hong, M.-H. Chang, C.-C. Liu, H.-F. Cheng, X. J. Loh, C.-H. Chen, C.-D. Liao, and K. V. Kong, "Metal carbonyl-gold nanoparticle conjugates for highly sensitive SERS detection of organophosphorus pesticides," *Biosens. Bioelectron.*, vol. 96, pp. 167–172, 2017.

[73] Q. Xu, P. Pu, J. Zhao, C. Dong, C. Gao, Y. Chen, J. Chen, Y. Liu, and H. Zhou, "Preparation of highly photoluminescent sulfur-doped carbon dots for Fe(iii) detection," *J. Mater. Chem. A*, vol. 3, no. 2, pp. 542–546, 2015.

[74] X. Cui, L. Zhu, J. Wu, Y. Hou, P. Wang, Z. Wang, and M. Yang, "A fluorescent biosensor based on carbon dots-labeled oligodeoxyribonucleotide and graphene oxide for mercury (II) detection," *Biosens. Bioelectron.*, vol. 63, pp. 506–512, 2015.

[75] Q.-Y. Cai, J. Li, J. Ge, L. Zhang, Y.-L. Hu, Z.-H. Li, and L.-B. Qu, "A rapid fluorescence 'switch-on' assay for glutathione detection by using carbon dots–MnO2 nanocomposites," *Biosens. Bioelectron.*, vol. 72, pp. 31–36, 2015.

[76] L. L. Li, J. Ji, R. Fei, C. Z. Wang, Q. Lu, J. R. Zhang, L. P. Jiang, and J. J. Zhu, "A facile microwave avenue to electrochemiluminescent two-color graphene quantum dots," *Adv. Funct. Mater.*, vol. 22, no. 14, pp. 2971–2979, 2012.

[77] M. Arvand and S. Hemmati, “Magnetic nanoparticles embedded with graphene quantum dots and multiwalled carbon nanotubes as a sensing platform for electrochemical detection of progesterone,” *Sensors Actuators B Chem.*, vol. 238, pp. 346–356, 2017.

[78] X. Li, J. Wei, K. E. Aifantis, Y. Fan, Q. Feng, F.-Z. Cui, and F. Watari, “Current investigations into magnetic nanoparticles for biomedical applications,” *J. Biomed. Mater. Res. Part A*, vol. 104, no. 5, pp. 1285–1296, May 2016.

[79] R. Gao, X. Cui, Y. Hao, L. Zhang, D. Liu, and Y. Tang, “A highly-efficient imprinted magnetic nanoparticle for selective separation and detection of 17β-estradiol in milk,” *Food Chem.*, vol. 194, pp. 1040–1047, 2016.

[80] Z. Xi, R. Huang, Z. Li, N. He, T. Wang, E. Su, and Y. Deng, “Selection of HBsAg-Specific DNA Aptamers Based on Carboxylated Magnetic Nanoparticles and Their Application in the Rapid and Simple Detection of Hepatitis B Virus Infection,” *ACS Appl. Mater. Interfaces*, vol. 7, no. 21, pp. 11215–11223, Jun. 2015.

[81] Y. Pang, C. Wang, J. Wang, Z. Sun, R. Xiao, and S. Wang, “Fe3O4@Ag magnetic nanoparticles for microRNA capture and duplex-specific nuclease signal amplification based SERS detection in cancer cells,” *Biosens. Bioelectron.*, vol. 79, pp. 574–580, 2016.

[82] P. Miao, Y. Tang, and L. Wang, “DNA Modified Fe3O4@Au Magnetic Nanoparticles as Selective Probes for Simultaneous Detection of Heavy Metal Ions,” *ACS Appl. Mater. Interfaces*, vol. 9, no. 4, pp. 3940–3947, Feb. 2017.

[83] K. El-Boubbou, C. Gruden, and X. Huang, “Magnetic glyco-nanoparticles: A unique tool for rapid pathogen detection, decontamination, and strain differentiation,” *J. Am. Chem. Soc.*, vol. 129, no. 44, pp. 13392–13393, 2007.

[84] J. M. Perez, F. J. Simeone, Y. Saeki, L. Josephson, and R. Weissleder, “Viral-induced self-assembly of magnetic nanoparticles allows the detection of viral particles in biological media,” *J. Am. Chem. Soc.*, vol. 125, no. 34, pp. 10192–

10193, 2003.

[85] H. Wei and E. Wang, “Fe3O4 magnetic nanoparticles as peroxidase mimetics and their applications in H2O2 and glucose detection,” *Anal. Chem.*, vol. 80, no. 6, pp. 2250–2254, 2008.

[86] T. T. T. Yang, *Rare earth nanotechnology*. CRC Press, 2012.

[87] A. R. Jha, *Rare earth materials: Properties and applications*. 2014.

[88] M. Haase and H. Schäfer, “Upconverting Nanoparticles,” *Angew. Chemie Int. Ed.*, vol. 50, no. 26, pp. 5808–5829, Jun. 2011.

[89] M. Wang, G. Abbineni, A. Clevenger, C. Mao, and S. Xu, “Upconversion nanoparticles: synthesis, surface modification and biological applications,” *Nanomedicine Nanotechnology, Biol. Med.*, vol. 7, no. 6, pp. 710–729, 2011.

[90] S. Kim, S.-H. Hwang, S.-G. Im, M.-K. Lee, C.-H. Lee, J. S. Son, and H.-B. Oh, “Upconversion Nanoparticle-Based Förster Resonance Energy Transfer for Detecting DNA Methylation,” *Sensors* , vol. 16, no. 8. 2016.

[91] M. Wu, X. Wang, K. Wang, and Z. Guo, “Sequence-specific detection of cytosine methylation in DNA via the FRET mechanism between upconversion nanoparticles and gold nanorods,” *Chem. Commun.*, vol. 52, no. 54, pp. 8377–8380, 2016.

[92] R. Zou, Y. Chang, T. Zhang, F. Si, Y. Liu, Y. Zhao, Y. Liu, M. Zhang, X. Yu, X. Qiao, G. Zhu, and Y. Guo, “Up-Converting Nanoparticle-Based Immunochromatographic Strip for Multi-Residue Detection of Three Organophosphorus Pesticides in Food,” *Front. Chem.*, vol. 7, p. 18, Feb. 2019.

[93] G. Wang, Y. Fu, Z. Ren, J. Huang, S. Best, X. Li, and G. Han, “Upconversion nanocrystal ‘armoured’ silica fibres with superior photoluminescence for miRNA detection,” *Chem. Commun.*, vol. 54, no. 49, pp. 6324–6327, 2018.

[94] J. Han, C. Zhang, F. Liu, B. Liu, M. Han, W. Zou, L. Yang, and Z. Zhang, "Upconversion nanoparticles for ratiometric fluorescence detection of nitrite," *Analyst*, vol. 139, no. 12, pp. 3032–3038, 2014.

[95] S. Wu, N. Duan, X. Ma, Y. Xia, Y. Yu, Z. Wang, and H. Wang, "Simultaneous detection of enterovirus 71 and coxsackievirus A16 using dual-colour upconversion luminescent nanoparticles as labels," *Chem. Commun.*, vol. 48, no. 40, pp. 4866–4868, 2012.

[96] A. Qu, X. Wu, L. Xu, L. Liu, W. Ma, H. Kuang, and C. Xu, "SERS- and luminescence-active Au–Au–UCNP trimers for attomolar detection of two cancer biomarkers," *Nanoscale*, vol. 9, no. 11, pp. 3865–3872, 2017.

[97] Y. Chen, H. T. T. Duong, S. Wen, C. Mi, Y. Zhou, O. Shimoni, S. M. Valenzuela, and D. Jin, "Exonuclease III-Assisted Upconversion Resonance Energy Transfer in a Wash-Free Suspension DNA Assay," *Anal. Chem.*, vol. 90, no. 1, pp. 663–668, Jan. 2018.

[98] D. M. Rissin, C. W. Kan, T. G. Campbell, S. C. Howes, D. R. Fournier, L. Song, T. Piech, P. P. Patel, L. Chang, A. J. Rivnak, E. P. Ferrell, J. D. Randall, G. K. Provuncher, D. R. Walt, and D. C. Duffy, "Single-molecule enzyme-linked immunosorbent assay detects serum proteins at subfemtomolar concentrations," *Nat. Biotechnol.*, vol. 28, no. 6, pp. 595–599, 2010.

[99] A. Hlaváček, Z. Farka, M. Hübner, V. Horňáková, D. Němeček, R. Niessner, P. Skládal, D. Knopp, and H. H. Gorris, "Competitive Upconversion-Linked Immunosorbent Assay for the Sensitive Detection of Diclofenac," *Anal. Chem.*, vol. 88, no. 11, pp. 6011–6017, 2016.

[100] L. Lu, D. Tu, Y. Liu, S. Zhou, W. Zheng, and X. Chen, "Ultrasensitive detection of cancer biomarker microRNA by amplification of fluorescence of lanthanide nanoprobes," *Nano Res.*, vol. 11, no. 1, pp. 264–273, 2018.

[101] M. Zhang, W. Zheng, Y. Liu, P. Huang, Z. Gong, J. Wei, Y. Gao, S. Zhou, X. Li, and X. Chen, "A New Class of Blue-LED-Excitable NIR-II Luminescent

Nanoprobes Based on Lanthanide-Doped CaS Nanoparticles," *Angew. Chemie Int. Ed.*, vol. 0, no. 0, May 2019.

[102] S. Yu, D. Tu, W. Lian, J. Xu, and X. Chen, "Lanthanide-doped near-infrared II luminescent nanoprobes for bioapplications," *Sci. China Mater.*, vol. 62, no. 8, pp. 1071–1086, 2019.

[103] Y. Liu, S. Zhou, Z. Zhuo, R. Li, Z. Chen, M. Hong, and X. Chen, "In vitro upconverting/downshifting luminescent detection of tumor markers based on Eu3+-activated core–shell–shell lanthanide nanoprobes," *Chem. Sci.*, vol. 7, no. 8, pp. 5013–5019, 2016.

[104] Y. Liu, D. Tu, H. Zhu, and X. Chen, "Lanthanide-doped luminescent nanoprobes: controlled synthesis, optical spectroscopy, and bioapplications," *Chem. Soc. Rev.*, vol. 42, no. 16, pp. 6924–6958, 2013.

[105] J. Xu, S. Zhou, D. Tu, W. Zheng, P. Huang, R. Li, Z. Chen, M. Huang, and X. Chen, "Sub-5 nm lanthanide-doped lutetium oxyfluoride nanoprobes for ultrasensitive detection of prostate specific antigen," *Chem. Sci.*, vol. 7, no. 4, pp. 2572–2578, 2016.

[106] A. R. Jha, *Rare earth materials: properties and applications*. CRC Press, 2014.

[107] Wikipedia, "Gadolinium." [Online]. Available: https://en.wikipedia.org/wiki/Gadolinium. [Accessed: 01-Jun-2019].

[108] A. Sedlmeier and H. H. Gorris, "Surface modification and characterization of photon-upconverting nanoparticles for bioanalytical applications," *Chem. Soc. Rev.*, vol. 44, no. 6, pp. 1526–1560, 2015.

[109] L. M. Liz-Marzán, M. Giersig, and P. Mulvaney, "Synthesis of nanosized gold− silica core− shell particles," *Langmuir*, vol. 12, no. 18, pp. 4329–4335, 1996.

[110] L. M. Liz-Marzán and P. Mulvaney, "The assembly of coated nanocrystals," *J.*

Phys. Chem. B, vol. 107, no. 30, pp. 7312–7326, 2003.

[111] H. S. Park, G. Dodbiba, L. F. Cao, and T. Fujita, "Synthesis of silica-coated ferromagnetic fine powder by heterocoagulation," *J. Phys. Condens. Matter*, vol. 20, no. 20, p. 204105, 2008.

[112] C. T. Kresge, M. E. Leonowicz, W. J. Roth, J. C. Vartuli, and J. S. Beck, "Ordered mesoporous molecular sieves synthesized by a liquid-crystal template mechanism," *Nature*, vol. 359, no. 6397, p. 710, 1992.

[113] I. Gorelikov and N. Matsuura, "Single-step coating of mesoporous silica on cetyltrimethyl ammonium bromide-capped nanoparticles," *Nano Lett.*, vol. 8, no. 1, pp. 369–373, 2008.

[114] J. Kim, J. E. Lee, J. Lee, J. H. Yu, B. C. Kim, K. An, Y. Hwang, C.-H. Shin, J.-G. Park, and J. Kim, "Magnetic fluorescent delivery vehicle using uniform mesoporous silica spheres embedded with monodisperse magnetic and semiconductor nanocrystals," *J. Am. Chem. Soc.*, vol. 128, no. 3, pp. 688–689, 2006.

[115] T. Sakura, T. Takahashi, K. Kataoka, and Y. Nagasaki, "One-pot preparation of mono-dispersed and physiologically stabilized gold colloid," *Colloid Polym. Sci.*, vol. 284, no. 1, pp. 97–101, 2005.

[116] T. Soukka, T. Rantanen, and K. Kuningas, "Photon upconversion in homogeneous fluorescence-based bioanalytical assays," *Ann. N. Y. Acad. Sci.*, vol. 1130, no. 1, pp. 188–200, 2008.

[117] D. Chen, L. Lei, A. Yang, Z. Wang, and Y. Wang, "Ultra-broadband near-infrared excitable upconversion core/shell nanocrystals," *Chem. Commun.*, vol. 48, no. 47, pp. 5898–5900, 2012.

[118] Z. Li, Y. Zhang, and S. Jiang, "Multicolor core/shell-structured upconversion fluorescent nanoparticles," *Adv. Mater.*, vol. 20, no. 24, pp. 4765–4769, 2008.

[119] F. Liu, Q. Zhao, H. You, and Z. Wang, “Synthesis of stable carboxy-terminated NaYF 4: Yb 3+, Er 3+@ SiO 2 nanoparticles with ultrathin shell for biolabeling applications,” *Nanoscale*, vol. 5, no. 3, pp. 1047–1053, 2013.

[120] S. Wilhelm, T. Hirsch, W. M. Patterson, E. Scheucher, T. Mayr, and O. S. Wolfbeis, “Multicolor upconversion nanoparticles for protein conjugation,” *Theranostics*, vol. 3, no. 4, p. 239, 2013.

[121] S. Gai, P. Yang, C. Li, W. Wang, Y. Dai, N. Niu, and J. Lin, “Synthesis of Magnetic, Up-Conversion Luminescent, and Mesoporous Core–Shell-Structured Nanocomposites as Drug Carriers,” *Adv. Funct. Mater.*, vol. 20, no. 7, pp. 1166–1172, 2010.

[122] C. Fang, S. Wu, N. Duan, S. Dai, and Z. Wang, “Highly sensitive aptasensor for oxytetracycline based on upconversion and magnetic nanoparticles,” *Anal. Methods*, vol. 7, no. 6, pp. 2585–2593, 2015.

[123] J. Tian, J. Bai, Y. Peng, Z. Qie, Y. Zhao, B. Ning, D. Xiao, and Z. Gao, “A core–shell-structured molecularly imprinted polymer on upconverting nanoparticles for selective and sensitive fluorescence sensing of sulfamethazine,” *Analyst*, vol. 140, no. 15, pp. 5301–5307, 2015.

[124] L. Fu, M. Morsch, B. Shi, G. Wang, A. Lee, R. Radford, Y. Lu, D. Jin, and R. Chung, “A versatile upconversion surface evaluation platform for bio–nano surface selection for the nervous system,” *Nanoscale*, vol. 9, no. 36, pp. 13683–13692, 2017.

[125] Z. Chen, H. Chen, H. Hu, M. Yu, F. Li, Q. Zhang, Z. Zhou, T. Yi, and C. Huang, “Versatile synthesis strategy for carboxylic acid− functionalized upconverting nanophosphors as biological labels,” *J. Am. Chem. Soc.*, vol. 130, no. 10, pp. 3023–3029, 2008.

[126] M. Darbandi and T. Nann, “One-pot synthesis of YF3@ silica core/shell nanoparticles,” *Chem. Commun.*, no. 7, pp. 776–778, 2006.

[127] A. Hlavacek, M. J. Mickert, T. Soukka, S. Lahtinen, T. Tallgren, N. Pizurova, A. Król, and H. H. Gorris, "Large-Scale Purification of Photon-Upconversion Nanoparticles by Gel Electrophoresis for Analogue and Digital Bioassays," *Anal. Chem.*, vol. 91, no. 2, pp. 1241–1246, 2018.

[128] R. P. Bagwe, L. R. Hilliard, and W. Tan, "Surface modification of silica nanoparticles to reduce aggregation and nonspecific binding," *Langmuir*, vol. 22, no. 9, pp. 4357–4362, 2006.

[129] L. Xiong, Z. Chen, Q. Tian, T. Cao, C. Xu, and F. Li, "High Contrast Upconversion Luminescence Targeted Imaging in Vivo Using Peptide-Labeled Nanophosphors," *Anal. Chem.*, vol. 81, no. 21, pp. 8687–8694, Nov. 2009.

[130] R. Naccache, F. Vetrone, V. Mahalingam, L. A. Cuccia, and J. A. Capobianco, "Controlled synthesis and water dispersibility of hexagonal phase NaGdF4: Ho3+/Yb3+ nanoparticles," *Chem. Mater.*, vol. 21, no. 4, pp. 717–723, 2009.

[131] Y. Liu, M. Chen, T. Cao, Y. Sun, C. Li, Q. Liu, T. Yang, L. Yao, W. Feng, and F. Li, "A cyanine-modified nanosystem for in vivo upconversion luminescence bioimaging of methylmercury," *J. Am. Chem. Soc.*, vol. 135, no. 26, pp. 9869–9876, 2013.

[132] J. Yuan, Y. Cen, X.-J. Kong, S. Wu, C.-L. Liu, R.-Q. Yu, and X. Chu, "MnO2-nanosheet-modified upconversion nanosystem for sensitive turn-on fluorescence detection of H2O2 and glucose in blood," *ACS Appl. Mater. Interfaces*, vol. 7, no. 19, pp. 10548–10555, 2015.

[133] R. Deng, X. Xie, M. Vendrell, Y.-T. Chang, and X. Liu, "Intracellular glutathione detection using MnO2-nanosheet-modified upconversion nanoparticles," *J. Am. Chem. Soc.*, vol. 133, no. 50, pp. 20168–20171, 2011.

[134] J. Shen, L.-D. Sun, Y.-W. Zhang, and C.-H. Yan, "Superparamagnetic and upconversion emitting Fe 3 O 4/NaYF 4: Yb, Er hetero-nanoparticles via a crosslinker anchoring strategy," *Chem. Commun.*, vol. 46, no. 31, pp. 5731–5733, 2010.

[135] H. Zhou, C. Xu, W. Sun, and C. Yan, “Clean and Flexible Modification Strategy for Carboxyl/Aldehyde-Functionalized Upconversion Nanoparticles and Their Optical Applications,” *Adv. Funct. Mater.*, vol. 19, no. 24, pp. 3892–3900, 2009.

[136] S. Wu, G. Han, D. J. Milliron, S. Aloni, V. Altoe, D. V Talapin, B. E. Cohen, and P. J. Schuck, “Non-blinking and photostable upconverted luminescence from single lanthanide-doped nanocrystals,” *Proc. Natl. Acad. Sci.*, vol. 106, no. 27, pp. 10917–10921, 2009.

[137] G.-S. Yi and G.-M. Chow, “Water-soluble NaYF4: Yb, Er (Tm)/NaYF4/polymer core/shell/shell nanoparticles with significant enhancement of upconversion fluorescence,” *Chem. Mater.*, vol. 19, no. 3, pp. 341–343, 2007.

[138] L. Cheng, K. Yang, M. Shao, S.-T. Lee, and Z. Liu, “Multicolor in vivo imaging of upconversion nanoparticles with emissions tuned by luminescence resonance energy transfer,” *J. Phys. Chem. C*, vol. 115, no. 6, pp. 2686–2692, 2011.

[139] S. Liang, X. Zhang, Z. Wu, Y. Liu, H. Zhang, H. Sun, H. Sun, and B. Yang, “Decoration of up-converting NaYF 4: Yb, Er (Tm) nanoparticles with surfactant bilayer. A versatile strategy to perform oil-to-water phase transfer and subsequently surface silication,” *CrystEngComm*, vol. 14, no. 10, pp. 3484–3489, 2012.

[140] S. Cui, H. Chen, H. Zhu, J. Tian, X. Chi, Z. Qian, S. Achilefu, and Y. Gu, “Amphiphilic chitosan modified upconversion nanoparticles for in vivo photodynamic therapy induced by near-infrared light,” *J. Mater. Chem.*, vol. 22, no. 11, pp. 4861–4873, 2012.

[141] W. Ren, G. Tian, S. Jian, Z. Gu, L. Zhou, L. Yan, S. Jin, W. Yin, and Y. Zhao, “TWEEN coated NaYF 4: Yb, Er/NaYF4 core/shell upconversion nanoparticles for bioimaging and drug delivery,” *Rsc Adv.*, vol. 2, no. 18, pp. 7037–7041, 2012.

[142] L. Li, R. Zhang, L. Yin, K. Zheng, W. Qin, P. R. Selvin, and Y. Lu, “Biomimetic surface engineering of lanthanide-doped upconversion nanoparticles as versatile

bioprobes," *Angew. Chemie Int. Ed.*, vol. 51, no. 25, pp. 6121–6125, 2012.

[143] K. W. Ferrara, M. A. Borden, and H. Zhang, "Lipid-shelled vehicles: engineering for ultrasound molecular imaging and drug delivery," *Acc. Chem. Res.*, vol. 42, no. 7, pp. 881–892, 2009.

[144] M. Longmire, P. L. Choyke, and H. Kobayashi, "Clearance properties of nano-sized particles and molecules as imaging agents: considerations and caveats," 2008.

[145] D. I. Gittins and F. Caruso, "Biological and Physical Applications of Water-Based Metal Nanoparticles Synthesised in Organic Solution," *ChemPhysChem*, vol. 3, no. 1, pp. 110–113, 2002.

[146] G. P. Mitchell, C. A. Mirkin, and R. L. Letsinger, "Programmed assembly of DNA functionalized quantum dots," *J. Am. Chem. Soc.*, vol. 121, no. 35, pp. 8122–8123, 1999.

[147] J. Aldana, Y. A. Wang, and X. Peng, "Photochemical instability of CdSe nanocrystals coated by hydrophilic thiols," *J. Am. Chem. Soc.*, vol. 123, no. 36, pp. 8844–8850, 2001.

[148] A. Hoshino, K. Fujioka, T. Oku, S. Nakamura, M. Suga, Y. Yamaguchi, K. Suzuki, M. Yasuhara, and K. Yamamoto, "Quantum dots targeted to the assigned organelle in living cells," *Microbiol. Immunol.*, vol. 48, no. 12, pp. 985–994, 2004.

[149] Q. Zhang, K. Song, J. Zhao, X. Kong, Y. Sun, X. Liu, Y. Zhang, Q. Zeng, and H. Zhang, "Hexanedioic acid mediated surface–ligand-exchange process for transferring NaYF4: Yb/Er (or Yb/Tm) up-converting nanoparticles from hydrophobic to hydrophilic," *J. Colloid Interface Sci.*, vol. 336, no. 1, pp. 171–175, 2009.

[150] J. Zhou, M. Yu, Y. Sun, X. Zhang, X. Zhu, Z. Wu, D. Wu, and F. Li, "Fluorine-18-labeled Gd3+/Yb3+/Er3+ co-doped NaYF4 nanophosphors for multimodality

PET/MR/UCL imaging," *Biomaterials*, vol. 32, no. 4, pp. 1148–1156, 2011.

[151] T. Cao, T. Yang, Y. Gao, Y. Yang, H. Hu, and F. Li, "Water-soluble NaYF4: Yb/Er upconversion nanophosphors: Synthesis, characteristics and application in bioimaging," *Inorg. Chem. Commun.*, vol. 13, no. 3, pp. 392–394, 2010.

[152] Q. Liu, Y. Sun, T. Yang, W. Feng, C. Li, and F. Li, "Sub-10 nm hexagonal lanthanide-doped NaLuF4 upconversion nanocrystals for sensitive bioimaging in vivo," *J. Am. Chem. Soc.*, vol. 133, no. 43, pp. 17122–17125, 2011.

[153] Y. Liu, D. L. Purich, C. Wu, Y. Wu, T. Chen, C. Cui, L. Zhang, S. Cansiz, W. Hou, Y. Wang, S. Yang, and W. Tan, "Ionic Functionalization of Hydrophobic Colloidal Nanoparticles to Form Ionic Nanoparticles with Enzymelike Properties," *J. Am. Chem. Soc.*, vol. 137, no. 47, pp. 14952–14958, 2015.

[154] M. Kamimura, D. Miyamoto, Y. Saito, K. Soga, and Y. Nagasaki, "Design of poly (ethylene glycol)/streptavidin coimmobilized upconversion nanophosphors and their application to fluorescence biolabeling," *Langmuir*, vol. 24, no. 16, pp. 8864–8870, 2008.

[155] N. J. J. Johnson, N. M. Sangeetha, J.-C. Boyer, and F. C. J. M. van Veggel, "Facile ligand-exchange with polyvinylpyrrolidone and subsequent silica coating of hydrophobic upconverting β-NaYF 4: Yb3+/Er3+ nanoparticles," *Nanoscale*, vol. 2, no. 5, pp. 771–777, 2010.

[156] L. Xiong, T. Yang, Y. Yang, C. Xu, and F. Li, "Long-term in vivo biodistribution imaging and toxicity of polyacrylic acid-coated upconversion nanophosphors," *Biomaterials*, vol. 31, no. 27, pp. 7078–7085, 2010.

[157] H. Zhang, Y. Li, I. A. Ivanov, Y. Qu, Y. Huang, and X. Duan, "Plasmonic modulation of the upconversion fluorescence in NaYF4: Yb/Tm hexaplate nanocrystals using gold nanoparticles or nanoshells," *Angew. Chemie Int. Ed.*, vol. 49, no. 16, pp. 2865–2868, 2010.

[158] C. L. Schofield, A. H. Haines, R. A. Field, and D. A. Russell, “Silver and gold glyconanoparticles for colorimetric bioassays,” *Langmuir*, vol. 22, no. 15, pp. 6707–6711, 2006.

[159] F. Pinaud, D. King, H.-P. Moore, and S. Weiss, “Bioactivation and cell targeting of semiconductor CdSe/ZnS nanocrystals with phytochelatin-related peptides,” *J. Am. Chem. Soc.*, vol. 126, no. 19, pp. 6115–6123, 2004.

[160] J. Lu, Y. Chen, D. Liu, W. Ren, Y. Lu, Y. Shi, J. Piper, I. Paulsen, and D. Jin, “One-Step Protein Conjugation to Upconversion Nanoparticles,” *Anal. Chem.*, vol. 87, no. 20, pp. 10406–10413, 2015.

[161] L. Le Li, P. Wu, K. Hwang, and Y. Lu, “An exceptionally simple strategy for DNA-functionalized Up-conversion nanoparticles as biocompatible agents for nanoassembly, DNA delivery, and imaging,” *J. Am. Chem. Soc.*, vol. 135, no. 7, pp. 2411–2414, 2013.

[162] H. T. T. Duong, Y. Chen, S. A. Tawfik, S. Wen, M. Parviz, O. Shimoni, and D. Jin, “Systematic investigation of functional ligands for colloidal stable upconversion nanoparticles,” *RSC Adv.*, vol. 8, no. 9, pp. 4842–4849, 2018.

[163] Y. Liu, D. L. Purich, C. Wu, Y. Wu, T. Chen, C. Cui, L. Zhang, S. Cansiz, W. Hou, and Y. Wang, “Ionic functionalization of hydrophobic colloidal nanoparticles to form ionic nanoparticles with enzymelike properties,” *J. Am. Chem. Soc.*, vol. 137, no. 47, pp. 14952–14958, 2015.

Chapter 2 Select UCNP targeted antibodies by phage display

2.1 Motivation

Before applying upconversion nanoparticles (UCNPs) in the cancer in-vitro diagnosis assays, we need to use different surface functionalization methods to conjugate biomolecules that can recognize targeted biomarkers, such as antibodies, nuclear acids, and peptides, to their surfaces. Most of these surface functionalization methods begin with surface modification of hydrophilic and biocompatible ligands.

In this study, we aimed to apply the phage display technology to search for antibodies that can bind to the surface of UCNPs with high affinity and specificity. These proteins can be used to replace the original surfactant on the surface of UCNPs and be worked as linkers to conjugate other biological molecules. An exciting application that results from these anti-UCNP antibodies is the possibility of a biocompatible fluorescent nanoprobe that has ultra-stability in biological samples.

2.2 Background and significance

2.2.1 Challenges in UCNPs surface modification

Since most highly monodisperse UCNPs of uniform size are synthesized in high-boiling organic solvents and the oleic acid is typically used as surfactant to prevent nanoparticle aggregation, these UCNPs are coated with a hydrophobic layer and have no functional groups for linking biomolecules. [1]–[4] Therefore, post-synthesis surface modification is necessary to transfer UCNPs to hydrophilic and biocompatible, and functional groups are also needed for further bioconjugation with antibodies, DNA, etc.

We have introduced the most common used UCNPs surface modification methods include silica coating, ligand exchange, ligand oxidization, ligand interaction, and layer-by-layer coating in Chapter 1. All these introduced methods can make UCNPs disperse into an aqueous solution and modified with carboxyl groups, amine groups, etc. for further bioconjugation. However, the binding affinity between the new ligands and

UCNPs is still not strong enough. In most biological environments, there are many phosphate groups that have a quite strong affinity to UCNPs surfaces, and they can replace these modified surfactants, resulted in aggregation of UCNPs. Furthermore, for biological applications, we should also consider the biocompatibility of these modified surfactants. Polyethylene glycol (PEG) is often used to make new modified UCNPs hydrophilic and more biocompatible. [5], [6] However, as PEG is not a human or animal source molecule, it also can cause immunoreaction and become harmful. [7] Ronnie H. Fang etc. have reported one method that using cell membrane to coat nanoparticles which results in much more biocompatible ones. [8] However, the experiment is quite complex and limits its applications. DNA has also been used in the ligand exchange method to replace the oleic acid, but its binding affinity is not strong enough to ensure good stability. [9], [10] So a suitable molecule with good biocompatibility and strong binding to UCNPs surface is needed to be modified on the UCNPs surface.

2.2.2 Phage display

The peptide is a good choice as it can bind to the target like an antibody as they have the same basic structure, amino acid. [11]–[13] And it is very easy to produce antibodies using cell engineering. Phage display is a popular technology to select the peptide that can bind to the target.

Phage display is a technique for the production and screening of novel proteins and polypeptides by inserting a gene fragment into a gene responsible for the surface protein of a bacteriophage (viruses that infect bacteria). In this technique, the gene inserted into a phage, causing the phage to "display" the protein on its outside while containing the gene for the protein on its inside, resulting in a connection between genotype and phenotype. These displaying phages can then be screened against other biomolecules such as proteins, peptides and DNA/RNA, metals, or inorganic crystals in order to detect the interaction between the displayed protein and those targets. [14]–[19]

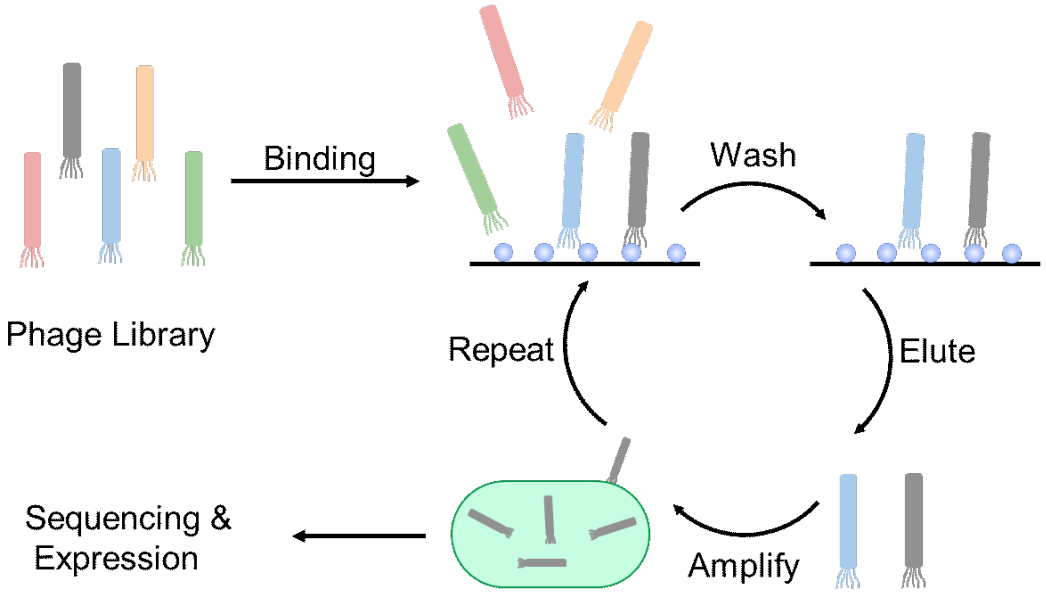

Figure 2-1. Schematic illustration of phage display.

Phage display was first described by George P. Smith in 1985 when he demonstrated the display of peptides on filamentous phage by creating a fusion of the virus's capsid protein to a library of peptide sequences. [20] This displayed the peptides on the viral surface, where those with the highest binding affinity could be selected. A patent by George Pieczenik claiming priority from 1985 also describes the generation of phage display libraries. [21] In 1988, Parmley and Smith described biopanning for affinity selection and demonstrated that recursive rounds of selection could enrich for clones present at 1 in a billion or less. [22] This technology was further developed and improved by groups at the Laboratory of Molecular Biology with Greg Winter and John McCafferty, The Scripps Research Institute with Lerner and Barbas and the German Cancer Research Center with Breitling and Dübel for the display of proteins such as antibodies for therapeutic protein engineering. Smith and Winter were awarded a half share of the 2018 Nobel Prize in chemistry for their contribution to developing phage display.

Phage display can also be applied to inorganic materials. Sandra R. Whaley, etc. used combinatorial phage-display libraries to evolve peptides that bind to a range of semiconductor surfaces with high specificity, depending on the crystallographic orientation and composition of the structurally similar materials they have used. As electronic devices contain structurally related materials in close proximity, such peptides

may find a use for the controlled placement and assembly of a variety of practically important materials, thus broadening the scope for `bottom-up' fabrication approaches. [23]

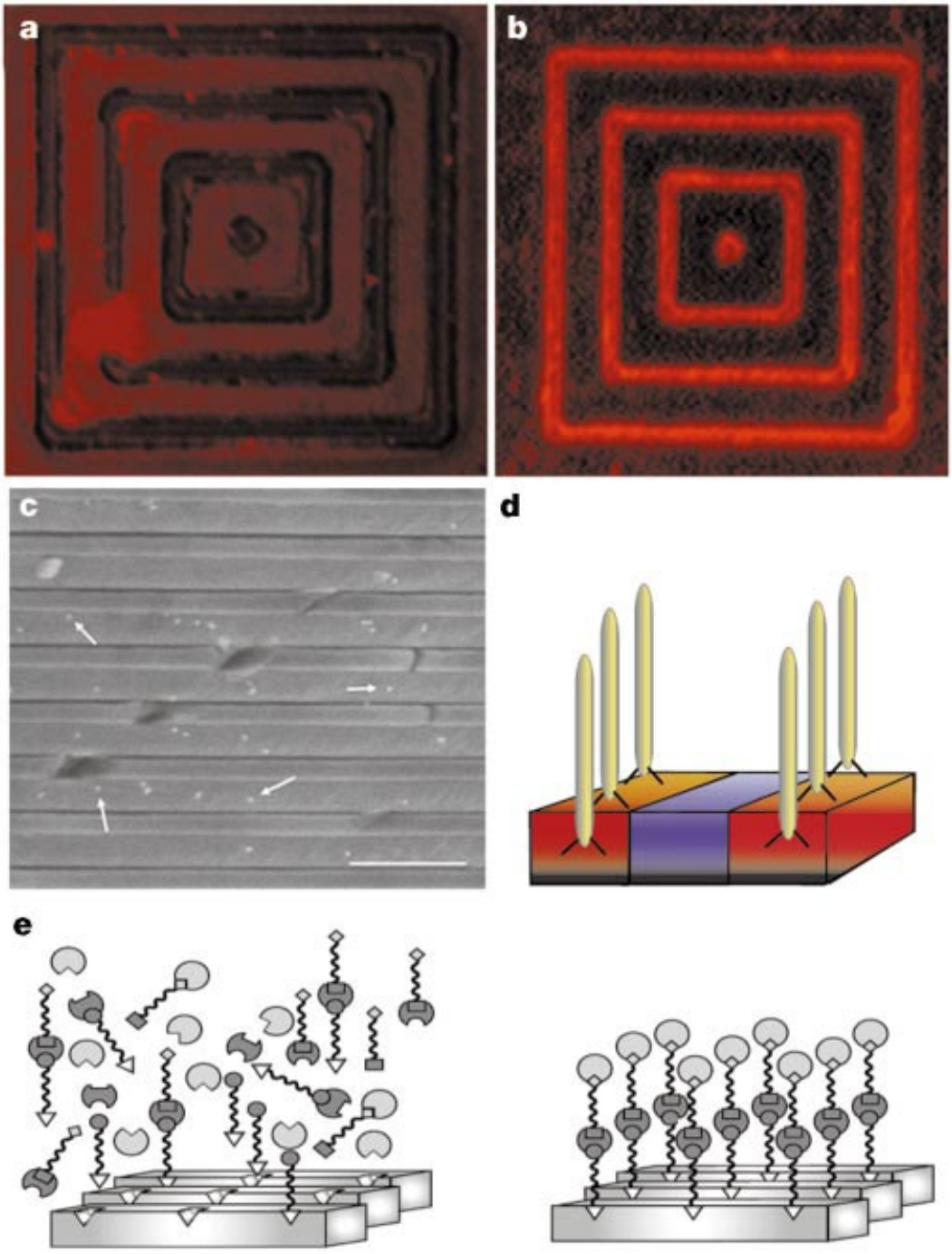

Figure 2-2. Phage recognition of semiconductor heterostructures. ***a-c****. Fluorescence images related to GaAs recognition by phage.* ***a****. Control experiment: no phage is present,*

but primary antibody and streptavidin-tetramethyl rhodamine (TMR) is present. ***b.*** *The GaAs clone G12-3 interacted with a substrate patterned with 1-mm GaAs lines and 4 μm SiO_2 spaces. The phage was then fluorescently labelled with TMR. The G12-3 clone specifically recognized the GaAs and not the SiO2 surface; scale bar, 4mm. A diagram of this recognition process is shown in d, in which phage specifically attach to one semiconductor rather than another, in a heterostructure.* ***c****. An SEM image of a heterostructure containing alternating layers of GaAs and $Al_{0.98}Ga_{0.02}As$, used to demonstrate that this recognition is element-specific. The cleaved surface interacted with G12-3 phage, and the phage was then tagged with 20 nm gold particles. These nanoparticles (shown arrowed in c) are located on GaAs and not AlGaAs layers. Scale bar, 500 nm.* ***e****, Diagram illustrating the use of this specificity to design nanoparticle heterostructures using proteins with multiple recognition sites. Reproduced from Ref. [23]*

Rajesh R. Naik, etc. reported silver-selected peptides in the phage display library. Moreover, they used these silver-binding peptides for *in vitro* biosynthesis of silver nanoparticles. [24]

		Isoelectric pH(pI)[a]
AG3	A Y S S G A P P M P P F	5.57
AG4	N P S S L F R Y L P S D	6.09
AG5	S L A T Q P P R T P P V	9.47
	● ● ● ★ ●	

[a] pI calculated using pI/Mass program at www.expasy.ch

Amino acids with functional side groups.
★ Amino acids conserved in all three sequences.
● Amino acids conserved in two of the sequences.

Figure 2-3. Amino acid sequences and properties of the silver-selected peptides. Reproduced from Ref. [24]

Seung-Wuk Lee, etc. found bacteriophage that was coupled with ZnS quantum dots and reported the fabrication of a highly ordered composite material from genetically engineered M13 bacteriophage and ZnS nanocrystals. The bacteriophage was coupled

with ZnS solution precursors and spontaneously evolved a self-supporting hybrid film material that was ordered at the nanoscale and the micrometer scale into ~72-micrometer domains, which were continuous over a centimeter length scale. [25]

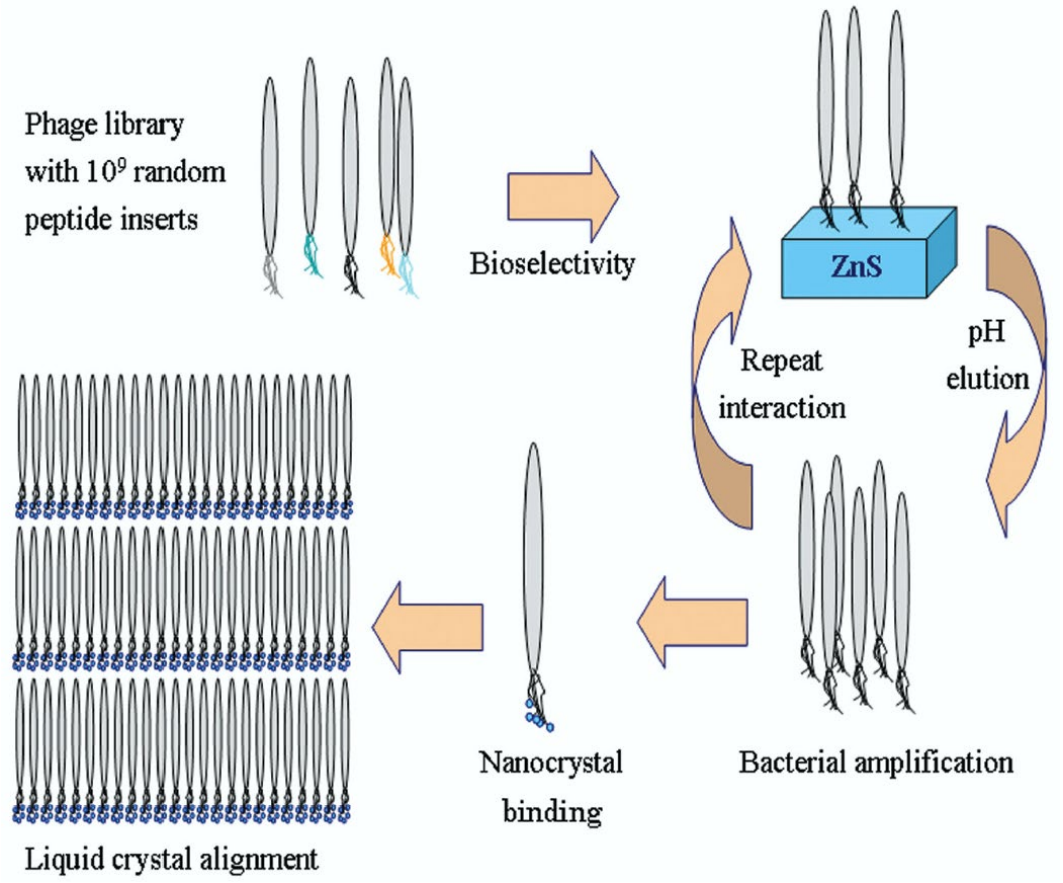

Figure 2-4. Schematic diagram of the process used to generate nanocrystal alignment by the phage display method. Reproduced from Ref. [25]

In this study, we want to select phage that has high binding affinity to UCNPs and use the phage-expressed protein to act as the ligand to modify on UCNPs surface.

2.3 Methods

2.3.1 Materials

2.3.1.1 Single-chain variable fragment (scFv) displayed phage library

NBF phage display library (National Biologics Facility, Creative Biolabs), a naive human scFv phagemid library, is used in this study. The library stock contains 1×10^{13} cfu/mL.

2.3.1.2 M13K07 helper phage

The helper phage is from *New England Biolabs* and amplified to 2.94×10^{13} cfu/mL.

2.3.1.3 *E.coli.* XL1-Blue Strain

The bacteria strain stocked as 50% glycerol culture is from *Stratagene*.

2.3.1.4 Media and buffer

All media and buffers were prepared using ultrapure water (Milli Q) with a resistance of 18 MΩ at 25 °C and stored at room temperature unless otherwise stated.

2YT Medium: 4 g of yeast extraction, 6.4 g of tryptone and 2 g of NaCl were dissolved in 400 mL of water. The 2YT medium was sterilized by autoclaving.

2YT Agar: 6 g of agar was dissolved in 400 mL 2YT medium. The solution was sterilized by autoclaving. Required antibiotics, at 1/1000 dilution, were added after medium had cooled such that the bottle was still quite warm but can be touched comfortably. Then the solution was poured into 100 mm and 150 mm plates and stored at 4 °C.

Antibiotic stock solutions: 100 mg of ampicillin (Sigma) was dissolved in 1 mL of water. 30 mg of kanamycin (Sigma) was dissolved in 1 mL of water. 3 mg of tetracycline (Sigma) was dissolved in 1 mL of water. All antibiotics were added to media at 1/1000 dilution. Antibiotics were stored in 0.5 mL aliquots at -20 °C.

Glucose-40%: 80 g of glucose (Sigma) was slowly added to 100 mL of water while stirring, then more distilled water was added to bring total volume to 200 mL. The glucose solution was sterilized by autoclaving.

Glycerol-50%: 100 mL pf glycerol (Sigma) was added to 100 mL of water while stirring. The glycerol solution was sterilized by autoclaving.

PBS buffer: Commercial PBS tablet (Sigma) was dissolved in water. The buffer was sterilized by autoclaving.

Elution buffer: 1.5 g of glycine (Sigma) was dissolved in 100 mL of water and the pH was adjusted to 2.5 using HCl. The solution was sterilized by autoclaving.

PEG-NaCl Solution: 40 g of polyethylene glycol-6000 (Sigma) and 29.2 g of NaCl were dissolved in 200 mL of water. The PEG-NaCl solution was sterilized by autoclaving.

2.3.2 Prepare naked UCNP

In this work, NaYF4, one of the most common used host structure of UCNPs, was used as the target to select phage clones with scFv expressed which shows binding affinity to it. NaYF4: Yb^{3+}, Er^{3+} nanocrystals (1%Er/20%Yb) was synthesized according to our previously reported method. In a typical experiment, 1 mmol $RECl_3 \cdot 6H_2O$ (RE = Y, Yb, Tm, 99.99%, Sigma 464317, 204870, 204668) with the desired molar ratio were added to a flask containing 6 mL OA (90%) and 15 mL ODE (90%). The mixture was heated to 160 °C under argon flow for 30 min to obtain a clear solution and then cooled down to about 50 °C, followed by the addition of 5 mL methanol (anhydrous) solution of NH_4F (4 mmol) and NaOH (2.5 mmol). After stirring for 30 min, the solution was heated to 150 °C under argon flow for 20 min to expel methanol, and then the solution was further heated to 310 °C for another 90 min. Finally, the reaction solution was cooled down to room temperature. The products were precipitated by ethanol and centrifuged (9000 rpm for 5 min), then washed 3 times with cyclohexane (anhydrous), ethanol (anhydrous) and methanol to get the nanoparticles.

To make phage can bind to the surface directly, acid washing was used to remove the surfactant resulted in naked UCNPs. The synthesized UCNPs were transferred into HCl (pH = 4) and treated with ultrasonic for 30 min. The UCNPs were washed 3 times with water to get the naked UCNPs. The naked UCNPs were stored in PBS buffer with good stability for further biological experiments.

2.3.3 Panning library of phage on naked UCNP

In this step, the library of purified phage will be exposed to a purified antigen in order to isolate a pool of phage particles which bind to the antigen of interest. Phage particles remaining after washing away non-binders will be harvested and used to infect bacteria.

This step is repeated 3-5 times to enrich the pool with specific binders to the antigen. In my project, the antigen is the naked UCNP.

Coat immunotube. After removing all the surfactants, the naked UCNPs were diluted to 10 mg/mL in PBS buffer. Then 1 mL of naked UCNPs solution was added to one immunotube and 1 mL of PBS buffer was added to each of two immunotubes as negative controls. After that, all the immunotubes were capped and rotated overnight at room temperature.

Prepare starter culture. In the same time, the starter culture was prepared. 5 mL 2YT-Tet with a single colony of XL1-Blue was inoculated and incubated overnight at 37 °C with shaking. And 5 mL 2YT-AmpKana with a single colony of XL1-Blue was inoculated and incubated under the same situation as a control.

Binding. After one night, all the immunotubes were washed three times with PBS buffer and then filled with Milk-PBS to block remaining binding sites on tubes. At the same time, library phage particles were blocked with 2mL Milk-PBS in 2 mL Eppendorf tube. All the immunotubes and Eppendorf tube were rotated at room temperature for 1 hour. Then for the first negative control immunotube, blocking solution was discarded and the blocked phage particles solution was transferred from the Eppendorf tube to this immunotube. The immunotube was rotated at room temperature for 45 minutes. Then for the second negative control immunotube, blocking solution was discarded and the phage particles solution was transferred from the first negative control immunotube to this immunotube, and the immunotube was rotated at room temperature for 45 minutes. Then blocking solution in the positive immunotube was discarded and the phage particles solution was transferred from second negative immunotube to the positive one. The immunotube was rotated at room temperature for 1 hour.

Elution of bound phage. After 1 hour, phage suspension was removed from the positive immunotube and the immunotube was washed three times with PBS-Tween solution and three times with PBS buffer. Then 1 mL 200 mM glycine (pH 2.5) was added to the immunotube and the immunotube was rotated at room temperature for 8 minutes to elute phage. After elution, eluate was transferred equally to two 2 mL tubes, each containing

500 µL 1 M Tris buffer (pH 7.4) and 500 µL 50% glycerol. One of them was added with 500 µL 50% glycerol and stored at -80 °C.

Infection. After elution, 10 µL aliquot of second tube of eluted phage was kept for calculating the concentration of the phage and the remainder was transfer to 10 mL XL1-Blue culture with optical density (OD) around 0.6. The infected culture was incubated at 37 °C without shaking for 30 minutes. Then the solution was centrifuged at 2000 × g for 10 minutes. The cell pellet was resuspended in 0.5 mL 2YT media and the solution was spread evenly onto two 150 mm 2YT-AmpGlu plates. They were incubated overnight at 30 °C.

Determine titre of eluted phage. Serial dilutions (10 µL + 90 µL PBS) of the 10 µL eluted phage sample were made to 10^{-4}. Then 1 µL of each dilutions was transferred to fresh tubes and added with100 µL of log-phase XL1-Blue cells. They were incubated at 37 °C without shaking for 30 minutes. After incubation, 20 µL of each culture was spread onto individual 2YT-AmpGlu plates and incubated overnight at 37 °C. After one night, colonies on the plates were recorded to calculate the output titre of the eluted phage.

Titre of phage (cfu/mL) = colonies × dilution factor × 100/20 × 1000 µL/mL ×2

Prepare glycerol stock. After one night, 5 mL 2YT with 20% glycerol was added to one of the 150 mm plates and the bacteria from the plate was scraped until all bacteria was detached from the plate. Then the slurry was transferred to the second plate and the bacteria from the second plate was scraped. All the slurry was transferred into 1.5 mL Eppendorf tubes with 1 mL in each and these glycerol stocks were stored at -80 °C.

Phage rescue. 100 µL of the glycerol stock was added into 50 mL 2YT-AmpGlu media in a 500 mL flask. It was incubated at 37 °C with shaking until OD increased to 0.5. Then the helper phage particles were added and incubated at 37 °C without shaking for 30 minute then with shaking for another 30 minutes. After incubation, the culture was centrifuged at 2000 × g for 10 minutes and the pellet resuspended in 100 mL 2YT-AmpKana in a 500 mL flask. It was incubated at 30 °C with shaking overnight. After one night, the culture was centrifuged at 3000 × g for 15 minutes and 80 mL of supernatant

was transferred equally into two 50 mL Falcon tubes. Then each tube was added with 8 mL PEG-NaCl solution and left on ice. After 1 hour, two tubes were centrifuged at 11000 × g 4 °C for 15 minutes. The phage pellets were resuspended in two tubes in 10 mL cold PBS and transferred into one tube. Then the tube was added with 2 mL PEG-NaCl solution and left on ice. After 1 hour, the tube was centrifuged at 11000 × g 4 °C for 15 minutes. Finally, the phage pellet was resuspended in 3 mL cold PBS-glycerol solution and stored at -80 °C. This phage glycerol stock can be used for subsequent rounds of panning and polyclonal phage ELISA.

Determine phage titre. Serial dilutions (10 µL + 90 µL PBS) of the 10 µL phage glycerol stock was made to 10^{-10}. For dilutions 10^{-7} to 10^{-10}, 1 µL of each was transferred to a fresh 1.5 mL tube and 100 µL log-phase XL1-Blue cells was added to each tube. They were incubated at 37 °C without shaking for 30 minutes. After incubation, 20 µL of each culture was spread onto individual 2YT-AmpGlu plates and incubated overnight at 37 °C. After one night, colonies on the plates were recorded to calculate the output titre of the eluted phage.

Titre of phage (cfu/mL) = colonies × dilution factor × 100/20 × 1000 µL/mL

2.3.4 Polyclonal phage ELISA

In this step, the pool of phage particles obtained after each round of panning is tested to determine if it is being enriched for binders to the antigen of interest. The ELISA involves immobilising antigen onto plates, followed by addition of various dilution of the phage pool from each round and then detection of bound phage using an anti-M13 phage antibody.

Coat plate. For one ELISA plate (Nunc Maxisorp), 200 µL of PBS buffer was added to each well of Column 1 and 200 µL of 10 mg/mL naked UCNP in PBS buffer was added to each well of Column 2-6. The plate was incubated overnight at room temperature.

Block plate and phage. After one night, the plate was washed three times with PBS buffer and added with 400 µL of Milk-PBS solution into each well to block the wells. In separate 2 mL tubes, 90 µL of phage particles from library, round 1, round 2 and round 3

was added to 1800 µL Milk-PBS solution to block all the phage particles. The plate and all the tubes were incubated at room temperature for 1 hour.

Add phage. After 1 hour, all the plate contents were discarded. Then 180 µL of Milk-PBS solution was added to each well of Column 3-5 and 200 µL of Milk-PBS solution was added to each well of Columns 6. And 200 µL of blocked phage particles was added into each well as below:

Library Phage: A1, B1, A2, B2

Round 1: C1, D1, C2, D2

Round 1: E1, F1, E2, F2

Round 3: G1, H1, G2, H2

Serially dilution at 1/10 (20 µL transferred) across the plate from Column 2 to Column 5 was made. Then the plate was incubated at room temperature for 1 hour.

Add anti-phage antibody. After 1 hour, the plate was washed three times with PBS-Tween solution. Then 200 µL of anti-M13 antibody with HRP (GE Healthcare 27-9421-01) diluted 1/5000 in Milk-PBS solution was added to each well and the plate was incubated at room temperature. After 1 hour, the plate was washed three times with PBS-Tween solution. Then 100 µL of TMB solution (Sigma) was added to each well and the plate was incubated at room temperature. After a blue colour developed and the discrimination between dilutions was being lost, 100 µL of 1M sulfuric acid (Sigma) was added to each well to strop the reaction. To read the signal, the absorption of 450 nm was measured using a microplate reader.

2.3.5 Monoclonal phage ELISA

In this step, individual clones are isolated from cell glycerol stocks after panning of a phage display library. This step involves growing single colonies from the cell glycerol stock, then growing many of these in a 96-well plate format. Helper phage is added to

induce production of phage particles. The phage particles from each clone is tested by phage ELISA for specific binding to the antigen-of-interest.

Grow individual colonies from glycerol stock. To grow the phage, 40 μL of glycerol stock was spread over a small section on the edge of a 150 mm 2YT-AmpGlu plate and incubated overnight at 37 °C.

Grow individual cultures from colonies. 150 μL of 2YT-AmpGlu media was added into each well of a 96-well round bottom plate (Nunc). Individual colonies was transferred from overnight culture plate into wells of Rows A-G of the plate and incubated at 37 °C overnight with shaking.

Induce phage production. 150 μL of 2YT-AmpGlu media was added into each well of a new 96-well round bottom plate. Then 5 μL of culture from corresponding wells of the overnight plate was added into the new plate and incubated at 37 °C for 3 hours with shaking. For the overnight plate, 60 μL 50% glycerol was added into each well and the plate was stored at -80 °C as the glycerol stock plate. Then 50 μL helper phage in 2YT media was added into each well of the new plate and incubated at 37 °C for 30 minutes without shaking and for another 30 minutes with shaking. Then the plate was centrifuged at 3200 × g for 10 minutes at room temperature and the pellet in each well was resuspended with 200 μL 2YT-AmpKana media and incubated overnight at 30 °C with shaking.

Prepare ELISA plate. 200 μL of naked UCNP at 5 mg/mL was added to all wells, except wells H1 to H6, of one ELISA plate and 200 μL PBS buffer was added to wells H1 to H6 as negative controls. The plate was incubated overnight at room temperature.

Phage ELISA. The overnight culture was centrifuged at 3200 × g at room temperature for 10 minutes and 150 μL of supernatant was transferred from each well to corresponding well of a new 96-well round bottom plate. 150 μL of Milk-PBS blocking solution was added to each well. The overnight ELISA plate was washed three times with PBS buffer and filled with 400 μL of Milk-PBS solution in each well. Both two plates were incubated at room temperature for 1 hour. Then the ELISA plate was emptied by inversion and filled with 100 μL of Milk-PBS solution in each well. 100 μL of blocked phage solution was

transferred from corresponding wells (Rows A-G) of the culture plate to the ELISA plate. Wells H1 to H6 were added with additional 100 µL of block phage solution from various random wells as no antigen controls. The ELISA plate was incubated at room temperature. After 1 hour, the plate was washed three times with PBS-Tween solution. Then 200 µL of anti-M13 antibody with HRP diluted 1/5000 in Milk-PBS solution was added into each well and incubated at room temperature. After 1 hour, the plate was washed three times with PBS-Tween solution. Then 100 µL of TMB solution to was added into each well and incubated at room temperature. After a blue colour developed and the discrimination between dilutions was being lost, 100 µL of 1M sulfuric acid was added into each well to strop the reaction. To read the signal, the absorption of 450 nm was measured using a microplate reader.

2.3.6 Sequencing of positive clones

In this step, clones are selected based on the monoclonal ELISA results, and the phagemid DNA from these clones is isolated and sequenced using primers flanking the scFv or Fab sequences. The number of unique clones can then be determined by sequence alignment.

Grow clones from glycerol stock phage. Each 150 mm 2YT-AmpGlu plate was divided into 8 even segments using a marker pen and all the segments were labelled with individual clone designations. Glycerol stock plate (mentioned in 2.3.1.4 Monoclonal phage ELISA ->Induce phage production step) was removed from -80 °C freezer and the wells which show higher binding affinity in the monoclonal ELISA test were selected. The surface of selected wells was scraped using a small inoculation loop and spread onto corresponding segments of the plate. The plate was incubated at 37 °C overnight.

Expand cultures. Single colony from each clone was picked and inoculated into 5 mL 2YT-AmpGlu media. They were incubated at 37 °C overnight with shaking.

Extract phagemid DNA. DNA from 2 mL of overnight culture was extracted using commercial plasmid DNA extraction kit (Qiagen QiaPrep Mini Prep Kit) and the DNA concentration was determined by measuring the absorption of 260 nm.

Sequencing. Each reaction was set up in a 1.5 mL Eppendorf tube. For scFv library which was used in this work, two reactions were set up for each clone, one with pHEN_For primer and one with pHEN_Rev primer. 1 μL of primer and 200 ng DNA was added into one tube and the tube was filled with water to a final volume of 12 μL. All the samples were submitted to Australia Genome Research Facility (AGRF) for sequencing.

Sequence analysis. Contig sequence for each clone was determined using forward and reverse data. The forward and reverse data should overlap. Then each contig was translated in six frames and determine the correct reading frame by searching for conserved sequences.

2.4 Results and discussions

In this study, $NaYF_4$, one of the most common used host structure of UCNPs, was used as the target to select phage clones with single-chain variable fragment (scFv) expressed which shows binding affinity to it. As we introduced, the synthesized UCNPs are coated with oleic acid blocking the $NaYF_4$. To make phage can bind to the surface directly, acid washing was used to remove the surfactant resulted in naked UCNPs.

After acid washing, the TEM images shown in Figure 2.5 confirmed the surface morphology didn't change.

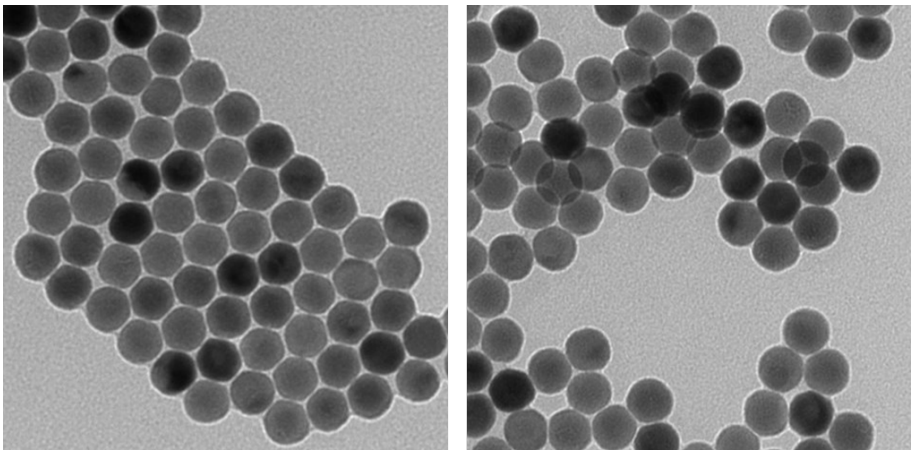

Figure 2.5 TEM images of OA coated UCNPs (left) and naked UCNPs (right).

The washed UCNPs showed a high positive surface potential (zeta potential value = 45.1) that fitted the exposure of RE^{3+}.

Begin with the library of phage, three rounds of panning were performed on naked UCNPs. After each round of panning, the concentration of eluted phage was calculated to make the same contribution of the phage amount for the next round. The output titres of eluted phage for each round are shown in Table 2-1.

Table 2-1. Phage concentration

	Concentration of eluted phage (cfu/mL)	Concentration of phage stock (cfu/mL)
Round 1	2.71×10^7	7.8×10^{12}
Round 2	8×10^5	8.9×10^{13}
Round 3	3×10^5	5.51×10^{13}

The decreasing concentration of the eluted phage indicated that the targeted phages were getting enriched after each panning. And the concentration of phage stocks was all over 10^{13} cfu/mL. This indicated that the eluted phage amplification step using XL-1 blue strain bacterial was successful.

To evaluate the properties of phage clones from different rounds in binding affinity to naked UCNPs, polyclonal phage enzyme linked immunosorbent assay (ELISA) was tested. Column 1 is negative control for no antigen coated and column 6 is negative control for no phage added.

Table 2-2. Polyclonal ELISA

	1	2	3	4	5	6
A	Library phage	UCNP + Lib phage	UCNP + 1/10 Lib phage	UCNP + 1/100 Lib phage	UCNP + 1/1000 Lib phage	UCNP
B						
C	Round 1 phage	UCNP + R1 phage	UCNP + 1/10 R1 phage	UCNP + 1/100 R1 phage	UCNP + 1/1000 R1 phage	UCNP
D						
E	Round 2 phage	UCNP + R2 phage	UCNP + 1/10 R2 phage	UCNP + 1/100 R2 phage	UCNP + 1/1000 R2 phage	UCNP
F						
G	Round 3 phage	UCNP + R3 phage	UCNP + 1/10 R3 phage	UCNP + 1/100 R3 phage	UCNP + 1/1000 R3 phage	UCNP
H						

In the ELISA test, anti-M13 antibody, which was used to detect phages bond to the naked UCNPs, is labelled with horseradish peroxide (HRP). HRP can catalyze the oxidation reaction of 3,3',5,5'-Tetramethylbenzidine (TMB). The resulting diamine causes the solution to take on a blue colour and the reaction can be halted by addition of acid. Using sulphuric acid turns the blue solution to yellow. A deeper yellow means more phages. So that we can read the signal by measuring absorption at 450 nm.

However no significant differences between each round and different concentrations of phage were overserved. So further three rounds were did and the concentration of phage in these round is shown in Table 2-3.

Table 2-3. Phage concentration

	Concentration of eluted phage (cfu/mL)	Concentration of phage stock (cfu/mL)
Round 4	3×10^5	5.09×10^{13}
Round 5	Too low to detect	4.88×10^{13}
Round 6	Too low to detect	1.7×10^{14}

The polyclonal phage ELISA was tested again to evaluate the binding affinity of phage clones from these new rounds. But there was still no significant signal showed in the ELISA result.

For these results, we thought that because of the high surface positive potential of UCNPs, many different kinds of phages would bind to the UCNPs surface and were not easily eluted in the elution step. As a result, the eluted phage stocks from different rounds consisted of too many different phages that all have binding affinity to the target so that no significant differences were observed in these ELISA tests.

So the monoclonal ELISA was test to compare the binding affinity between these different kinds of phages in the phage stock we have selected for several rounds. In the monoclonal ELISA test, 240 different colonies from the culture plate were selected to be test for the binding affinity to the target, naked UCNPs.

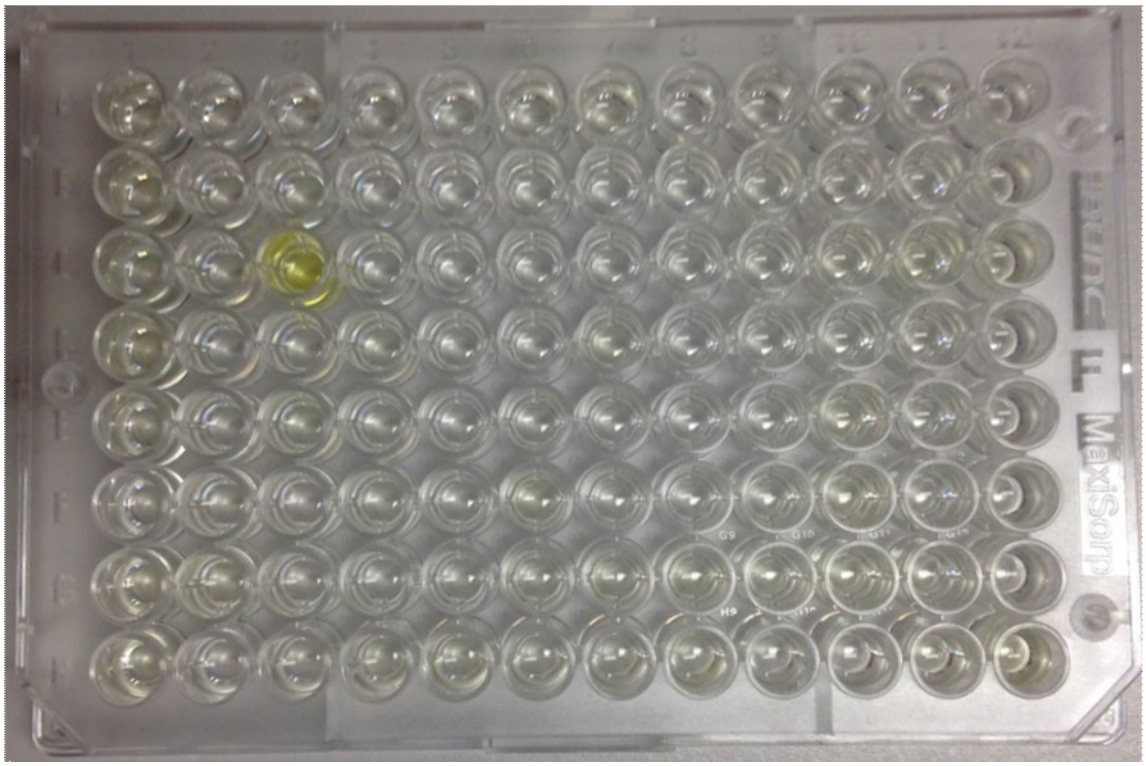

Figure 2-6. One monoclonal ELISA test for 84 different colonies.

Two colonies (C3, D1) that had higher signals in the monoclonal ELISA test were selected and confirmed again by the ELISA test.

Figure 2-7. ELISA results of the two selected phage C3 and D1.

The phagemid DNA of these two colonies was extracted and the concentration of the DNA is tested by measuring the absorption of 260 nm (Table 2-4).

Table 2-4. Concentration of phagemid DNA

	Concentration of phagemid DNA (ng/μL)			
	1	2	3	Average
C3	85.1	84.2	84.1	84.5
D1	152.3	151.2	151.7	151.7

For the DNA sequencing, at least 200 ng of NDA was needed, so different volumes of DNA extract solution of these two colonies were added in the tube (Table 2-5).

Table 2-5. DNA sequencing sample preparation.

Volume added (μL)	C3	D1
DNA	2.4	1.3
Primer	0.5	0.2
H_2O	9.1	10.2
Total	12	12

The DNA sequencing is tested by AGRF. After analysis and translation, the amino acids sequences of the two selected phages are shown in Figure 2-8.

- MAQVTLRESGPALVKPTQTLTLTCTFSGFSLSTSGVGVGWIRQPPGKALEWLALIYW
  NDDKRYSPSLKSRLTITKDTSKNQVVLTMTNMDPVDTATYYCAHVPPGYRRLAVEYF
  DYWGQGTLVTVSSGGGGSGGGGSGGGASDIQLTQSPSSSASVGDRVTISCRAS
  QPISMYLNWFQQKPGKAPKLLIYAASALQDGVPSRFSGSGSGTDFTLVISSLHPDDF
  ATYYCQQTHSDPRTFSQGTKLESNVRPHIIITIMVQQNRN

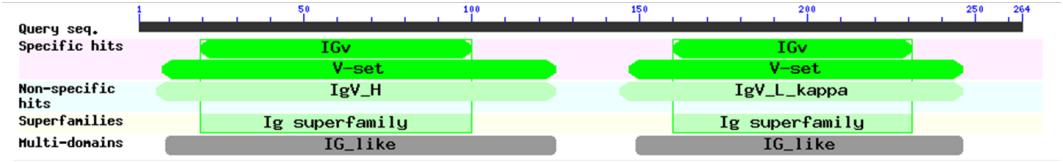

- MAQVQLQESGPGLVKPSQTLSLTCTVSGGSITSGGYYWSWIRQHPGKGLEWIGYI
  YYSGSTYYNPSLKSRVTISVDTSKNQFSLKLSSVTAADTAVYYCARDLVLPYCSSTSCY
  YYYGMDVWGQGTTVTVSSGGGGSRGGGSGGGASQAVVTQPPAASGTPGQ
  RVSIFCSGSSSNVEINNVYWYQQFPGAAPKLLIYRNNQRPSGVPDRFSASKSGTSAS
  LAISGLRSEDEADYYCATWDDKVNEMLFGGGTKVTVLGAAAHHHHHHGAAEQK
  LISEEDLNGAA

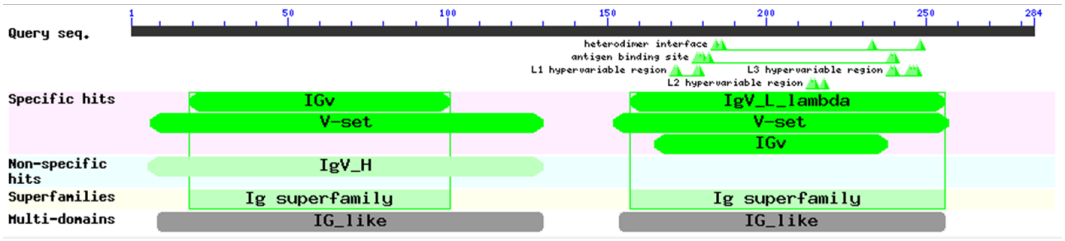

Figure 2-8. Amino acids sequences and structures of the scFv fragments from the two selected phage.

2.5 Conclusion and further works

From NBF phage display library, we have selected two phage colonies that have higher binding affinity to UCNPs surface. The DNA sequences and protein structures of these two scFv fragments are also analysed.

To finish our aim that explore new UCNPs surface modification strategy, we still need to finish some further works. The sequences of two selected phage have been analysed and we will use protein engineering technology to produce the scFv fragments. And then these scFv fragments can be used to modify UCNPs surface by ligand exchange method. Further characterization experiments can be done to check the performance of the new ligands.

Reference

[1] J. Zhao, Z. Lu, Y. Yin, C. McRae, J. A. Piper, J. M. Dawes, D. Jin, and E. M. Goldys, "Upconversion luminescence with tunable lifetime in $NaYF_4$:Yb,Er nanocrystals: role of nanocrystal size," *Nanoscale*, vol. 5, no. 3, pp. 944–952, 2013.

[2] J. Zhao, D. Jin, E. P. Schartner, Y. Lu, Y. Liu, A. V Zvyagin, L. Zhang, J. M. Dawes, P. Xi, J. A. Piper, E. M. Goldys, and T. M. Monro, "Single-nanocrystal sensitivity achieved by enhanced upconversion luminescence," *Nat. Nanotechnol.*, vol. 8, p. 729, Sep. 2013.

[3] D. Liu, X. Xu, Y. Du, X. Qin, Y. Zhang, C. Ma, S. Wen, W. Ren, E. M. Goldys, J. A. Piper, S. Dou, X. Liu, and D. Jin, "Three-dimensional controlled growth of monodisperse sub-50 nm heterogeneous nanocrystals," *Nat. Commun.*, vol. 7, p. 10254, Jan. 2016.

[4] Y. Zhang, L. Zhang, R. Deng, J. Tian, Y. Zong, D. Jin, and X. Liu, "Multicolor barcoding in a single upconversion crystal," *J. Am. Chem. Soc.*, vol. 136, no. 13, pp. 4893–4896, 2014.

[5] G. Zhao, L. Tong, P. Cao, M. Nitz, and M. A. Winnik, "Functional PEG-PAMAM-tetraphosphonate capped NaLnF4 nanoparticles and their colloidal stability in phosphate buffer," *Langmuir*, vol. 30, no. 23, pp. 6980–6989, 2014.

[6] Y. Shi, B. Shi, A. V. E. Dass, Y. Lu, N. Sayyadi, L. Kautto, R. D. Willows, R. Chung, J. Piper, H. Nevalainen, B. Walsh, D. Jin, and N. H. Packer, "Stable Upconversion Nanohybrid Particles for Specific Prostate Cancer Cell Immunodetection," *Sci. Rep.*, vol. 6, p. 37533, Nov. 2016.

[7] H.-J. Jang, C. Y. Shin, and K.-B. Kim, "Safety Evaluation of Polyethylene Glycol (PEG) Compounds for Cosmetic Use," *Toxicol. Res.*, vol. 31, no. 2, pp. 105–136, Jun. 2015.

[8] R. H. Fang, C.-M. J. Hu, B. T. Luk, W. Gao, J. A. Copp, Y. Tai, D. E. O'Connor, and L. Zhang, "Cancer Cell Membrane-Coated Nanoparticles for Anticancer

Vaccination and Drug Delivery," *Nano Lett.*, vol. 14, no. 4, pp. 2181–2188, Apr. 2014.

[9] J. Lu, Y. Chen, D. Liu, W. Ren, Y. Lu, Y. Shi, J. Piper, I. Paulsen, and D. Jin, "One-Step Protein Conjugation to Upconversion Nanoparticles," *Anal. Chem.*, vol. 87, no. 20, pp. 10406–10413, 2015.

[10] L. Le Li, P. Wu, K. Hwang, and Y. Lu, "An exceptionally simple strategy for DNA-functionalized Up-conversion nanoparticles as biocompatible agents for nanoassembly, DNA delivery, and imaging," *J. Am. Chem. Soc.*, vol. 135, no. 7, pp. 2411–2414, 2013.

[11] Y. Aoki, T. Uenaka, J. Aoki, M. Umeda, and K. Inoue, "A novel peptide probe for studying the transbilayer movement of phosphatidylethanolamine," *J. Biochem.*, vol. 116, no. 2, pp. 291–297, 1994.

[12] E. M. Barnett, X. U. Zhang, D. Maxwell, Q. Chang, and D. Piwnica-Worms, "Single-cell imaging of retinal ganglion cell apoptosis with a cell-penetrating, activatable peptide probe in an in vivo glaucoma model," *Proc. Natl. Acad. Sci.*, vol. 106, no. 23, pp. 9391–9396, 2009.

[13] J. E. Dover, G. M. Hwang, E. H. Mullen, B. C. Prorok, and S.-J. Suh, "Recent advances in peptide probe-based biosensors for detection of infectious agents," *J. Microbiol. Methods*, vol. 78, no. 1, pp. 10–19, 2009.

[14] Wikipedia, "Phage display." [Online]. Available: https://en.wikipedia.org/wiki/Phage_display. [Accessed: 01-Jun-2019].

[15] S. Ghoshal, V. Bondada, K. E. Saatman, R. P. Guttmann, and J. W. Geddes, "Phage display for identification of serum biomarkers of traumatic brain injury," *J. Neurosci. Methods*, vol. 272, pp. 33–37, 2016.

[16] R. M. A. El-Magd, N. F. Vozza, J. A. Tuszynski, and D. S. Wishart, "Isolation of soluble scFv antibody fragments specific for small biomarker molecule, L-Carnitine, using phage display," *J. Immunol. Methods*, vol. 428, pp. 9–19, 2016.

[17] K. Omidfar and M. Daneshpour, “Advances in phage display technology for drug discovery,” *Expert Opin. Drug Discov.*, vol. 10, no. 6, pp. 651–669, 2015.

[18] A. Munke, J. Persson, T. Weiffert, E. De Genst, G. Meisl, P. Arosio, A. Carnerup, C. M. Dobson, M. Vendruscolo, and T. P. J. Knowles, “Phage display and kinetic selection of antibodies that specifically inhibit amyloid self-replication,” *Proc. Natl. Acad. Sci.*, vol. 114, no. 25, pp. 6444–6449, 2017.

[19] G. Winter, A. D. Griffiths, R. E. Hawkins, and H. R. Hoogenboom, “Making antibodies by phage display technology,” *Annu. Rev. Immunol.*, vol. 12, no. 1, pp. 433–455, 1994.

[20] G. P. Smith, “Filamentous fusion phage: novel expression vectors that display cloned antigens on the virion surface,” *Science (80-.).*, vol. 228, no. 4705, pp. 1315–1317, 1985.

[21] G. Pieczenik, “Method of inserting unique DNA sequences into DNA vectors.” Google Patents, 09-Jul-1985.

[22] S. F. Parmley and G. P. Smith, “Antibody-selectable filamentous fd phage vectors: affinity purification of target genes,” *Gene*, vol. 73, no. 2, pp. 305–318, 1988.

[23] S. R. Whaley, D. S. English, E. L. Hu, P. F. Barbara, and A. M. Belcher, “Selection of peptides with semiconductor binding specificity for directed nanocrystal assembly,” *Nature*, vol. 405, no. 6787, p. 665, 2000.

[24] R. R. Naik, S. J. Stringer, G. Agarwal, S. E. Jones, and M. O. Stone, “Biomimetic synthesis and patterning of silver nanoparticles,” *Nat. Mater.*, vol. 1, no. 3, p. 169, 2002.

[25] S.-W. Lee, C. Mao, C. E. Flynn, and A. M. Belcher, “Ordering of quantum dots using genetically engineered viruses,” *Science (80-.).*, vol. 296, no. 5569, pp. 892–895, 2002.

Chapter 3 Bispecific Antibody Functionalized Upconversion Nanoprobe

Hao He, Christopher B. Howard, Yinghui Chen, Shihui Wen, Gungun Lin, Jiajia Zhou, Kristofer J. Thurecht, and Dayong Jin

Analytical Chemistry, **2018**, 90, 3024-3029
DOI: 10.1021/acs.analchem.7b05341

Contributions:

Planning of experiments, modification of UCNPs, characterization of upconversion nanoprobe by spectrometer, Nanodrop, DLS, ELISA-like assay, cell labelling, data processing, manuscript writing.

3.1 Motivation

After transferring upconversion nanoparticles (UCNPs) from hydrophobic to hydrophilic and modifying with functional groups, suitable bioconjugation method is needed to conjugate UCNPs with biomolecules. However, conventional approaches are not only time-consuming, but also less efficient in keeping the antibodies active and maintaining correct presentation to analytes.

In this chapter in a format of a published paper, we report a new bioconjugation strategy for UCNPs by using bispecific antibody.

3.2 Manuscript

3.2.1 Abstract

Upconversion nanoparticles (UCNPs) are new optical probes for biological applications. To realize specific biomolecular recognition for diagnosis and imaging, the key lies in developing a stable and easy-to-use bioconjugation method for antibody modification. Current methods are not yet satisfactory regarding conjugation time, stability, and binding efficiency. Here we report a facile and high-yield approach based on a bispecific antibody (BsAb), free of chemical reaction steps. One end of the BsAb is designed to recognize methoxy polyethylene glycol (mPEG) coated UCNPs, and the other end of the BsAb is to recognize the cancer antigen biomarker. Through simple vortexing, BsAb-UCNP nanoprobes form within 30 min and show higher (up to 54%) association to the target than the traditional UCNP nanoprobes in the ELISA-like assay. We further demonstrate its successful binding to the cancer cells with high efficiency and specificity for background-free fluorescence imaging under near-infrared excitation. This method suggests a general approach broadly suitable for functionalizing a range of nanoparticles to specifically target biomolecules.

3.2.2 Introduction

Photon upconversion is an anti-Stokes process, in which sequential absorption of two or more photons results in the emission of light at a shorter wavelength than the excitation wavelength. Upconversion nanoparticles (UCNPs), one kind of luminescent

nanomaterials that utilize such an anti-Stokes process, have attracted tremendous interest in recent years[1], [2]. UCNPs can be designed to absorb near-infrared (NIR) excitation photons and emit tunable shorter-wavelength luminescence from the deep-UV to the NIR range by controlling the doped sensitizers and activators[3], [4]. They are exceptionally photostable and low toxic, making them attractive over traditional organic dyes and quantum dots as fluorescent probes for single molecule tracking[5], deep-tissue optical imaging[6]–[8], early disease diagnosis[9], [10] and cell-targeted imaging[11], [12].

A variety of immunoassays and imaging applications rely on specific and stable binding of fluorescent nanoparticles to antibodies, which accordingly require surface functionalization of the nanoparticles with antibodies[13], [14]. Despite the great potential of UCNPs, up to date, the facile and efficient conjugation of antibodies to UCNPs remains the critical bottleneck for its widespread applications in biological and biomedical fields[15].

A primary reason is that UCNPs are typically synthesized in a nonpolar solvent, and they are capped with hydrophobic surfactant molecules, such as oleic acid (OA)[16]. At least two steps are needed to conjugate antibodies to the surface of UCNPs, including first transferring UCNPs from hydrophobic to hydrophilic, followed by conjugating hydrophilic UCNPs with antibodies[15]. Ligand exchange is an universal way to functionalize the surface of UCNPs with hydrophilic and active groups, such as carboxyl or amino moiety[12], [17]. After that, carbodiimide chemistry, such as EDC method, is generally used to further conjugate antibodies to these active groups, but this approach is not only time-consuming, but it is less efficient in keeping the antibodies active and maintaining correct presentation to antigens on cell surfaces. This is because the chemical conjugation is not site-specific and often leads to blocking of the antibody binding area[18].

Here we report for the first time bispecific antibody (BsAb) as both linker and binder for efficient conjugation of antibodies to UCNPs. BsAbs are artificial antibodies containing two different binding sites with specificity to two different targets[19]. In this work, we produce BsAbs through a recombinant DNA technology, for which a DNA sequence is designed to generate BsAbs with two active domains linked by a G4s linker, one domain

recognizing methoxy polyethylene glycol molecules (mPEG) and the other capturing cancer cell surface antigen EphA2. This design allows direct conjugation of BsAbs with mPEG coated UCNPs in 30 min with a high bioconjugation yield, free of chemical reaction steps. We further demonstrate that BsAb conjugated UCNPs can increase the binding signal to EphA2 biomarker and enhance specific binding to prostate cancer cells, unveiling its enormous potential for cancer diagnosis and cell imaging.

3.2.3 Experiments and materials

3.2.3.1 Materials

$YCl_3 \cdot 6H_2O$ (99.99%), $TmCl_3 \cdot 6H_2O$ (99.99%), NaOH (99.9%), NH_4F (99.99%), oleic acid (OA, 90%), 1-octadecene (ODE, 90%), tetrahydrofuran (THF, anhydrous, ≥99.9%, inhibitor-free), hexane (anhydrous, 95%), N-(3-Dimethylaminopropyl)-N′-ethylcarbodiimide hydrochloride (EDC, BioXtra), 2-(N-Morpholino)ethanesulfonic acid hydrate (MES, 99.5%), H_2SO_4 (95%), Tween 20, Ephrin type-A receptor 2 (EphA2) and anti-EphA2 antibody (IgG, produced in rabbit), are purchased from Sigma-Aldrich and used as received without further purification. Methoxy polyethylene glycol modified with phosphate group on one end (mPEG, Mw 3500) and polyethylene glycol modified with a carboxy group and a phosphate group on each end (cPEG, Mw 3500) are purchased from JenKem Technology, USA. Roswell Park Memorial Institute 1640 Medium (RPMI 1640 medium, GlutaMAX^{TM} supplement), Fetal Bovine Serum (FBS, certified, US origin) and cell dissociation buffer (enzyme-free, PBS) are purchased from ThermoFisher.

3.2.3.2 Synthesis of UCNPs.

$NaYF_4$: 20%Yb^{3+}/4%Tm^{3+} UCNPs with a size of 22 nm are prepared using our previous reported method[3]. 5 mL of a methanol solution of $RECl_3$ (2.0 mmol, RE = Y, Yb, Tm) is magnetically mixed with 12 mL of oleic acid and 30 mL of 1-octadecene in a 100 mL three-neck round-bottom flask. The mixture is degassed under an Ar flow and heated to 150 °C for 30 min to form a clear solution and then cooled to room temperature. 15 mL methanol solution containing 0.296 g of NH_4F and 0.2 g of NaOH is added and stirred for 60 min. The solution is slowly heated to 150 °C and then held at this temperature for a further 30 min to completely remove methanol and some water. The reaction mixture is

then quickly heated to 310 °C and aged for 1.5 h. After the solution is cooled, absolute ethanol is added to precipitate the UCNPs. After centrifuge, the precipitate is washed with cyclohexane, ethanol, and methanol four times. The washed UCNPs are redispersed in cyclohexane and stored for further experiments.

3.2.3.3 Preparation of BsAb.

The BsAb fragment consists of a single chain variable region (scFv) specific for mPEG linked to a variable region specific for EphA2, a receptor overexpressed in cancer cells. Both scFvs are linked by a glycine serine (G4s) linker. A c-myc tag is added for purification and ELISA tests. Genes encoding BsAb fragment which bind to mPEG and EphA2 are synthesized by Geneart and the gene sequence is attached in SI 3. Genes are transfected into CHO cells for expression. The BsAb production and purification were performed as outlined in our previous work[20]. These sequence information of the BsAb used in this work is show below.

a. Gene sequence

>4B3_G4S_PEG15-2

AAGCTTGCCACCATGGGCTGGTCCTGCATCATCCTGTTTCTGGTGGCTACCGC
CACCGGCGTGCACTCCCACCACCATCACCATCACGAGGTGCAGGTGCAGCA
GTCCGGACCCGAGCTCGTGAAACCTGGCGCCTCCGTGAAGATCTCCTGCAA
GGCCTCCGGCTACACCTTCACCGACTACGACATGAACTGGATGAAGCAGTCC
CACGGCAAGTCCCTGGAATGGATCGGCGACATCAACCCCAACAACGGCGGA
GCCTCCTACAACCAGAAGTTCCGGGGCAAGGCCACCCTGACCGTGGACAAG
TCCTCCTCCACCGCCTACATGGAACTGCGGTCCCTGACCTCCGAGGACAGCG
CCGTGTACTACTGCGCCAGACGGTCCACCATGACCTACTTCGACTACTGGGG
CCAGGGCACCACACTGACAGTGTCTAGCGGAGGCGGAGGATCTGGTGGTGG
TGGATCTGGCGGAGGGGGCTCTCAGATCGTGCTGACCCAGTCCCCTGCCATC
ATGTCTGCTAGCCCTGGCGAGAAAGTGACAATCTCCTGCTCCGCCAGCTCCT
CCGTGTCCTACATGTACTGGTATCAGCAGAAGCCCGGCTCCAGCCCCAAGCC
CTGGATCTACAGAACCTCCAACCTGGCCTCTGGCGTGCCCGCTAGATTCTCC
GGCTCTGGCTCTGGCACCTCCTACTCCCTGACCATCTCCACCATGGAAGCCG

AGGACGCCGCCACCTACTACTGCCAGCAGTACCACTCCTACCCTCTGACCTT
CGGCGCTGGCACCAAGCTGGAACTGAAGTCTGGTGGCGGAGGCAGCGAAGT
GAAGCTGGAAGAATCCGGCGGAGGCCTGGTGCAGCCTGGCGGATCTATGAA
GCTGTCCTGTGTGGCCAGCGGCTTCACCTTCTCTAACTATTGGATGAACTGGG
TGCGACAGTCCCCCGAGAAGGGACTGGAATGGGTCACCGAGATCCGGTCCA
AGTCCAACAACTACGCCACCCACTACGCCGAGTCCGTGAAGGGCCGGTTCA
CCATCTCTCGGGACGACTCCAAGGGCTCCGTGTACCTGCAGATGAACAACCT
GCGGGCCGAGGACACCGGCATCTATTATTGCTCCAACCGGTATTATTGGGGGC
AGGGAACCCTCGTGACCGTGTCTGCTGGGGGAGGCGGTAGTGGCGGCGGAG
GAAGTGGGGGAGGGGGATCTGACATTGTGATGACACAGTCCCACAAGTTCAT
GAGCACCTCCGTGCGGGACAGAGTGACCATCACATGCAAGGCCAGCCAGGA
CGTGAACACCAGCGTGGCATGGTATCAGCAGAAACCTGGCCAGTCCCCCAA
GCTCGTGATCTACTGGGCCTCTACCCGGCACACAGGCGTGCCAGATCGGTTC
ACCGGATCTGGCAGCGGCACCGACTTCACCCTGACAATCAGCAACGTGCAG
TCCGAGGACCTGGCCGACTACTTCTGTCTGCAATATATCAACTACCCTTACAC
CTTCGGAGGCGGGACAAAGCTGGAAATCAAAGAGCAGAAGCTGATCTCCGA
AGAGGACCTGAACTGAGCGGCCGC

b. Protein sequence

>4B3_G4S_PEG15-2

MGWSCIILFLVATATGVHSHHHHHHEVQVQQSGPELVKPGASVKISCKASGYTF
TDYDMNWMKQSHGKSLEWIGDINPNNGGASYNQKFRGKATLTVDKSSSTAYM
ELRSLTSEDSAVYYCARRSTMTYFDYWGQGTTLTVSSGGGGSGGGGSGGGGSQ
IVLTQSPAIMSASPGEKVTISCSASSSVSYMYWYQQKPGSSPKPWIYRTSNLASG
VPARFSGSGSGTSYSLTISTMEAEDAATYYCQQYHSYPLTFGAGTKLELKSGGG
GSEVKLEESGGGLVQPGGSMKLSCVASGFTFSNYWMNWVRQSPEKGLEWVTEI
RSKSNNYATHYAESVKGRFTISRDDSKGSVYLQMNNLRAEDTGIYYCSNRYYW
GQGTLVTVSAGGGGSGGGGSGGGGSDIVMTQSHKFMSTSVRDRVTITCKASQD
VNTSVAWYQQKPGQSPKLVIYWASTRHTGVPDRFTGSGSGTDFTLTISNVQSED
LADYFCLQYINYPYTFGGGTKLEIKEQKLISEEDLN*

3.2.3.4 Preparation of mPEG coated UCNPs and cPEG coated UCNPs.

To convert OA capped UCNPs to mPEG or cPEG (polyethylene glycol modified with a carboxy group) coated ones, ligand exchange method is used. 1.5 mL of 20 mg/mL UCNPs in cyclohexane are precipitated with ethanol. After centrifuge and discarding the solution, UCNPs are redispersed in 3 mL of THF with vortex and sonication. Then 1.5 mL of 200 mg mPEG or cPEG in THF solution is added. The mixed solution is stirred at room temperature for 24 h. After that, 3 mL of MiliQ water is added and mixed with shaking. Then the solution is extracted with 1 mL of hexane to remove the OA molecules. After removing the oil phase, the solution is put in vacuo overnight to evaporate organic solvents. Then the solution is dialyzed in 1 L of MiliQ water for 24 h to remove the excessive PEG molecules.

3.2.3.5 Bioconjugation of BsAb to mPEG-UCNPs.

After the converting step, the mPEG-UCNPs are changed into MES buffer (pH 6.8) using a centrifuge method at a final concentration of 1 mg/mL. Then 10 μL of mPEG-UCNPs and 10 μL of 0.5 mg/mL of BsAb are mixed in 80 μL of MES buffer and the solution is incubated under 37 °C with vortex for 30 min. After washing with MES buffer twice (centrifuge at 14,000 rpm for 20 min), the final settlement of conjugates is dissolved in 100 μL of MES buffer with sonication for 5 s.

The reaction time of 30 min is determined by testing the concentration of BsAb in the conjugates under different reaction time (Figure 3-1).

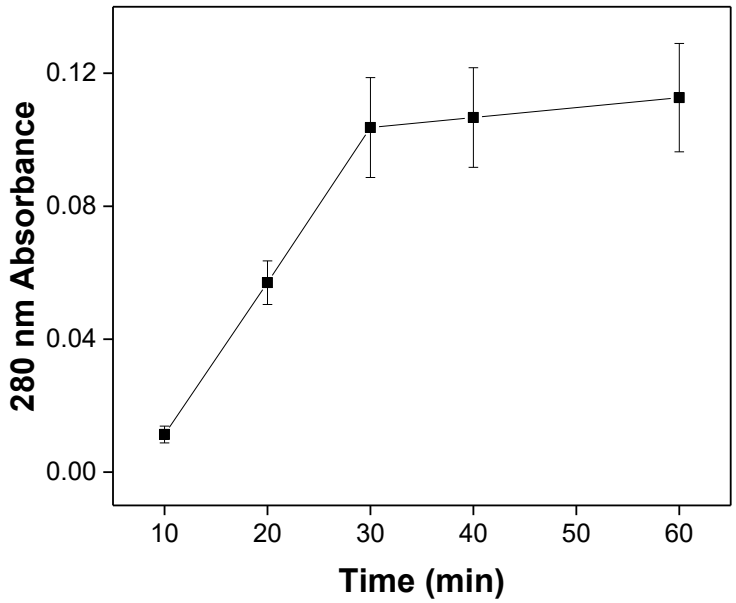

Figure 3-1. 280 nm absorbance intensity of BsAb-UCNP nanoprobe under different reaction time.

3.2.3.6 Optical Characterization.

The mPEG-UCNPs and BsAb-UCNPs are separately diluted at a concentration of 10 μg/mL in MES buffer and tested for the emission spectra using a Horiba550 spectrometer and the absorption spectra using a Nanodrop2000.

3.2.3.7 Indirect ELISA.

The binding between BsAbs and mPEG-UCNPs is evaluated by indirect ELISA methods using mPEG-UCNPs immobilized on ELISA plates.

Individual wells of a 96-well plate (Nunc) are coated with 100 μL of 50 μg/mL of mPEG-UCNPs or without mPEG-UCNPs as negative controls overnight at room temperature. After discarding all the solution in the plate and washing each well with MEST buffer (MES + 0.05% Tween 20) three times, 400 μL of the milk-MES buffer (MES + 2% skim milk) is added to each well and incubated for 60 min to block nonspecific binding. Then the blocking solution is discarded and 200 μL of 50 ng/mL of BsAbs in milk-MES buffer is added to relevant wells. As control groups, 200 μL of 50 ng/mL of control BsAbs that

cannot bind to mPEG and only the buffer is also added to relevant wells, respectively. The plate is incubated at room temperature for 2 h and then washed three times with the MEST buffer. Then 100 μL of HRP labeled anti-c-myc antibody diluted 1/5000 in milk-MES buffer is added to each well and incubated for 1 h. All the solutions are discarded and the wells are washed with the MEST buffer three times. Then 100 μL TMB solution is added to each well. After 45 s, 100 μL of 1 M H_2SO_4 is added to end the reaction. The colorimetric reactions in each well are analyzed at an absorbance of 450 nm using the plate reader. Average absorbance and standard deviation are determined for each sample.

3.2.3.8 Dynamic Light Scanning Characterization.

To determine the size of BsAbs, mPEG-UCNPs and the BsAb-UCNP nanoprobes, dynamic light scanning (DLS) test is used. For each sample, 1 mL of 50 μg /mL sample in MES buffer is added into a cuvette and tested by Zetasizer.

3.2.3.9 Bioconjugation of IgG Antibody to cPEG-UCNPs.

After the converting step, the cPEG-UCNPs are changed into MES buffer (pH 4.5) using a centrifuge method at a final concentration of 1 mg/mL. Then 10 μL of cPEG-UCNPs, 100 μg of EDC and 100 μg of NHS are mixed in 90 μL MES buffer (pH 4.5). After 2 h gentle shaking, the sample is washed with the MES buffer twice (centrifuge at 14,000 rpm for 20 min). After the final centrifuge step, the precipitate is suspended with 50 μL MES buffer. The solution is mixed with 50 μL of anti-EphA2 IgG antibody (0.1 mg/mL) and put into a 37 °C shaker overnight. After twice washing with MES buffer (centrifuge at 14,000 rpm for 20 min), the sample is finally suspended in 100 μL of MES buffer with sonication for 5 s.

3.2.3.10 Direct ELISA-like Assay.

A direct ELISA-like assay is used to compare the binding efficiency of BsAb-mPEG-UCNPs and IgG-cPEG-UCNPs to the target EphA2.

Individual wells of a 96-well plate (Falcon) are coated with 100 μL of EphA2 at different concentrations (0.1, 1, 10 and 100 ng/mL) overnight at 4 °C. After discarding all the solution in the plate and washing each well with MEST buffer three times, 400 μL of

milk-MES buffer is added to each well for 60 min to block nonspecific binding. Then the blocking solution is discarded and 200 μL of 50 μg/mL of BsAb-mPEG-UCNPs or IgG-cPEG-UCNPs in milk-MES buffer is added. The plate is incubated at room temperature for 2 h and then washed three times with MEST buffer. The plate is dried under 60 °C. The signal in each well is analyzed using the emission of UCNPs by a homemade plate reader. Average signal and standard deviation are determined for each sample.

3.2.3.11 Cancer Cell Targeted Imaging.

To further broaden the application of the BsAb-UCNP nanoprobes, we test it in cell targeted imaging experiments.

PC3 prostate cancer cells which overexpress the EphA2 and LNCaP prostate cancer cells which express undetectable levels of EphA2 are used to test the targeting of BsAb-UCNP probes.

PC3 cells and LNCaP cells are cultured in RPMI medium with 10% FBS at 37 °C and 5% CO_2. Cells are subcultured using cell dissociation buffer for cell detachment when approximately 80% confluency is reached. The cells slides are prepared one day before, 1×10^4 cells in 2 mL cell medium are pipetted into a 6-well plate with one glass cover slide in each well and incubated overnight until the cells became adherent to the cover slide. After the medium is aspirated, 500 μL of 50 μg/mL UCNP probes in cell medium is added to each well. As a negative control, 500 μL of 50 μg/mL mPEG-UCNPs in cell medium is added to PC3 cells wells. After 1 h incubation, excess particles are removed by washing with MES buffer three times. After fixed by 4% paraformaldehyde, the sample slides are sealed by vector. All the slides are imaged by an Olympus Microscopy modified with a 980 nm laser (Pigtailed DBR Single-Frequency Lasers, 1W, Thorlabs) as excitation. Average intensity and standard deviation are determined for each cell.

3.2.4 Results and Discussion

3.2.4.1 Preparation of BsAb-UCNP nanoprobes and characterization

As the schematic shown in Figure 3-2A, we use 22 nm UCNPs with a composition of NaYF4: 20%Yb/4%Tm due to it super bright emission[3]. To convert UCNPs into a

hydrophilic phase and modify them with mPEG molecules for BsAb conjugation, we use ligand exchange method to replace OA surfactant with mPEG onto UCNPs surface.

The BsAb in this work is designed with two active domains linked by a G4s linker and one domain recognizes mPEG molecules with another one capturing cancer cell surface antigen EphA2. It also has a c-myc tag which is mainly used for purification and detection purposes. Although the BsAb preparation is more complicated and expensive compared with traditional IgG antibody for now, current commercial production will make it accessible to researchers as it's popular not only in the lab but also the market[19].

The BsAb in this work consists of 517 amino acids and has a molecular weight of 55.7 kD. According to our previous work, the BsAb shows high binding affinity to both mPEG (K_D 10 nM) and EphA2 (K_D 1 nM)[20], which is comparable to the normal EphA2 IgG antibody (K_D 0.1 nM) and binders (K_D 10~100 nM)[21].

We merely mix mPEG modified UCNPs and the designed BsAb in buffer and vortex gently for a short time and get the BsAb-UCNP nanoprobes. TEM photos in Figure 3-2B-D show that the morphology of UCNPs does not change after the surface modification of mPEG and BsAbs. Further emission spectra in Figure 3-2E show that the BsAb conjugation has no effect on optical properties of the UCNPs. And the 280 nm absorption peak (refers to protein) change in Figure 3-2F confirms that BsAbs bind to UCNPs.

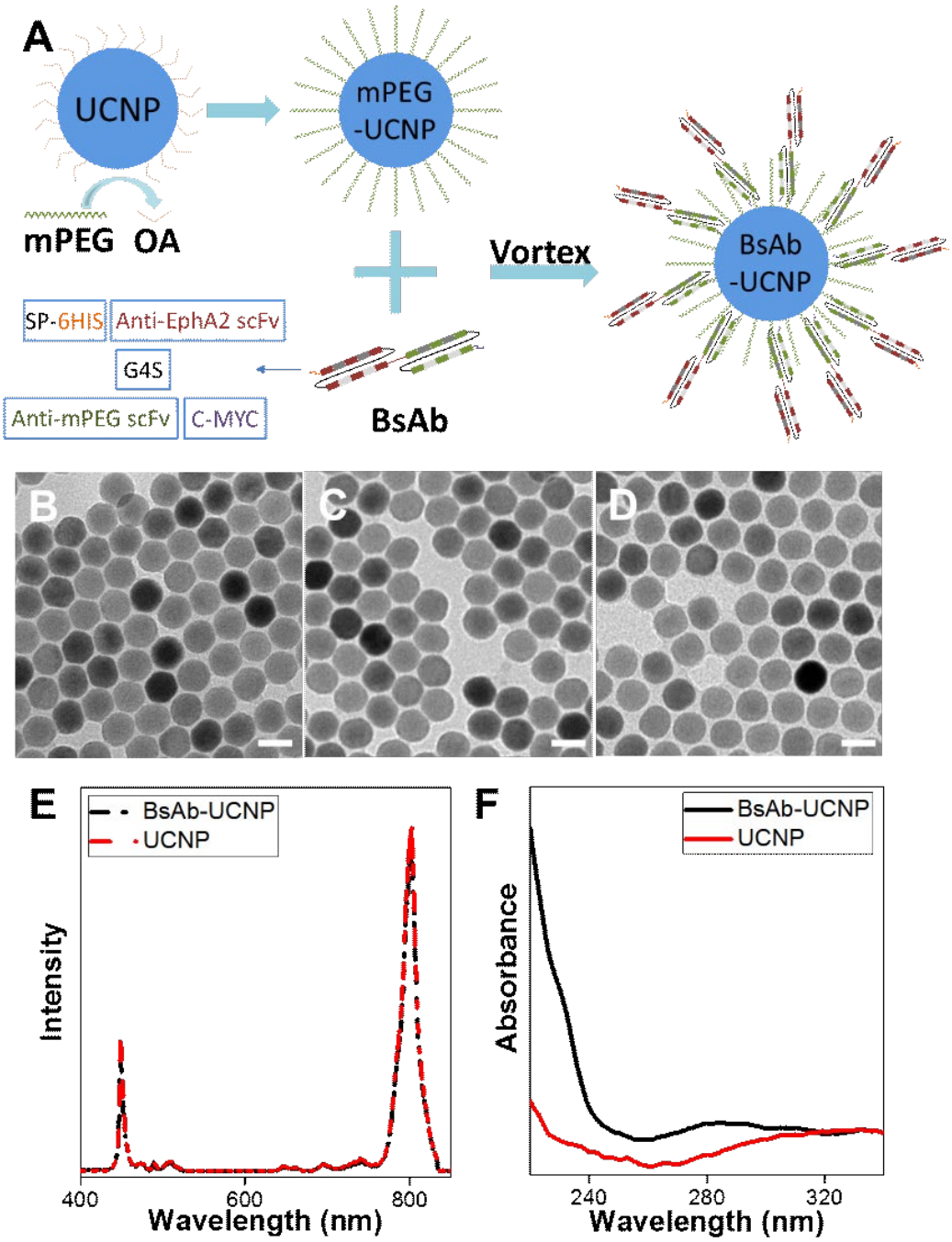

Figure 3-2. A. Scheme of the formation of BsAb-UCNP nanoprobes. And TEM pictures of UCNPs (B), mPEG-UCNPs (C), BsAb-UCNP nanoprobes (D) (Scale Bar: 20 nm). E. Emission spectra under 980 nm laser excitation of BsAb-UCNP nanoprobes and mPEG-UCNPs (at the same concentration of 10 μg/mL). F. Absorption spectra of BsAb-UCNP nanoprobes and mPEG-UCNPs (at the same concentration of 10 μg/mL).

3.2.4.2 Validation of binding between BsAb and mPEG-UCNPs.

We use indirect ELISA to verify the successful binding of BsAb and mPEG-UCNPs (Figure 3-3A). The control groups include adding a BsAb that doesn't have mPEG binding ability to immobilized mPEG-UCNPs, adding second antibody alone to immobilized mPEG-UCNPs, adding BsAb to wells without mPEG-UCNPs and a blank control.

As shown in Figure 3-3B, the experiment group shows the significantly higher signal ($P<0.01$) than the other control groups, suggesting that the mPEG-recognizing BsAb has been successfully conjugated to mPEG-UCNPs, while neither the control BsAb nor the second antibody alone shows binding. This result indicates that the BsAb can effectively and specifically bind to mPEG-UCNPs, while mPEG-UCNPs show no binding to other proteins. Due to the high binding affinity and specificity of the BsAb, we expect mPEG-UCNPs and BsAb can self-assemble under the aqueous condition to form the BsAb-UCNP nanoprobes.

To further prove the successful self-assembly of BsAb and mPEG-UCNPs in solution, and verify the structure of BsAb-UCNP nanoprobes (Figure 3-3C), we use DLS to measure the mean size of each sample. From Figure 3-3D, each sample shows a single peak with low PdI value which means all samples are in well monodispersed. It shows the conjugate has a diameter of 43 nm, which indicates that BsAb has formed a single layer on top of each UCNP, because the size of BsAb is 6 nm in diameter and the mPEG-UCNPs have a diameter of 28 nm, i.e., the size of BsAb-UCNP nanoprobes is approximately the sum of one mPEG-UCNP and two BsAbs from both sides, denoting full coverage of the UCNPs with antibodies at this concentration range.

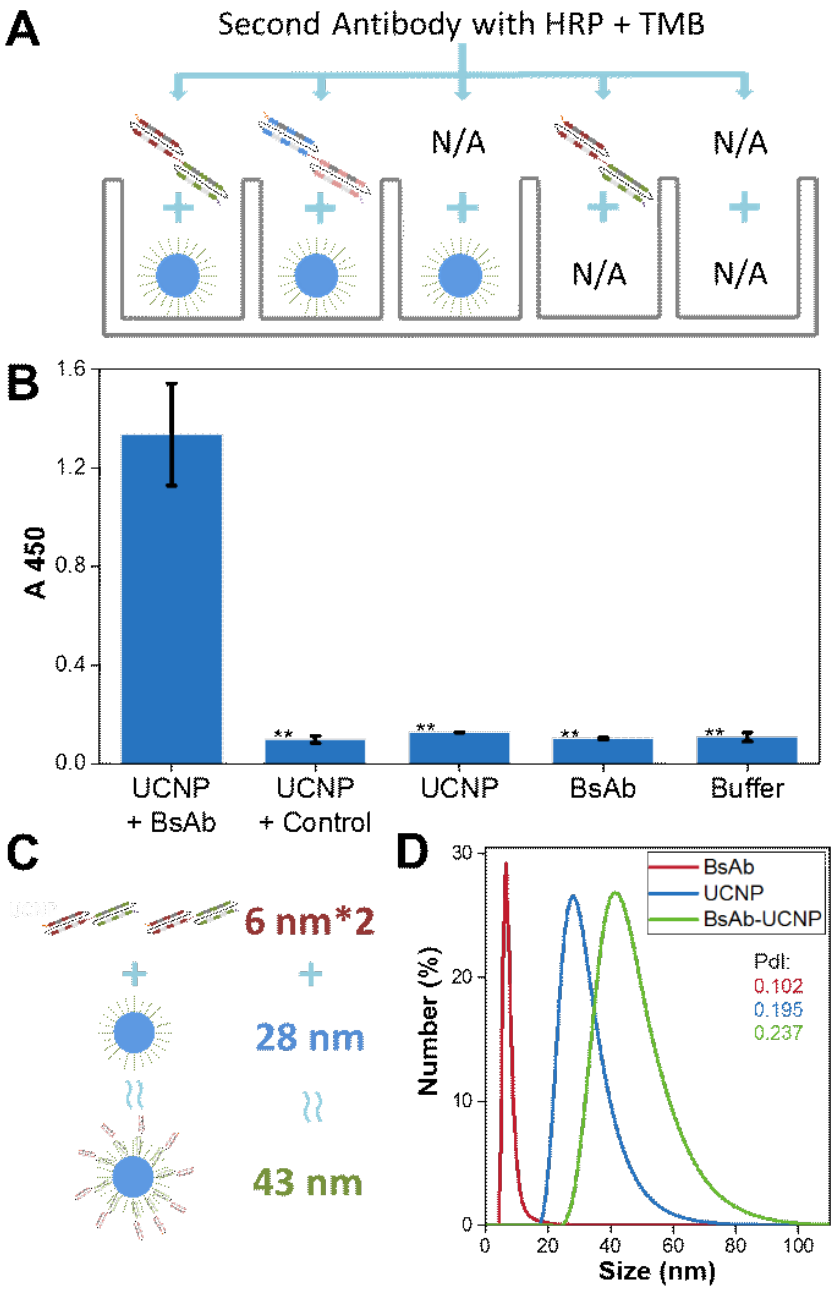

*Figure 3-3. A. Scheme of the binding ELISA test. B. Results of binding ELISA tests. Each group is tested three times and error bars are shown. (Significant Difference is shown and **: P<0.01) C. Schematic of BsAb-UCNP structure D. DLS results of BsAb, mPEG-UCNPs and BsAb-UCNP nanoprobes.*

To test its stability, we use DLS to monitor the size of BsAb-UCNP nanoprobes for 8 hours after the bioconjugation and find the negligible change in size distribution as shown in Figure 3-4.

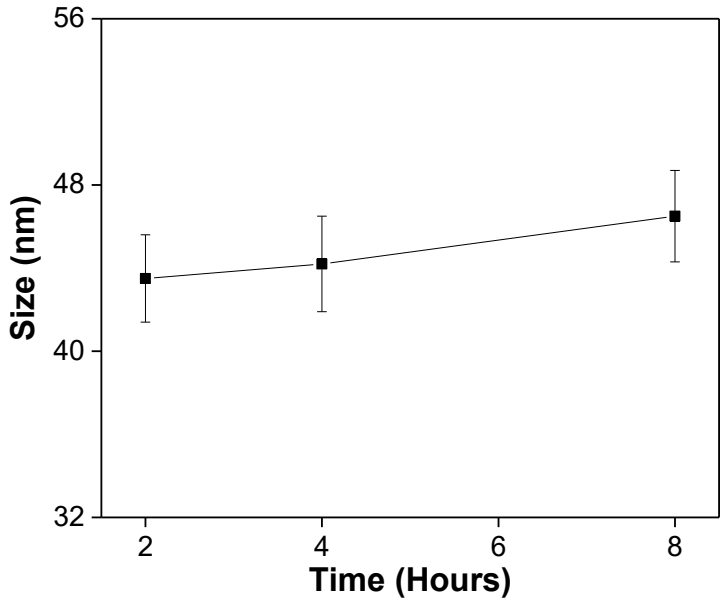

Figure 3-4. DLS results of BsAb-UCNP nanoprobe after 2 h, 4 h and 8 h.

3.2.4.3 Comparing BsAb and EDC conjugation methods

Figure 3-5A shows the schematic outlining of conventional EDC-coupling method that needs two time-consuming steps, while our BsAb conjugation method is a one-step approach which is achieved with more straightforward operation and far shorter time under mild conditions.

Due to the drawback of the EDC method described previously, we assume that using the BsAb conjugation method will result in a higher binding efficiency. Therefore, we use a direct ELISA-like assay to compare the binding efficiency of the BsAb-UCNP nanoprobes and the IgG-UCNP nanoprobes to prostate cancer biomarker EphA2. We add these two nanoprobes separately to immobilized EphA2 at various concentrations of 0.1, 1, 10 and 100 ng/mL. From the results shown in Figure 3-5B, both of the nanoprobes show binding to EphA2, while the binding efficiencies of BsAb-UCNP nanoprobes are consistently higher than that of IgG-UCNP nanoprobes. The efficiency differences become more significant with the increasing of immobilized target concentration. When the immobilized target concentration is 100 ng/mL, BsAb-UCNP nanoprobes show 54% higher signal ($P<0.01$) than the IgG-UCNP nanoprobe. The results indicate that the

nanoprobes developed using BsAb perform better than the nanoprobe conjugated by the traditional EDC chemical linkage method. This is because all the binding domains cannot be blocked and are shown directly to the outside by using the BsAb. Also, the BsAb has a smaller size than the normal IgG. This means that more capture molecules can be placed on the surface of the particles, which helps to increase the binding efficiency to the target.

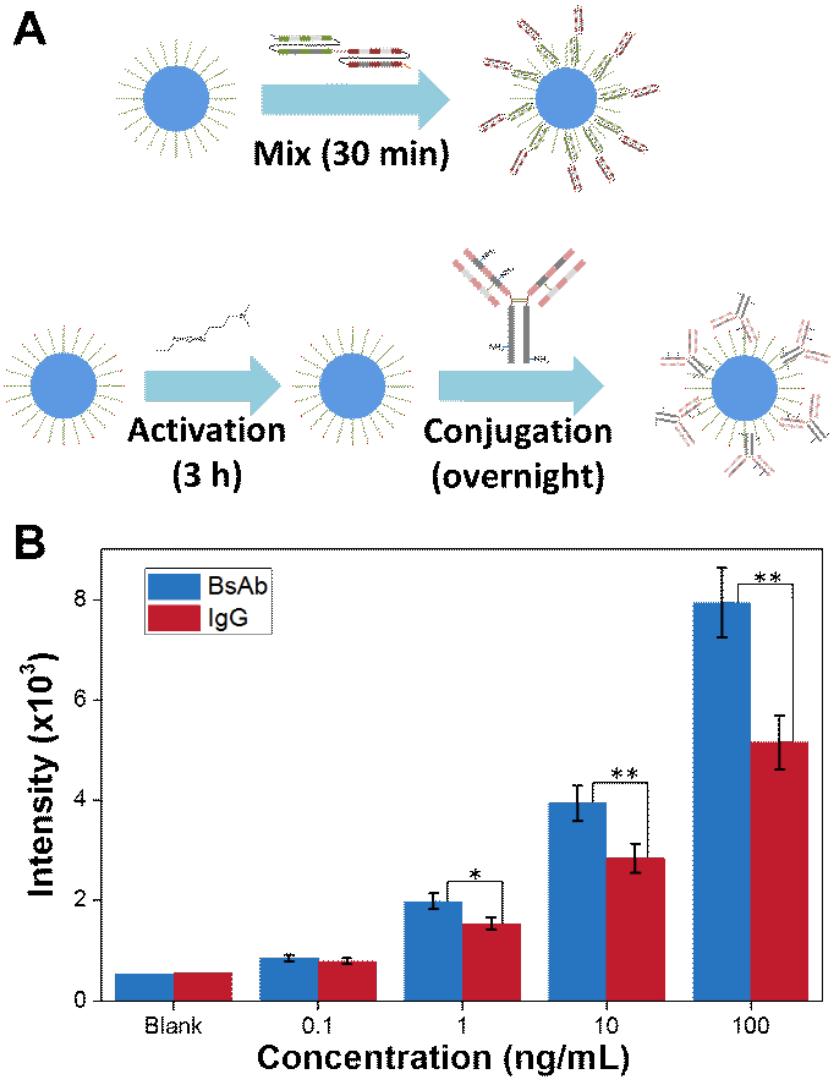

*Figure 3-5. A. Scheme showing two different conjugation methods using in this study. B. Results of direct ELISA-like assay tests. Each group is tested three times and error bars are shown. (Significant Difference is shown and **: P<0.01, *: P<0.05)*

3.2.4.4 Cell Imaging

After validating the higher binding efficiency of BsAb-UCNPs nanoprobes to the cancer

biomarker, we further explore its use for cell imaging application, using confocal microscopy.

From the top panel of confocal images in Figure 3-6, overlays of fluorescence and bright-field images show that the fluorescence is mainly from the surface of the cells, confirming the accumulation of nanoprobes on the EphA2 expressed surface of PC3 cells (middle panel). In comparison, particles without BsAb show much less accumulation on PC3 cells. The effect of targeting surface receptors is also demonstrated by the negligible binding of the BsAb-UCNP nanoprobes to a negative cell line that only exhibits minimal expression of the EphA2 protein (LNCaP) which validates the specificity of the targeting (bottom panel). Subsequent analysis of the blue upconversion intensity per cell reveals that the experiment group shows the most intense upconversion fluorescence. All the results indicate that the BsAb-UCNP nanoprobes show excellent performance in cell targeted imaging experiments and can be applied as an excellent bioprobe candidate for such protein biomarkers.

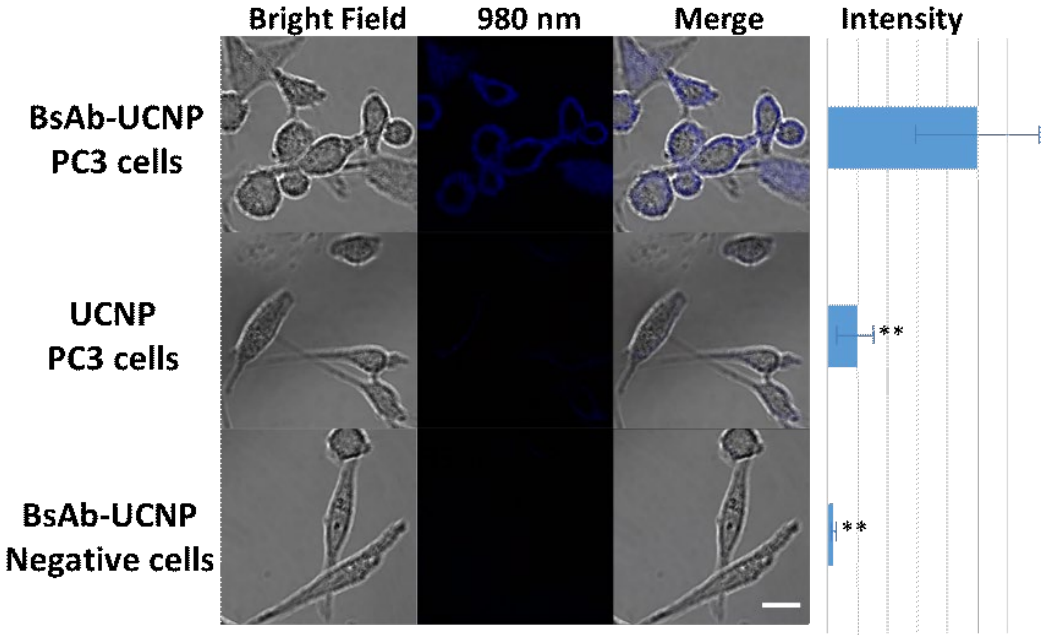

Figure 3-6. Confocal microscopic images of PC3 cells treated with BsAb-UCNPs, PC3 cells treated with UCNPs and negative cells (LNCaP cell line) treated with BsAb-UCNPs. Fluorescence images (labeled with 980 nm) are obtained by collecting the blue emission in the range of 400-500 nm under the excitation of 980 nm laser. Intensity equals to the

*blue upconversion intensity per cell. Scale bar, 20 μm. (Significant Difference is shown and **: P<0.01, *: P<0.05)*

3.2.5 Conclusion

In conclusion, we have developed a straightforward method for direct conjugation of UCNPs and antibodies through applying BsAb. The approach is a one-step strategy and avoids chemical reaction. And it owns a better performance in operation time and binding efficiency than the commonly used EDC conjugation method. We subsequently demonstrated that the BsAb-UCNP nanoprobes conjugated by the developed approach could be applied in cell targeted imaging with high specific binding efficiency. This approach will promote the applicability of UCNPs and can be applied to all nanomaterials with a variety of compositions, sizes and shapes and utilize a variety of antibodies for broad applications in imaging and diagnosis.

Reference:

[1] J. Wang, R. Deng, M. A. Macdonald, B. Chen, J. Yuan, F. Wang, D. Chi, T. S. Andy Hor, P. Zhang, G. Liu, Y. Han, and X. Liu, "Enhancing multiphoton upconversion through energy clustering at sublattice level," *Nat. Mater.*, vol. 13, no. 2, pp. 157–162, 2014.

[2] B. Zhou, B. Shi, D. Jin, and X. Liu, "Controlling upconversion nanocrystals for emerging applications," *Nat. Nanotechnol.*, vol. 10, no. 11, pp. 924–936, 2015.

[3] J. Zhao, D. Jin, E. P. Schartner, Y. Lu, Y. Liu, A. V Zvyagin, L. Zhang, J. M. Dawes, P. Xi, J. A. Piper, E. M. Goldys, and T. M. Monro, "Single-nanocrystal sensitivity achieved by enhanced upconversion luminescence," *Nat. Nanotechnol.*, vol. 8, p. 729, Sep. 2013.

[4] Y. Lu, J. Zhao, R. Zhang, Y. Liu, D. Liu, E. M. Goldys, X. Yang, P. Xi, A. Sunna, J. Lu, Y. Shi, R. C. Leif, Y. Huo, J. Shen, J. A. Piper, J. P. Robinson, and D. Jin, "Tunable lifetime multiplexing using luminescent nanocrystals," *Nat. Photonics*, vol. 8, no. 1, pp. 32–36, 2014.

[5] D. J. Gargas, E. M. Chan, A. D. Ostrowski, S. Aloni, M. V. P. Altoe, E. S. Barnard, B. Sanii, J. J. Urban, D. J. Milliron, B. E. Cohen, and P. J. Schuck, "Engineering bright sub-10-nm upconverting nanocrystals for single-molecule imaging," *Nat. Nanotechnol.*, vol. 9, no. 4, pp. 300–305, 2014.

[6] L. Xiong, Z. Chen, Q. Tian, T. Cao, C. Xu, and F. Li, "High Contrast Upconversion Luminescence Targeted Imaging in Vivo Using Peptide-Labeled Nanophosphors," *Anal. Chem.*, vol. 81, no. 21, pp. 8687–8694, Nov. 2009.

[7] C. Yao, P. Wang, L. Zhou, R. Wang, X. Li, D. Zhao, and F. Zhang, "Highly Biocompatible Zwitterionic Phospholipids Coated Upconversion Nanoparticles for Efficient Bioimaging," *Anal. Chem.*, vol. 86, no. 19, pp. 9749–9757, Oct. 2014.

[8] E. S. Levy, C. A. Tajon, T. S. Bischof, J. Iafrati, A. Fernandez-Bravo, D. J. Garfield, M. Chamanzar, M. M. Maharbiz, V. S. Sohal, P. J. Schuck, B. E. Cohen, and E. M. Chan, "Energy-Looping Nanoparticles: Harnessing Excited-State Absorption for Deep-Tissue Imaging," *ACS Nano*, vol. 10, no. 9, pp. 8423–8433, 2016.

[9] Z. Farka, M. J. Mickert, A. Hlaváček, P. Skládal, and H. H. Gorris, "Single

Molecule Upconversion-Linked Immunosorbent Assay with Extended Dynamic Range for the Sensitive Detection of Diagnostic Biomarkers," *Anal. Chem.*, vol. 89, no. 21, pp. 11825–11830, Nov. 2017.

[10] M. He and Z. Liu, "Paper-Based Microfluidic Device with Upconversion Fluorescence Assay," *Anal. Chem.*, vol. 85, no. 24, pp. 11691–11694, Dec. 2013.

[11] H. Wang, R. L. Han, L. M. Yang, J. H. Shi, Z. J. Liu, Y. Hu, Y. Wang, S. J. Liu, and Y. Gan, "Design and Synthesis of Core-Shell-Shell Upconversion Nanoparticles for NIR-Induced Drug Release, Photodynamic Therapy, and Cell Imaging," *ACS Appl. Mater. Interfaces*, vol. 8, no. 7, pp. 4416–4423, 2016.

[12] L. Le Li, P. Wu, K. Hwang, and Y. Lu, "An exceptionally simple strategy for DNA-functionalized Up-conversion nanoparticles as biocompatible agents for nanoassembly, DNA delivery, and imaging," *J. Am. Chem. Soc.*, vol. 135, no. 7, pp. 2411–2414, 2013.

[13] J.-M. Nam, "Nanoparticle-Based Bio-Bar Codes for the Ultrasensitive Detection of Proteins," *Science (80-.).*, vol. 301, no. 5641, pp. 1884–1886, 2003.

[14] K. Pu, A. J. Shuhendler, J. V Jokerst, J. Mei, S. S. Gambhir, Z. Bao, and J. Rao, "Semiconducting polymer nanoparticles as photoacoustic molecular imaging probes in living mice," *Nat Nano*, vol. 9, no. 3, pp. 233–239, 2014.

[15] Q. Liu, W. Feng, and F. Li, "Water-soluble lanthanide upconversion nanophosphors: Synthesis and bioimaging applications in vivo," *Coord. Chem. Rev.*, vol. 273–274, pp. 100–110, 2014.

[16] J. Zhao, Z. Lu, Y. Yin, C. McRae, J. A. Piper, J. M. Dawes, D. Jin, and E. M. Goldys, "Upconversion luminescence with tunable lifetime in $NaYF_4$:Yb,Er nanocrystals: role of nanocrystal size," *Nanoscale*, vol. 5, no. 3, pp. 944–952, 2013.

[17] Y. Shi, B. Shi, A. V. E. Dass, Y. Lu, N. Sayyadi, L. Kautto, R. D. Willows, R. Chung, J. Piper, H. Nevalainen, B. Walsh, D. Jin, and N. H. Packer, "Stable Upconversion Nanohybrid Particles for Specific Prostate Cancer Cell Immunodetection," *Sci. Rep.*, vol. 6, p. 37533, Nov. 2016.

[18] G. T. Hermanson, *Bioconjugate Techniques 2nd Edition*. Academic Press, 2013.

[19] G. Fan, Z. Wang, M. Hao, and J. Li, "Bispecific antibodies and their applications,"

J. Hematol. Oncol., vol. 8, no. 1, p. 130, Dec. 2015.

[20] C. B. Howard, N. Fletcher, Z. H. Houston, A. V Fuchs, N. R. B. Boase, J. D. Simpson, L. J. Raftery, T. Ruder, M. L. Jones, C. J. De Bakker, S. M. Mahler, and K. J. Thurecht, "Overcoming Instability of Antibody-Nanomaterial Conjugates : Next Generation Targeted Nanomedicines Using Bispecifi c Antibodies," *Adv. Healthc. Mater.*, vol. 5, pp. 2055–2068, 2016.

[21] C. Ullman, P. Mathonet, A. Oleksy, A. Diamandakis, L. Tomei, A. Demartis, C. Nardi, S. Sambucini, A. Missineo, K. Alt, C. E. Hagemeyer, M. Harris, A. Hedt, R. Weis, and K. R. Gehlsen, "High affinity binders to EphA2 isolated from Abdurin Scaffold libraries; Characterization, binding and tumor targeting," *PLoS One*, vol. 10, no. 8, pp. 1–25, 2015.

Chapter 4 Quantitative Lateral Flow Strip Sensor Using Highly Doped Upconversion Nanoparticles

Hao He, Baolei Liu, Shihui Wen, Jiayan Liao, Gungun Lin, Jiajia Zhou, and Dayong Jin

Analytical Chemistry, **2018**, 90, 12356−12360

DOI: 10.1021/acs.analchem.8b04330

Contribution:

Planning of experiments, modification of UCNPs, characterization of upconversion nanoprobe by spectrometer, power dependent intensity test, Nanodrop, DLS, strip fabrication, LFS assay, device design and 3D-print, data evaluation, manuscript writing.

4.1 Motivation

The applications of NPs bring IVD assays quite high sensitivity and flexibility. But as we introduced in Chapter 1, most of these assays can only be done under lab environment because they still need lab based equipment to read the signal. POC assays, such as AuNPs based paper strips make pregnant test can be done at home without any training, are needed in the early stage cancer screening and after treatment monitoring. However, these strips are not sensitive and remain indicative rather than quantitative, cannot be a good candidate.

In this chapter in a format of a published paper, we developed a quantitative lateral flow strip assay using highly doped UCNPs and all the test can be finished with only a smartphone. This simplicity and sensitive quantitative assay makes cancer detection as easy as just take a photo.

4.2 Manuscript

4.2.1 Abstract

Paper based lateral flow assays, though being low-cost and widely used for rapid in-vitro diagnostics, are indicative and do not provide sufficient sensitivity for the detection and quantification of low abundant biomarkers for early stage cancer diagnosis. Here we design a compact device to create a focused illumination spot with high irradiance, which activates a range of highly doped 50 nm upconversion nanoparticles (UCNPs) to produce orders of magnitude more brighter emissions. The device employs a very low-cost laser diode, simplified excitation and collection optics, and permits a mobile phone camera to record the results. Using highly erbium ions (Er^{3+}) and thulium ions (Tm^{3+}) doped UCNPs as two independent reporters on two-color lateral flow strips, new records of limit of detection (LOD), 89 pg/mL and 400 pg/mL, have been achieved for the ultra-sensitive

detection of PSA and EphA2 biomarkers, respectively without crosstalk. The technique and device presented in this work suggests a broad scope of low-cost, rapid and quantitative lateral flow assays in early detection of bio-analytes.

4.2.2 Introduction

The simple and low-cost lateral flow strip (LFS), like pregnancy testing sticks, have been widely used for point-of-care applications, at home and clinics, without any training required. However, the current visually interpreted tests are indicative rather than quantitative, which are limited by their low visibility of the traditionally used reporters, such as colloidal gold nanoparticles[1] and dye encapsulated latex beads[2]. To overcome their inadequate sensitivity issue towards high performance in analytical assays, and to meet the increasing demand in the quantitative detection of low abundance disease biomarker and toxins, new fluorescence nanoparticles are needed in LFS devices. Using semiconductor quantum dots[3] and ceramic upconversion nanoparticles (UCNPs)[4], fluorescence-based LFS sensors have high sensitivity. To do this, simple-to-use optical readers are also essential in fluorescence-based LFS sensors, as it not only produces quantitative results but also offers less subjective interpretation of results.

The other aspect that affects the detection sensitivity and accuracy in quantitative assays is the background noise, e.g. scatterings and autofluorescence of paper substrates under excitation illumination. For this reason, UCNPs have attracted more attentions[5]–[8], as they only require near infrared excitation to emit signals in the visible wavelength range, in which case the autofluorescence from paper substrates are minimized. Moreover, different doping of lanthanide ions can produce a collection of choices of photo-stable multi-color emissions for high throughput multiplexed assays[9].

In early days, large UCNPs with size of 400 nm have been used in LFS sensors[4], because high brightness of emission signals is needed and large particles encapsulate a

large number of emitters to meet this requirement. But such big particles often block the pores of paper substrate, and end up with higher noise from non-specific blockage[10]. Enlarging pore size is not an option as the flow speed is too high to allow sufficient time for immunoassays, therefore the pore size has to be within the range from a few microns to sub-micron scales in nitrocellulose strips[11]. Recently controlled synthesis of small monodispersed UCNPs[12], and at large quantity[13], have been realized, and UCNPs in the range of tens of nanometers have been introduced for LFS sensors[14]. But the intensity of smaller UCNPs drops significantly compared to the larger ones, due to the reduced volume of emitters and increased level of surface quenching. Therefore LFS sensors using smaller UCNPs are often less sensitive, though UCNP based strips have been suggested for the detection of analytes, such as *E. coli* (10^3 org/mL)[15], *Vibrio anguillarum* (10^2 cfu/mL)[16], cephalexin (0.6 ng/mL)[17] and prostate specific antigen (PSA, 556 ng/mL)[18]. The key towards real world applications of UCNP based LFS sensors is to significantly improve their limit of detection (LOD).

Instead of using large crystal host to increase the number of emitters, we have recently developed strategies to increase the concentration of emitters within small nanocrystals and to produce a range of highly-doped UCNPs displaying exceptional brightness and sensitivity[19]–[21]. Conventionally, the doping level has been kept relatively low to ensure a sizable separation between the dopants to prevent parasitic interaction, which limits the concentration of dopants. To overcome the issue of concentration quenching of upconversion luminescence, we use a high irradiance, either by using a high-power laser or focusing the excitation beam, and an inert shell passivation, to alleviate the threshold of concentration quenching, which ensures each highly doped UCNP exceptionally bright, sufficient for naked eye inspection through a simple microscope[22].

On the other hand, the small cameras built in the smartphone have enabled the increased capabilities and ubiquity of smartphones to be used for point of care applications[23].

Together with the fast growing fields of low-cost laser diode and 3D-printing technologies, compact and low-cost readers can be made for fluorescent based LFS sensors for quantification of low abundant biomarkers, but the sensitivity of phone cameras is yet to be improved.

In this study, we apply two kinds of UCNPs, highly doped by Er^{3+} ions to emit yellowish upconversion emissions and Tm^{3+} ions to emit purple upconversion emissions, as multi-color reporters in LFS. We print a plastic holder that aligns a low-cost excitation laser diode and collection optics (shown in Figure 4-1), with a total cost less than $100. The key is to tightly focus the excitation beam to only illuminate a small region on the paper substrate, which unlocks the high brightness of highly doped UCNPs to deliver high sensitivity detection of smaller volume of samples. We demonstrate here that highly doped UCNPs provide significant higher brightness than the conventional UCNPs, which allows a limit of detection of 89 pg/mL for PSA and 400 pg/mL for ephrin type-A receptor 2 (EphA2) achieved in a quantitative multiplexed assay without crosstalk.

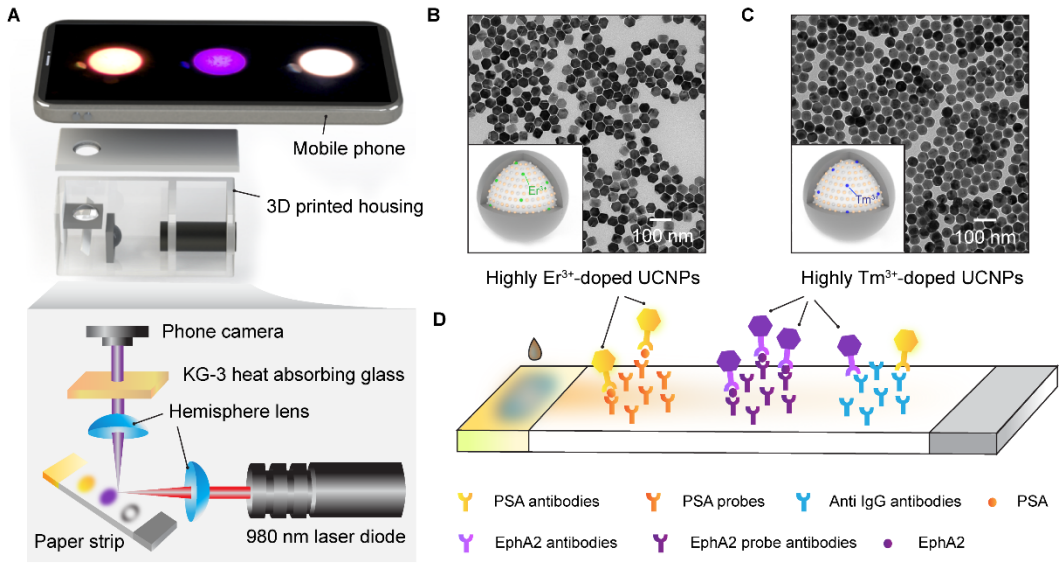

Figure 4-1. Schematic illustration of the LFS sensor. A. A mobile phone based reader and the optics layout. B. Structure of highly Er^{3+} doped core-shell UCNPs and the

corresponding TEM image. C. Structure of highly Tm^{3+} doped core-shell UCNPs and the corresponding TEM image. D. Two-color LFS assays for PSA and EphA2 analytes.

4.2.3 Methods, results and discussion

4.2.3.1 Synthesis of UCNPs and TEM characterization

To obtain smaller and brighter UCNPs, we synthesize two kinds of inert shell passivated UCNPs highly doped with Er^{3+} and Tm^{3+}, i.e. 8%Er/60%Yb@$NaYF_4$ and 8%Tm/60%Yb@$NaYF_4$, and evaluate their performance against the conventional UCNPs with the same size, i.e. 2%Er/20%Yb and 0.5%Tm/20%Yb.

NaYF4: Yb^{3+}, Er^{3+}/Tm^{3+} nanocrystals with different doping (2%Er/20%Yb, 8%Er/60%Yb, 0.5%Tm/20%Yb and 8%Tm/60%Yb) were synthesized according to our previously reported method. In a typical experiment, 1 mmol $RECl_3 \cdot 6H_2O$ (RE = Y, Yb, Tm, 99.99%, Sigma) with the desired molar ratio were added to a flask containing 6 mL OA (90%, Sigma) and 15 mL ODE (90%, Sigma). The mixture was heated to 160 °C under argon flow for 30 min to obtain a clear solution and then cooled down to about 50 °C, followed by the addition of 5 mL methanol (anhydrous, Sigma) solution of NH_4F (4 mmol, Sigma) and NaOH (2.5 mmol, Sigma). After stirring for 30 min, the solution was heated to 150 °C under argon flow for 20 min to expel methanol, and then the solution was further heated to 310 °C for another 90 min. Finally, the reaction solution was cooled down to room temperature. The products were precipitated by ethanol and centrifuged (9000 rpm for 5 min), then washed 3 times with cyclohexane (anhydrous, Sigma), ethanol (anhydrous, Sigma) and methanol to get the nanoparticles.

To get the nanoparticles with core-shell structure, layer-by-layer epitaxial growth has been employed. The shell precursors preparation is similar with that for the core nanoparticles synthesis, until the step where the reaction solution was slowly heated to

150°C and kept for 20 min. Instead of further heating to 300 °C to trigger nanocrystal growth, the solution was cooled down to room temperature to yield the shell precursors. For epitaxial growth, 0.15 mmol as-prepared core nanocrystals were added to a containing 6 ml OA and 6 ml ODE. The mixture was heated to 170 °C under argon for 30 min, and then further heated to 300 °C. Next, 0.25 ml as prepared shell precursors were injected into the reaction mixture and ripened at 300 °C for 4 min, followed by the same injection and ripening cycles for several times to get the nanocrystals with the desired size. Finally, the slurry was cooled down to room temperature and the formed nanocrystals were purified according to the same procedure used for the core nanocrystals.

The uniformity of each UCNPs sample is confirmed by TEM characterization shown in Figure 4-2

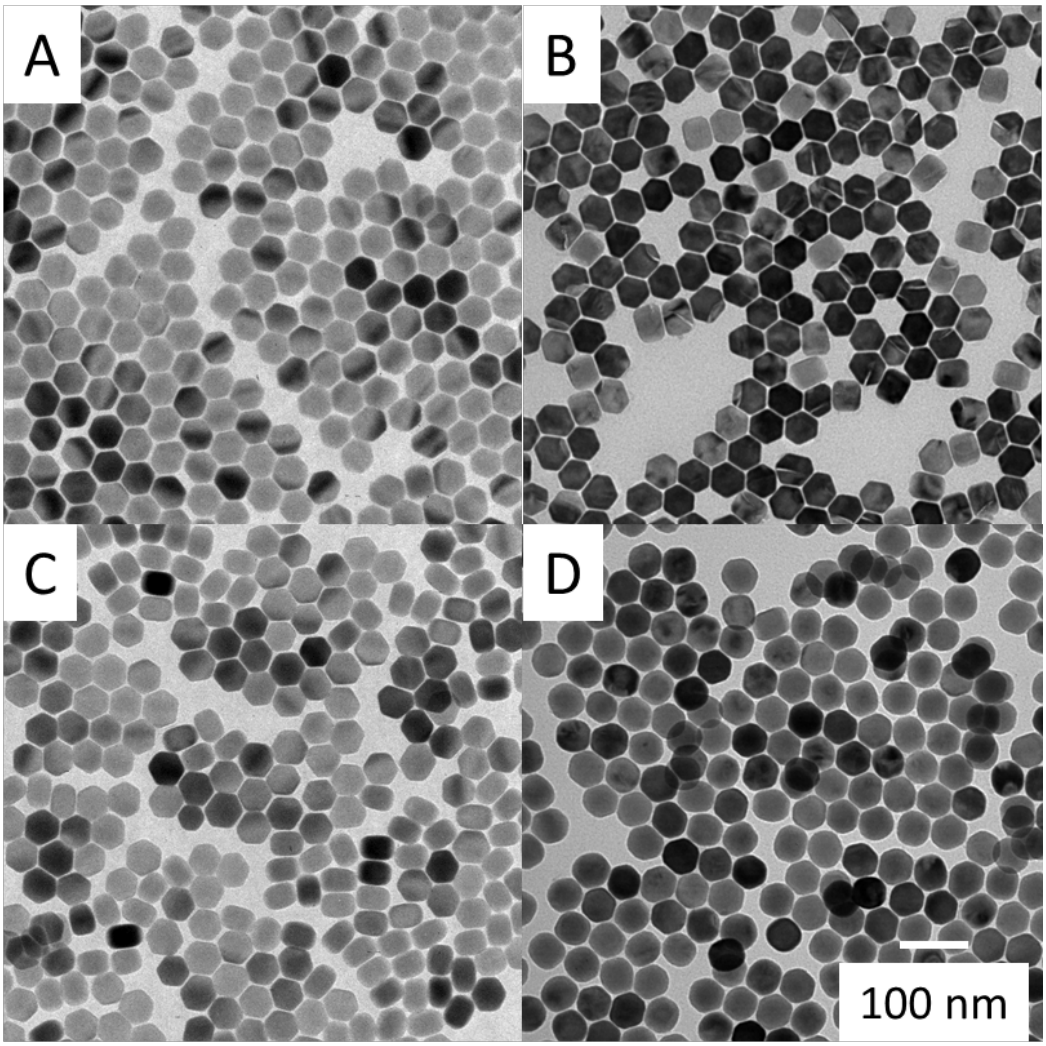

Figure 4-2. TEM photos of A. 2%Er/20%Yb UCNPs, B. 8%Er/60%Yb@$NaYF_4$ UCNPs, C. 0.5%Tm/20%Yb UCNPs and D. 8%Tm/60%Yb@$NaYF_4$ UCNPs. Scale bar: 100 nm.

4.2.3.2 UCNP surface functionalization and characterization

We use a ligand exchange method to modify the surfaces of UCNPs with carboxyl groups, followed by an EDC/NHS method to conjugate antibodies. To convert OA capped UCNPs to cPEG (polyethylene glycol modified with a carboxy group, M_w = 3500, JenKem Technology, USA) coated ones, ligand exchange method is used. 1.5 mL of 20 mg/mL UCNPs in cyclohexane are precipitated with ethanol. After centrifuge and discarding the solution, UCNPs are redispersed in 3 mL of THF (anhydrous) with vortex and sonication.

Then 1.5 mL of 200 mg cPEG in THF solution is added. The mixed solution is stirred at room temperature for 24 h. After that, 3 mL of MiliQ water is added and mixed with shaking. Then the solution is extracted with 1 mL of hexane to remove the OA molecules. After removing the oil phase, the solution is put in vacuo overnight to evaporate organic solvents. Then the solution is dialyzed in 1 L of MiliQ water for 24 h to remove the excessive PEG molecules.

After the converting step, the cPEG-UCNPs are changed into MES buffer (pH 4.5) using a centrifuge method at a final concentration of 1 mg/mL. Then 10 μL of cPEG-UCNPs, 100 μg of EDC and 100 μg of NHS are mixed in 90 μL MES buffer (pH 4.5). After 2 h gentle shaking, the sample is washed with the MES buffer twice (centrifuge at 14,000 rpm for 20 min). After the final centrifuge step, the precipitate is suspended with 50 μL MES buffer. The solution is mixed with 50 μL of IgG antibody (0.1 mg/mL anti-PSA monoclonal antibody produced in rabbit/anti-EphA2 monoclonal antibody produced in rabbit, Sigma) and put into a 37 °C shaker overnight. After twice washing with MES buffer (centrifuge at 14,000 rpm for 20 min), the sample is finally suspended in 100 μL of MES buffer with sonication for 5 s.

The successful conjugation of antibodies is confirmed by UV absorption spectra with a characteristic peak appearance at 280 nm and the dynamic light scattering revealing a slight increase in size. We use Nanodrop2000 to test the UV absorption spectra (Figure 4-3) of the cPEG coated different UCNPs and IgG conjugated ones to confirm that antibodies have been conjugated to the surface of UCNPs.

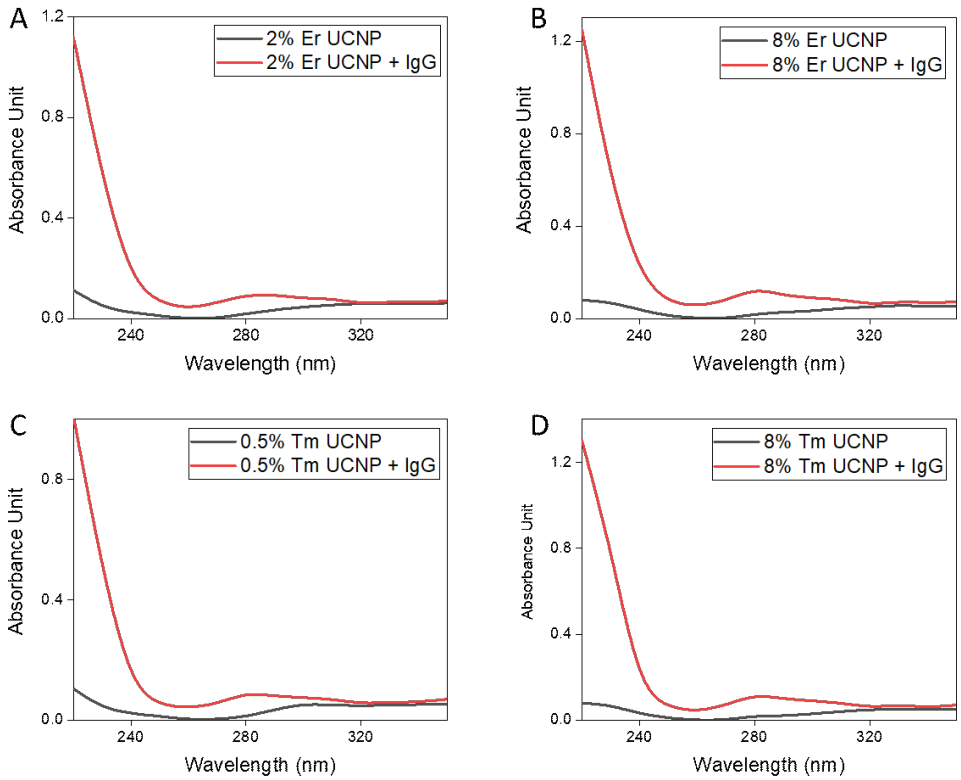

Figure 4-3: UV absorption spectrum of cPEG coated and IgG modified UCNPs: A. 2%Er/20%Yb, B. 8%Er/60%Yb@$NaYF_4$, C. 0.5%Tm/20%Yb, D. 8%Tm/60%Yb@$NaYF_4$.

And we use dynamic scattering to test the size distribution of these samples in MES buffer (pH 6.8). The results also give an evidence of IgG on UCNPs surfaces.

Table 4-1: DLS size distribution

	cPEG- UCNP	IgG-cPEG-UCNP
2%Er/20%Yb	50.6 nm	64.4 nm
8%Er/60%Yb	58.1 nm	75.1 nm
0.5%Tm/20%Yb	52.4 nm	66.8 nm
8%Tm/60%Yb	60.4 nm	76.2nm

We particularly test the power dependent properties of the as-prepared UCNPs reporters, in terms of their emission intensities and spectrum profiles using a purpose-built single

nanoparticle characterization system[22]. As shown in Figure 4-6A, the brightness of highly doped UCNPs increases much more significantly than the lower doped ones with increasing excitation power density. The enhancement ratios of the emission brightness for highly Er^{3+} and Tm^{3+} doped UCNPs are 5 times and 12 times more than that of lower doped ones when the power reaches above 0.5 MW/cm^2. As shown in Figure 4-6B, the emission spectrum of highly Er^{3+} doped UCNP reporters emit a lot more intensity in red around 650 nm under higher excitation power, which results in a bright yellowish emission. This paint mixing effect also happens in the highly Tm^{3+} doped UCNP reporters with appearance in purple from the phone camera. The power dependent spectrum profiles of lower doped UCNP reporters are shown in Figure 4-4.

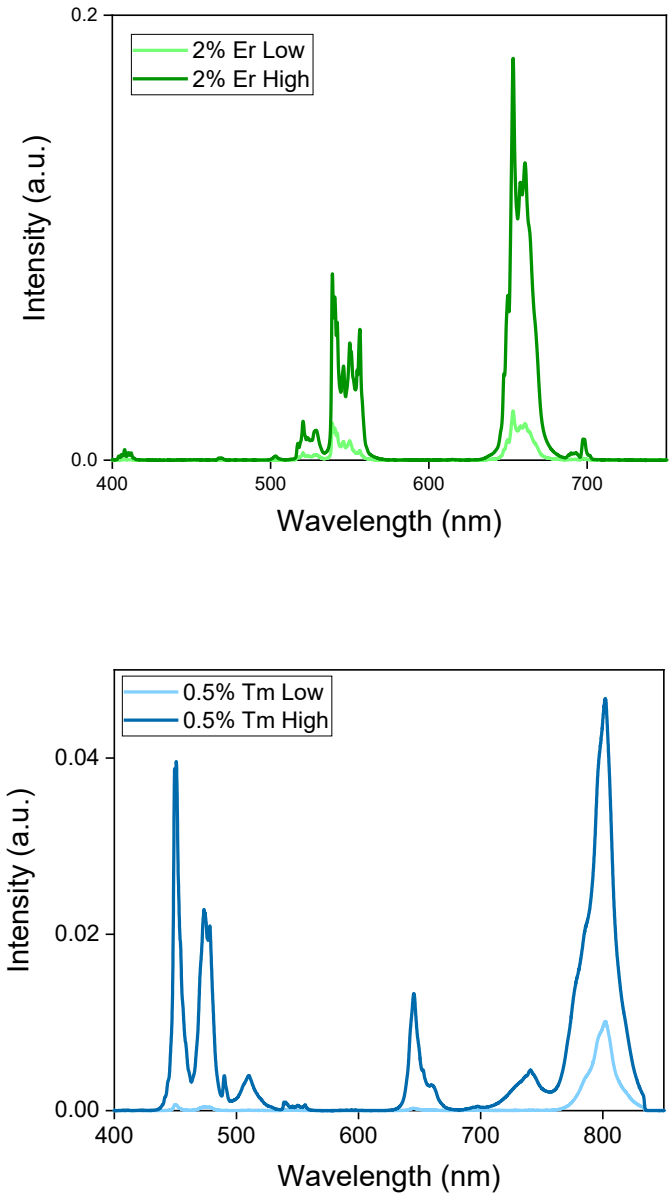

Figure 4-4. Power dependent spectra of 2%Er/20%Yb (left) and 0.5%Tm/20%Yb (right) under low and high excitation power.

To quantify the higher brightness of highly doped UCNPs as reporters on LFS, we compare highly Er^{3+} doped UCNP reporter and lower doped one by detecting different concentrations of target PSA using lateral flow strips.

The strip structure is shown in Figure 4-1 consist of an adhesive PVC back pad, a

nitrocellulose membrane (FF120HP membrane, GE Life Science), a sample pad (CF4, GE Life Science) and an absorbent pad (CF5, GE Life Science). The sample pad, nitrocellulose membrane and absorbent pad are orderly mounted on the PVC back pad with 2 mm overlap. The assembled pads are cut into strips with width of 3 mm. Test area and control area are coated by 0.5 μL of 0.2 mg/mL anti-PSA/EphA2 polyclonal antibodies produced in mouse (Sigma) and 0.5 μL 2 mg/mL anti-rabbit IgG antibodies (Sigma) separately and incubated under 4°C overnight.

To test the samples, UCNP reporters are transferred to a working buffer (pH6.8 MES buffer, 0.5% w/v tween 20, 1% w/v BSA). After mixing, sample solutions with UCNP reporters solutions are added to the sample pad of strip. After 10 mins, washing buffer (pH6.8 MES buffer, 0.5% w/v tween 20) is added to the sample pad. After 20 mins, the strip is detected by reader. To read the emission signal of UCNPs reporters on strips, we use a purpose-built scanning confocal system, which is shown in Figure 4-5.

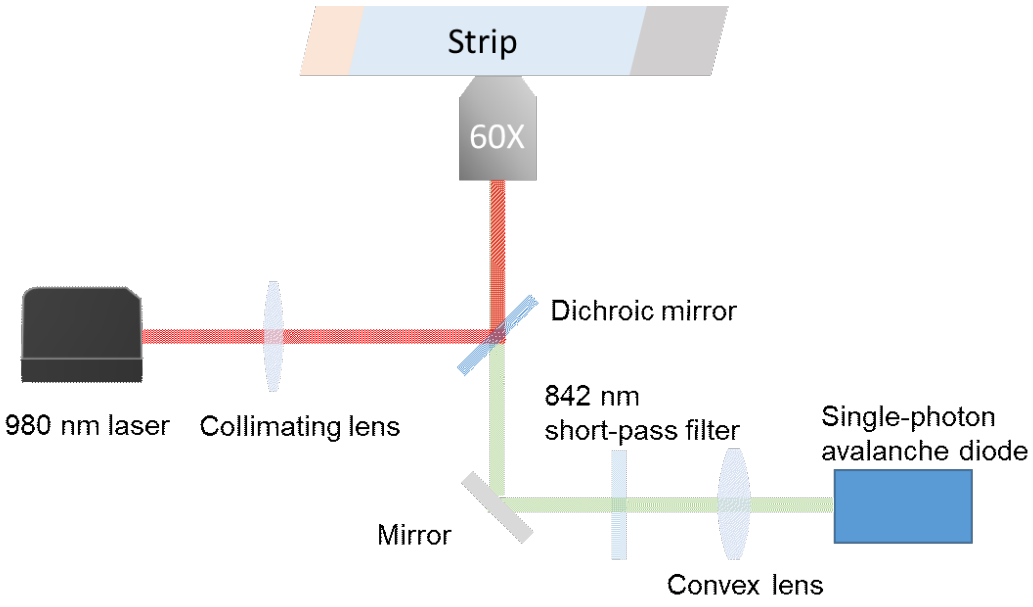

Figure 4-5. Optical layout of strip test system based on single photon counting detector. A 976 nm laser is used to excite the UCNPs, with a home built power control unit including a half wave plate and a polarizer. The emission of UCNPs is collected by an

objective lens (60X, NA 0.85 Edmund), then focused by a tube lens to an optical fibre, which is linked to a single photon avalanche detector (SPAD). We use x-y movement of the stage to read 10 different points of one testing area.

Under an excitation power density of 0.5 MW/cm^2, the signals from test area and background area are recorded by a single photon counting detector. As shown in Figure 4-6D, the highly doped UCNP reporters show much higher signal compared to the lower doped ones and the brightness enhancement ratio is consistent with the single nanoparticle characterization results. Despite the difference in the brightness, both reporters show the same limit of detection of 50 pg/mL for PSA. The lower doped UCNP reporters require the use of a highly sensitive and costly single photon counting detector, which is not suitable for point of care applications. Only the highly doped UCNP reporters provide sufficient brightness for a normal phone camera to achieve the high sensitivity.

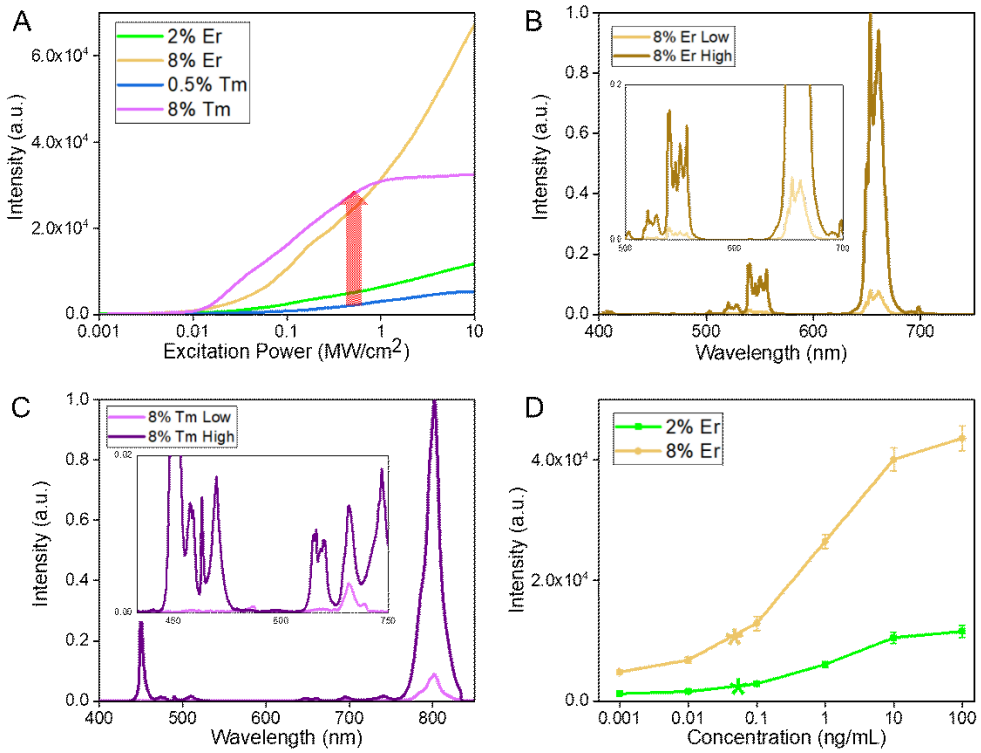

Figure 4-6. A. Power dependent emission intensity profiles of single highly doped UCNP reporter and lower doped one testes by a purpose-built single nanoparticle characterization system. The red arrow indicates the power density at 0.5 MW/cm^2. B. Emission spectra of single highly Er^{3+} doped UCNP reporter under high (0.5 MW/cm^2) and low (0.01 MW/cm^2) excitation powers testes by a purpose-built single nanoparticle characterization system. C. Emission spectra of single highly Tm^{3+} doped UCNP reporters under high (0.5 MW/cm^2) and low (0.01 MW/cm^2) excitation powers testes by a purpose-built single nanoparticle characterization system. D. The fluorescence signal intensities of test area on strips when detecting different concentrations of target PSA using highly Er^{3+} doped UCNP reporters and lower doped ones. Each data point represents the mean (±standard deviation) of triplicate experiments and the stars mark the LODs, defined as the concentration that corresponds to the sum of background noise and three times the standard deviation above the background. We use 3σ method to calculate the LOD of our strip test system. We set noise N = background + 3

SD(background) and liner fit S/N with target concentrations. The LOD is the concentration when S/N =1.

We build a compact device enclosed by a 3D-printed small housing as shown in Figure 4-1 and Figure 4-7A. The device consists of a 980 nm 300 mw laser diode as the light source, two hemisphere lenses with one to focus the excitation light beam to the strip and the other for collecting the emission signal to the phone camera, and a low-cost KG-3 heat absorbing glass as the short pass filter to remove the laser scattering. The spectral response of the phone camera CMOS (Sony IMX-214, the most common used one) [24] and the transmission curve of the KG-3 glass [25] are shown in Figure 4-7B, which indicates that the phone camera can read most of the visible emission signals of our highly doped UCNP reporters with negligible amount of excitation scattering light detected.

For demonstration purpose, we fix the optics and camera setting, but move the strip from one side to another at a constant speed, so that the average fluorescence intensity values of the testing area, the control area and the background area can be extracted from video analyses (Figure 4-7C). Using this method Figure 4-7D shows the advantage of highly doped UCNP reporters when the target concentration is at a very low range where the lower doped UCNP group shows no detectable signals. The LOD for PSA using highly Er^{3+} doped UCNP reporters is 61 pg/mL, more sensitive than using the lower doped ones (LOD: 8.5 ng/mL). The derived LOD indicates better performance in PSA detection than previous reported UCNP LFS assays (556 ng/mL) [18] and even a commercial dissociation-enhanced lanthanide fluoroimmunoassay (DELFIA) kit (100 pg/mL).

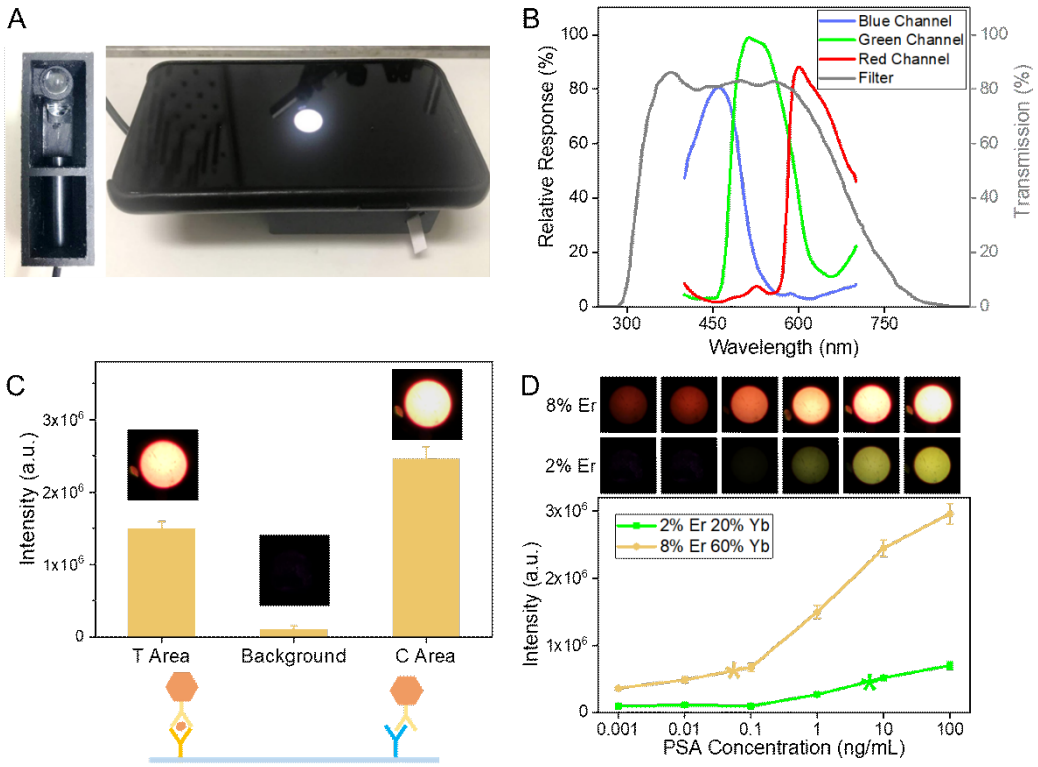

Figure 4-7. A. Photos of a 3D-printed box for housing optics (left) and the working state of the phone based LFS device (right). B. Spectral response (Color lines) of the phone camera CMOS (Sony IMX-214) and the transmission curve (grey line) of KG-3 absorbing glass. C. A representative result from a typical PSA assay showing the signals from testing area, background and control area. D. Results of detecting different concentrations of target PSA on strips using highly Er^{3+} doped UCNP reporters and lower doped ones. Each data point represents the mean (±standard deviation) of triplicate experiments and the stars mark the LODs, defined as the concentration that corresponds to the sum of background noise and three times the standard deviation above the background.

To show the potential of the smart phone based quantitative LFS for multiplexed assays, we use both highly Er^{3+} and Tm^{3+} doped UCNP reporters in a single strip for simultaneous testing of PSA and EphA2 target analytes. To achieve this, we modify highly Er^{3+} doped UCNPs with anti-PSA antibodies and highly Tm^{3+} doped UCNPs with anti-EphA2

antibodies. Figure 4-8A shows the two targets testing results. The yellowish and purple colors indicate the existence of PSA and EphA2 respectively, and their brightness increases along with the increase of concentrations of targets. This two-color LFS system achieves a LOD of 89 pg/mL for PSA (Figure 4-8B) that indicates this system maintains the high sensitivity as compared with single-color one. The LOD for EphA2 is of 400 pg/mL (Figure 4-8C). As the emission energy of highly Tm^{3+} doped UCNP reporters is mainly around 800 nm (Figure 4-6C) that is beyond the range of detection optics and phone camera (Figure 4-7B), the signal intensity is lower. We further evaluate the specificity of such a two-color LFS system by testing two targets PSA and EphA2 separately with 10% FBS as an interfering sample. Compared to the control groups, all the positive groups show much higher intensity with significant difference. The results indicate that there is negligible cross-interactions.

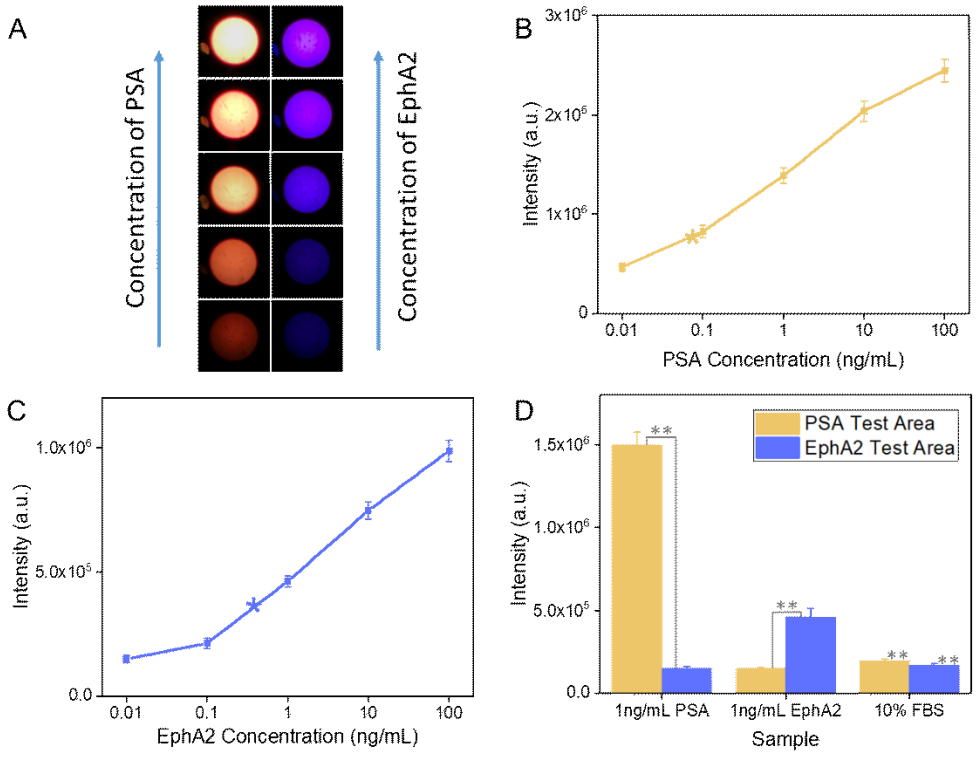

Figure 4-8. A. Result photos of two-color LFS assay for test different concentrations of PSA and EphA2. B. Fluorescence intensities of PSA test area for detecting different

*concentrations of PSA. C. Fluorescence intensities of EphA2 test area for detecting different concentrations of EphA2. D. Specificity evaluation of two-color LFS for 1 ng/mL PSA, EphA2 and 10% FBS. Each data point and bar represents the mean (±standard deviation) of triplicate experiments and the stars mark the LODs, defined as the concentration that corresponds to the sum of background noise and three times the standard deviation above the background. Significant difference is show with ** ($P < 0.01$).*

4.2.4 Conclusion and persperctive

The rapid progress in material science provides a large library of bright nanoparticles for biomolecular assays. The highly doped UCNPs, employed in this work, have presented major advances in this field of applications, due to their high brightness, mono-dispersity and uniformity in size and intensity, as well as being able to emit tunable colors according to the design of synthesis. Continuous development of more efficient and size controllable nanoparticle reporters will further improve the detection sensitivity in smart-phone based POCT applications. The quality of camera and the speed of CPU, built in smart phones, will continue to be improved and support more sophisticated image analysis and data processing, which shows a huge potential to drive the field of POCT from being indicative to being quantitative, and user-friendly. On the other hand, the accuracy of biomarker-based cancer diagnostics will be primarily improved by increasing the number of biomarkers being simultaneously tested. Therefore, the capacity of multiplexed LFS assays will play an essential role, which accordingly demands the development of both multicolor reporters and the capacity of the phone camera to decode these colors.

In conclusion, we have designed a quantitative LFS sensor using highly doped UCNPs as reporters and a phone camera as the readout element. The device eliminates the use of costly single photon counting detector and retains the high sensitivity of detecting low-

abundance target analyte. We have achieved a LOD of 61 pg/mL for PSA. By designing two types of highly doped UCNPs emitting two different colors as reporters, the sensor can simultaneously detect PSA and EphA2 with a LOD of 89 pg/mL and 400 pg/mL respectively without crosstalk. This portable device with ultra-bright luminesce reporters could be potentially applied in detecting a large range of biomarkers for early stage cancer diagnostics. This work provides a new strategy to design nanoparticle reporters that have great potential for POCT applications.

4.2.5 Acknowledgments

The authors acknowledge the financial support from the China Scholarship Council (201504910696), the Australian Research Council (ARC) Future Fellowship Scheme (D.J., FT130100517) and Australian Research Council (ARC) Research Hub for Integrated Device for End-user Analysis at Low levels (IDEAL) (IH150100028).

4.3 Development of this work

4.3.1 New design of the reader box and smartphone App

After the publication of this paper, we further patented our invention (AU2018903614) and developed this whole system. We have designed a new reader box with better stability and reproducibility as shown in Figure 4-9.

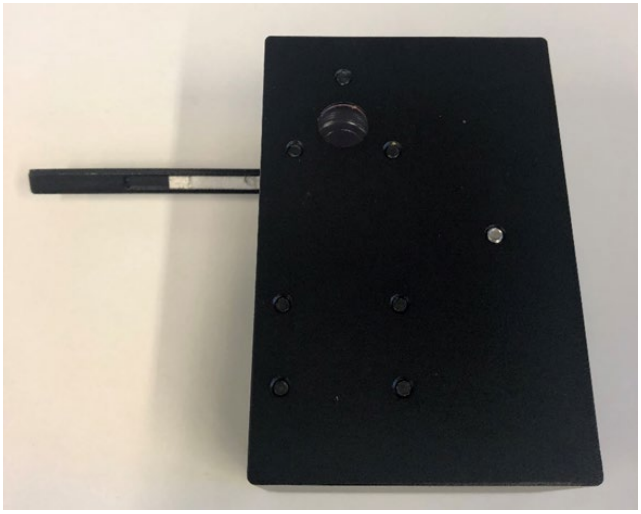

Figure 4-9. Photo of the new reader box.

For the real POC applications, we have programmed an Android based software that can read the strip, process the data and share the result.

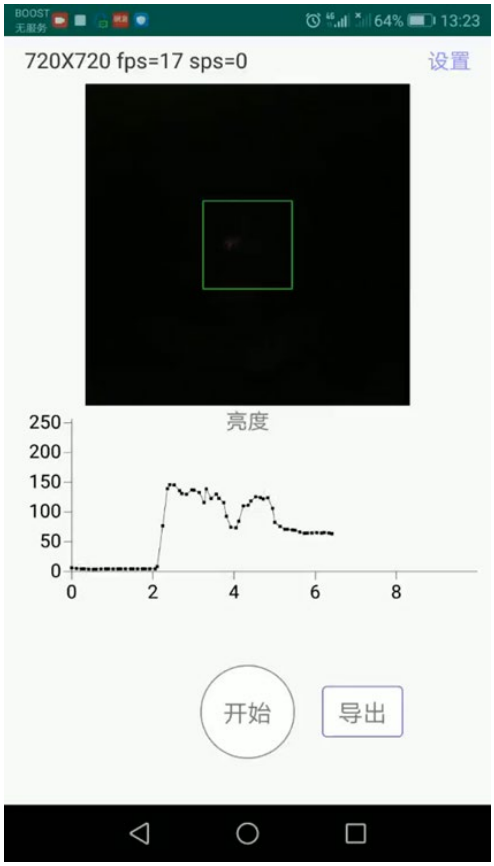

Figure 4-10. Interface of our new developed Android software.

4.3.2 Other disease test

We further applied this lateral flow strip sensor for detection of pre-eclampsia through testing another biomarker FKPBL and reached a limit of detection at 0.1 ng/mL for it.

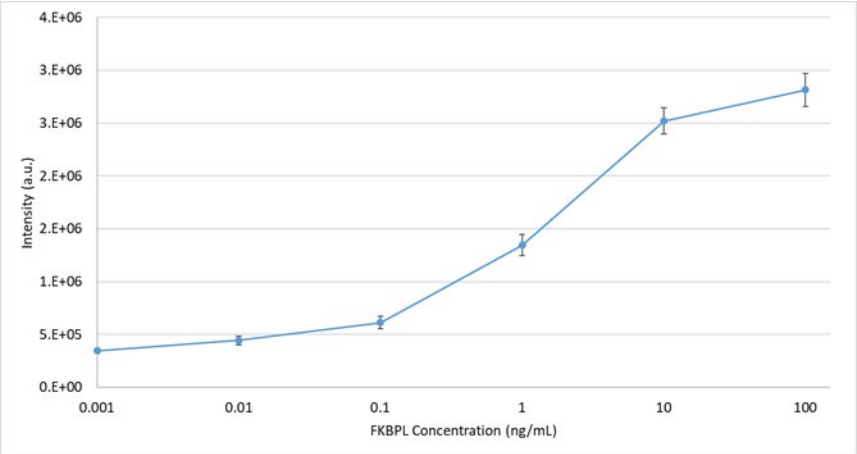

Figure 4-11. Result fluorescence intensities of testing areas for detecting different concentration of FKBPL in HEPES buffer.

Reference

[1] D. H. Choi, S. K. Lee, Y. K. Oh, B. W. Bae, S. D. Lee, S. Kim, Y.-B. Shin, and M.-G. Kim, "A dual gold nanoparticle conjugate-based lateral flow assay (LFA) method for the analysis of troponin I," *Biosens. Bioelectron.*, vol. 25, no. 8, pp. 1999–2002, 2010.

[2] S. Lee, S. Mehta, and D. Erickson, "Two-Color Lateral Flow Assay for Multiplex Detection of Causative Agents Behind Acute Febrile Illnesses," *Anal. Chem.*, vol. 88, no. 17, pp. 8359–8363, Sep. 2016.

[3] Z. Li, Y. Wang, J. Wang, Z. Tang, J. G. Pounds, and Y. Lin, "Rapid and Sensitive Detection of Protein Biomarker Using a Portable Fluorescence Biosensor Based on Quantum Dots and a Lateral Flow Test Strip," *Anal. Chem.*, vol. 82, no. 16, pp. 7008–7014, Aug. 2010.

[4] J. Hampl, M. Hall, N. A. Mufti, Y. M. Yao, D. B. MacQueen, W. H. Wright, and D. E. Cooper, "Upconverting Phosphor Reporters in Immunochromatographic Assays," *Anal. Biochem.*, vol. 288, no. 2, pp. 176–187, 2001.

[5] Y. Zhou, Y. Chen, H. He, J. Liao, H. T. T. Duong, M. Parviz, and D. Jin, "A Homogeneous DNA Assay by Recovering Inhibited Emission of Rare Earth Ions-Doped Upconversion Nanoparticles," *J. Rare Earths*, 2018.

[6] Y. Chen, H. T. T. Duong, S. Wen, C. Mi, Y. Zhou, O. Shimoni, S. M. Valenzuela, and D. Jin, "Exonuclease III-Assisted Upconversion Resonance Energy Transfer in a Wash-Free Suspension DNA Assay," *Anal. Chem.*, vol. 90, no. 1, pp. 663–668, Jan. 2018.

[7] C. Liu, L. Chang, H. Wang, J. Bai, W. Ren, and Z. Li, "Upconversion

Nanophosphor: An Efficient Phosphopeptides-Recognizing Matrix and Luminescence Resonance Energy Transfer Donor for Robust Detection of Protein Kinase Activity," *Anal. Chem.*, vol. 86, no. 12, pp. 6095–6102, Jun. 2014.

[8] J. Zhou, J. L. Leaño, Z. Liu, D. Jin, K.-L. Wong, R.-S. Liu, and J.-C. G. Bünzli, "Impact of Lanthanide Nanomaterials on Photonic Devices and Smart Applications," *Small*, vol. 0, no. 0, p. 1801882, Jul. 2018.

[9] M. You, M. Lin, Y. Gong, S. Wang, A. Li, L. Ji, H. Zhao, K. Ling, T. Wen, Y. Huang, D. Gao, Q. Ma, T. Wang, A. Ma, X. Li, and F. Xu, "Household Fluorescent Lateral Flow Strip Platform for Sensitive and Quantitative Prognosis of Heart Failure Using Dual-Color Upconversion Nanoparticles," *ACS Nano*, vol. 11, no. 6, pp. 6261–6270, Jun. 2017.

[10] M. P. A. Laitinen and M. Vuento, "Affinity immunosensor for milk progesterone: identification of critical parameters," *Biosens. Bioelectron.*, vol. 11, no. 12, pp. 1207–1214, 1996.

[11] K. Henderson and J. Stewart, "Factors influencing the measurement of oestrone sulphate by dipstick particle capture immunoassay," *J. Immunol. Methods*, vol. 270, no. 1, pp. 77–84, 2002.

[12] D. Liu, X. Xu, Y. Du, X. Qin, Y. Zhang, C. Ma, S. Wen, W. Ren, E. M. Goldys, J. A. Piper, S. Dou, X. Liu, and D. Jin, "Three-dimensional controlled growth of monodisperse sub-50 nm heterogeneous nanocrystals," *Nat. Commun.*, vol. 7, p. 10254, Jan. 2016.

[13] W. You, D. Tu, W. Zheng, X. Shang, X. Song, S. Zhou, Y. Liu, R. Li, and X. Chen, "Large-scale synthesis of uniform lanthanide-doped NaREF4 upconversion/downshifting nanoprobes for bioapplications," *Nanoscale*, vol. 10,

no. 24, pp. 11477–11484, 2018.

[14] Z. Liang, X. Wang, W. Zhu, P. Zhang, Y. Yang, C. Sun, J. Zhang, X. Wang, Z. Xu, Y. Zhao, R. Yang, S. Zhao, and L. Zhou, "Upconversion Nanocrystals Mediated Lateral-Flow Nanoplatform for in Vitro Detection," *ACS Appl. Mater. Interfaces*, vol. 9, no. 4, pp. 3497–3504, Feb. 2017.

[15] R. S. Niedbala, H. Feindt, K. Kardos, T. Vail, J. Burton, B. Bielska, S. Li, D. Milunic, P. Bourdelle, and R. Vallejo, "Detection of Analytes by Immunoassay Using Up-Converting Phosphor Technology," *Anal. Biochem.*, vol. 293, no. 1, pp. 22–30, 2001.

[16] P. Zhao, Y. Wu, Y. Zhu, X. Yang, X. Jiang, J. Xiao, Y. Zhang, and C. Li, "Upconversion fluorescent strip sensor for rapid determination of Vibrio anguillarum," *Nanoscale*, vol. 6, no. 7, pp. 3804–3809, 2014.

[17] C. Liu, W. Ma, Z. Gao, J. Huang, Y. Hou, C. Xu, W. Yang, and M. Gao, "Upconversion luminescence nanoparticles-based lateral flow immunochromatographic assay for cephalexin detection," *J. Mater. Chem. C*, vol. 2, no. 45, pp. 9637–9642, 2014.

[18] E. Juntunen, R. Arppe, L. Kalliomäki, T. Salminen, S. M. Talha, T. Myyryläinen, T. Soukka, and K. Pettersson, "Effects of blood sample anticoagulants on lateral flow assays using luminescent photon-upconverting and Eu(III) nanoparticle reporters," *Anal. Biochem.*, vol. 492, pp. 13–20, 2016.

[19] C. Ma, X. Xu, F. Wang, Z. Zhou, D. Liu, J. Zhao, M. Guan, C. I. Lang, and D. Jin, "Optimal Sensitizer Concentration in Single Upconversion Nanocrystals," *Nano Lett.*, vol. 17, no. 5, pp. 2858–2864, May 2017.

[20] S. Wen, J. Zhou, K. Zheng, A. Bednarkiewicz, X. Liu, and D. Jin, “Advances in highly doped upconversion nanoparticles,” *Nat. Commun.*, vol. 9, no. 1, p. 2415, 2018.

[21] J. Zhao, D. Jin, E. P. Schartner, Y. Lu, Y. Liu, A. V Zvyagin, L. Zhang, J. M. Dawes, P. Xi, J. A. Piper, E. M. Goldys, and T. M. Monro, “Single-nanocrystal sensitivity achieved by enhanced upconversion luminescence,” *Nat. Nanotechnol.*, vol. 8, p. 729, Sep. 2013.

[22] F. Wang, S. Wen, H. He, B. Wang, Z. Zhou, O. Shimoni, and D. Jin, “Microscopic inspection and tracking of single upconversion nanoparticles in living cells,” *Light Sci. &Amp; Appl.*, vol. 7, p. 18007, Apr. 2018.

[23] K. G. Shah, V. Singh, P. C. Kauffman, K. Abe, and P. Yager, “Mobile Phone Ratiometric Imaging Enables Highly Sensitive Fluorescence Lateral Flow Immunoassays without External Optical Filters,” *Anal. Chem.*, vol. 90, no. 11, pp. 6967–6974, Jun. 2018.

(24) Sony Semiconductor Solutions Corporation. (2018). IMX214 | Sony Semiconductor Solutions. [online] Available at: https://www.sony-semicon.co.jp/products_en/new_pro/april_2014/imx214_e.html [Accessed 30 Aug. 2018].

(25) Edmund Optics Inc. (2018). 12.5mm Dia. KG-3 Heat Absorbing Glass | Edmund Optics. [online] Edmundoptics.com. Available at: https://www.edmundoptics.com/p/125mm-dia-kg-3-heat-absorbing-glass/9438/ [Accessed 30 Aug. 2018].

(26) Järås K.; Adler B.; Tojo A.; Malm J.; Marko-Varga G.; Lilja H.; Laurell T. Porous silicon antibody microarrays for quantitative analysis: measurement of free and

total PSA in clinical plasma samples. Clin. Chim Acta, 2012, 414: 76-84.

Chapter 5 Single-molecule immunoaggregation assay detects biomarkers in microliter sample

5.1 Motivation

We used brighter UCNPs to bring a more sensitive lateral flow assay. However, the concentrations of some biomarkers in early stage cancers are thought to be even lower. To reach this ultralow limit of detection, a large volume of sample is used for pre-processing to enrich the concentration of biomarkers. However, it is not easy to get a lot of body fluid samples from the patients, especially the younger ones. So the development of new assays that can detect low trace of analytes using small volume samples is needed.

In this chapter consisting of one co-author published paper and one unpublished paper, we will first introduce our built single nanoparticle tracking system that makes detection of single nanoparticle possible. Then we used this system to develop a single-molecule level immunoaggregation assay for sub-microliter sample detection. This new in-vitro diagnosis assay can detect cancer biomarker with a concentration as low as 0.6 pg/mL in only 0.5 μL sample.

5.2 Introduction

A 1 mm^3 tumour composed of a million cells that each secrete 5,000 proteins into 5 litres of circulating blood in a patient body translates to a concentration of 2 fM. Most of conventional IVD assays cannot reach this limit of detection. Attempts to develop methods able to measure this concentration of proteins have focused on the single molecule assays.

5.2.1 Single molecule assay

To detect analytes at ultralow abundance level, single molecule assays, also called digital assays, attract more and more research interests. [1]–[6] Moreover, commercialized digital PCR and digital ELISA assays have been developed for detection of nuclear acids or proteins.

5.2.1.1 Digital PCR

Digital PCR is another refinement of conventional PCR. Compared with conventional qPCR, digital PCR measures the actual number of molecules (target DNA) as each molecule is in one droplet, thus making it a discrete “digital” measurement. It provides absolute quantification because dPCR measures the positive fraction of samples, which is the number of droplets that are fluorescing due to proper amplification. This positive fraction accurately indicates the initial amount of template nucleic acid. dPCR can be used to quantitate mutant alleles in circulating tumor DNA.

The first paper on dPCR was published by Dr Alec Morley and Pamela Sykes in 1992. [7] The purpose was to quantify PCR targets in an attempt to track and measure the absolute lowest number of leukemic cells in a patient with leukemia. The purpose was to monitor residual disease in leukemia patients, and thereby treat the patients at the earliest possible moment of detection of disease recurrence. Further evolutions of the technology allowed for more widespread distribution of this technique, with small partitions created by emulsion droplets and microfluidics.

Droplet Digital PCR technology is a digital PCR method utilizing a water-oil emulsion droplet system. [8], [9] Droplets are formed in a water-oil emulsion to form the partitions that separate the template DNA molecules. The droplets serve essentially the same function as individual test tubes or wells in a plate in which the PCR reaction takes place, albeit in a much smaller format. The massive sample partitioning is a key aspect of the ddPCR technique.

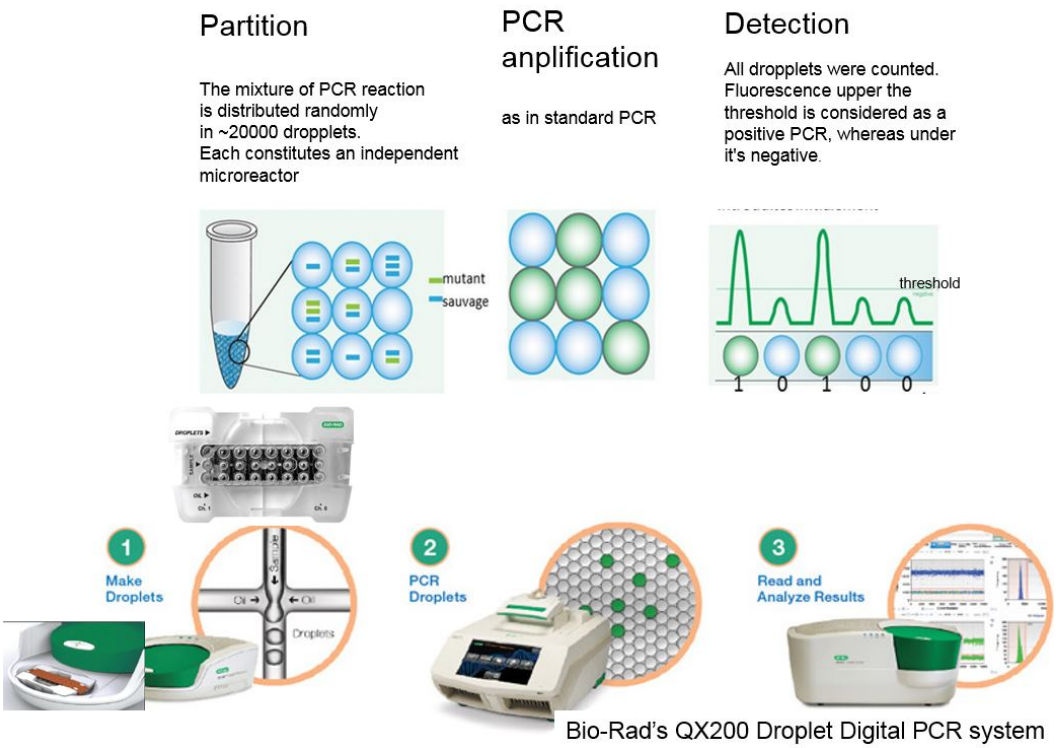

Figure 5-1. Workflow of Bio-Rad QX 200 Droplet Digital PCR. Reproduce from Ref. [9]

The Droplet Digital PCR System partitions nucleic acid samples into thousands of nanoliter-sized droplets, and PCR amplification is carried out within each droplet. This technique has a smaller sample requirement than other commercially available digital PCR systems, reducing cost and preserving precious samples.

ddPCR technology uses a combination of microfluidics and proprietary surfactant chemistries to divide PCR samples into water-in-oil droplets. The droplets support PCR amplification of the template molecules they contain and use reagents and workflows similar to those used for most standard TaqMan probe-based assays. Following PCR, each droplet is analyzed or read to determine the fraction of PCR-positive droplets in the original sample. These data are then analyzed using Poisson statistics to determine the target DNA template concentration in the original sample.

Droplet Digital PCR surpasses the performance of earlier digital PCR techniques by resolving the previous lack of scalable and practical technologies for digital PCR implementation. Serial dilution is laborious and introduces the possibility of pipetting error; competing chip-based systems rely on complex fluidics schemes for partitioning.

Droplet Digital PCR addresses these shortcomings by massively partitioning the sample in the fluid phase in one step. The creation of tens of thousands of droplets means that a single sample can generate tens of thousands of data points rather than a single result, bringing the power of statistical analysis inherent in digital PCR into practical application. Bio-Rad's Droplet Digital PCR System automates the ddPCR workflow of droplet generation, thermal cycling, droplet reading, and data analysis, making this technology accessible to the working research laboratory.

5.2.1.2 Digital ELISA

Traditional ELISA readout systems require large volumes that ultimately dilute reaction product, requiring millions of enzyme labels to generate signals that are detectable utilizing conventional plate readers. Sensitivity is therefore limited to the picomolar range and above. Single-molecule analysis provides a resolution that simply cannot be obtained with bulk ensemble measurements. Single molecule measurements are digital in nature: each molecule generates a signal that can be counted. It is much easier to measure the presence or absence of signal than to detect the absolute amount of signal—that is, counting is easier than integrating.

David M Rissin et al. reported the digital ELISA for detecting serum proteins at single molecular level. [10] This method has been used to measure proteins in a variety of different matrices (serum, plasma, cerebrospinal fluid, urine, cell extracts, etc.) at femtomolar (fg/mL) concentrations, offering a roughly 1000-fold improvement in sensitivity. This approach makes use of arrays of femtoliter-sized reaction chambers, which are termed single-molecule arrays, that can isolate and detect single enzyme molecules. Because the array volumes are approximately 2 billion times smaller than a conventional ELISA, a rapid buildup of fluorescent product is generated if a labeled protein is present. With diffusion defeated, this high local concentration of product can be readily observed. Only a single molecule is needed to reach the detection limit.

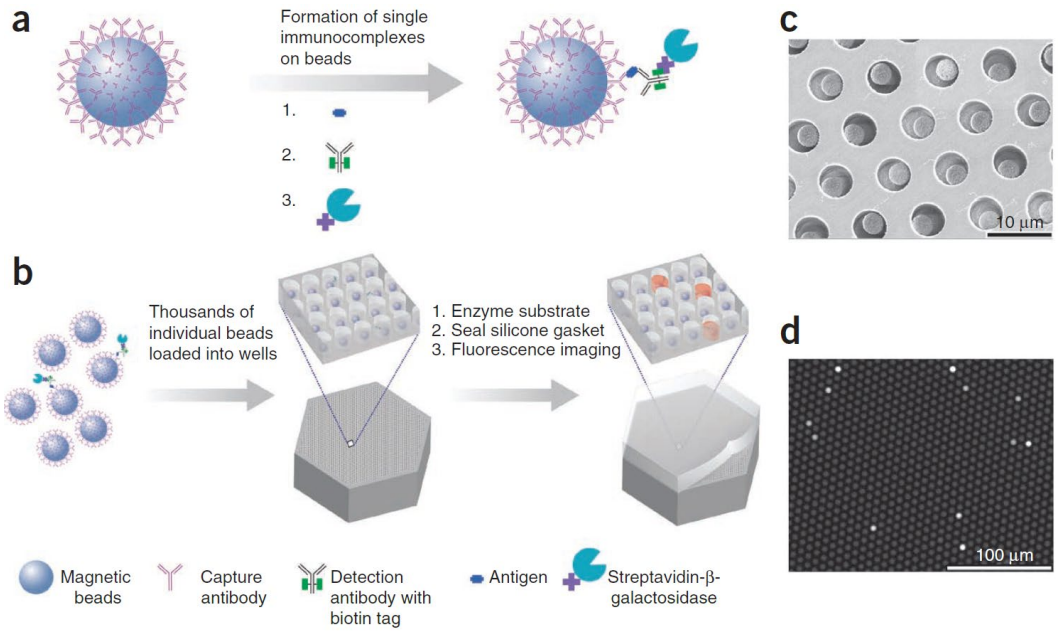

Figure 5-1. Digital ELISA based on arrays of femtoliter-sized wells. (a,b) Single protein molecules are captured and labelled on beads using standard ELISA reagents (a), and beads with or without a labelled immunoconjugate are loaded into femtoliter-volume well arrays for isolation and detection of single molecules by fluorescence imaging (b). (c) Scanning electron micrograph of a small section of a femtoliter-volume well array after bead loading. Beads (2.7 µm diameter) were loaded into an array of wells with diameters of 4.5 µm and depths of 3.25 µm. (d) Fluorescence image of a small section of the femtoliter volume well array after signals from single enzymes are generated. Whereas the majority of femtoliter volume chambers contain a bead from the assay, only a fraction of those beads possess catalytic enzyme activity, indicating a single, bound protein molecule. The concentration of protein in bulk solution is correlated to the percentage of beads that carry a protein molecule. Reproduced from Ref. [10]

In the first step of this single-molecule immunoassay, antibody capture agents are attached to the surface of paramagnetic beads (2.7 µm diameter) that will be used to concentrate a dilute solution of molecules. The beads typically contain approximately 250,000 attachment sites, so one can think of each bead as having a “lawn” of capture molecules. The beads are added to the sample solution such that there are many more beads than target molecules. Typically 500,000 beads will be added to a 100 µL sample. Adding so many beads confers two advantages. First, at a roughly 10:1 bead-to-molecule ratio, the percentage of beads that contain a labeled immunocomplex follows a Poisson

distribution. At low concentrations of protein, the Poisson distribution indicates that each bead will capture either a single immunocomplex or none. For example, if 1 fM of a protein in 0.1 mL (60,000 molecules) is captured and labeled on 500,000 beads, then 12% of the beads will carry one protein molecule and 88% will not carry any protein molecules. Second, with so many beads in solution, the bead-to-bead distance is small, so that every molecule encounters a bead in less than a minute. At this time scale, diffusion of the target analyte molecules, even large proteins, occurs quickly, and in theory all the molecules should have multiple collisions with multiple beads. In this manner, the slow binding to a fixed capture surface is avoided and the efficiency of binding increases dramatically. The beads are then washed to remove nonspecifically bound proteins and incubated with biotinylated detection antibody and then with β-galactosidase–labeled streptavidin. In this manner, each bead that has captured a single protein molecule is labelled with an enzyme. Beads that do not capture a molecule remain label-free. Rather than an ensemble readout, beads are loaded into arrays of 216,000 femtoliter-sized wells that have been sized to hold no more than one bead per well. Beads are added in the presence of substrate, and wells are subsequently sealed with oil and imaged. This assay permits the detection of very low concentrations of enzyme labels by confining the fluorophores generated by individual enzymes to extremely small volumes (~40 fL), ensuring a high local concentration of fluorescent product molecules. If a target analyte has been captured (that is, an immunocomplex has formed), then the substrate will be converted to a fluorescent product by the captured enzyme label. The ratio of the number of wells containing an enzyme labeled bead to the total number of wells containing a bead corresponds to the analyte concentration in the sample. By acquiring two fluorescence images of the array, it is possible to demonstrate an increase in signal, thereby confirming the presence of a true immunocomplex, and beads associated with a single enzyme molecule (an “on” well) can be distinguished from those not associated with an enzyme (an “off” well). The protein concentration in the test sample is determined by counting the number of wells containing both a bead and fluorescent product relative to the total number of wells containing beads. Because this assay enables concentration to be determined digitally rather than by measurement of the total analog signal, this approach to detecting single immunocomplexes has been termed digital ELISA.

The ability of digital ELISA to measure much lower concentrations of proteins than conventional ELISA derives from two effects: (1) the high sensitivity of digital ELISA to enzyme label and (2) the low level of background signal that can be achieved by digitizing protein detection. For antibodies of given affinity, the sensitivity of the immunoassay will be determined by the assay background. The high label sensitivity and decreased label concentration help reduce nonspecific binding to the capture surface, resulting in much lower background signal.

These two digital assays for nuclear acids and proteins detection have been well commercialized and applied into many different bioapplications. However, due to the limitation of the signal probes, both of them need signal amplification steps, PCR or enzyme, to make the single molecule detectable for the detectors.

5.2.2 Single UCNP tracking system

As we introduced in Chapter 1, NPs possess unique advantages compared with conventional organic fluorophores, especially the super bright emission. This makes NPs a suitable candidate as the probe for single molecule detection.

My colleagues and I have showed a series of monodispersed UCNPs with a brightness that already meets the requirement for our eyes to observe single nanoparticles through a microscope. This section of chapter is presented in a published journal paper in *Light: Science & Applications, 2018, 7(4), 18007* and my contribution is design intracellular experiments, including modification of UCNPs, cell experiments and data processing. [11] The upconversion fluorescence system built for the purpose of observing single nanoparticles is shown in Figure 5-3.

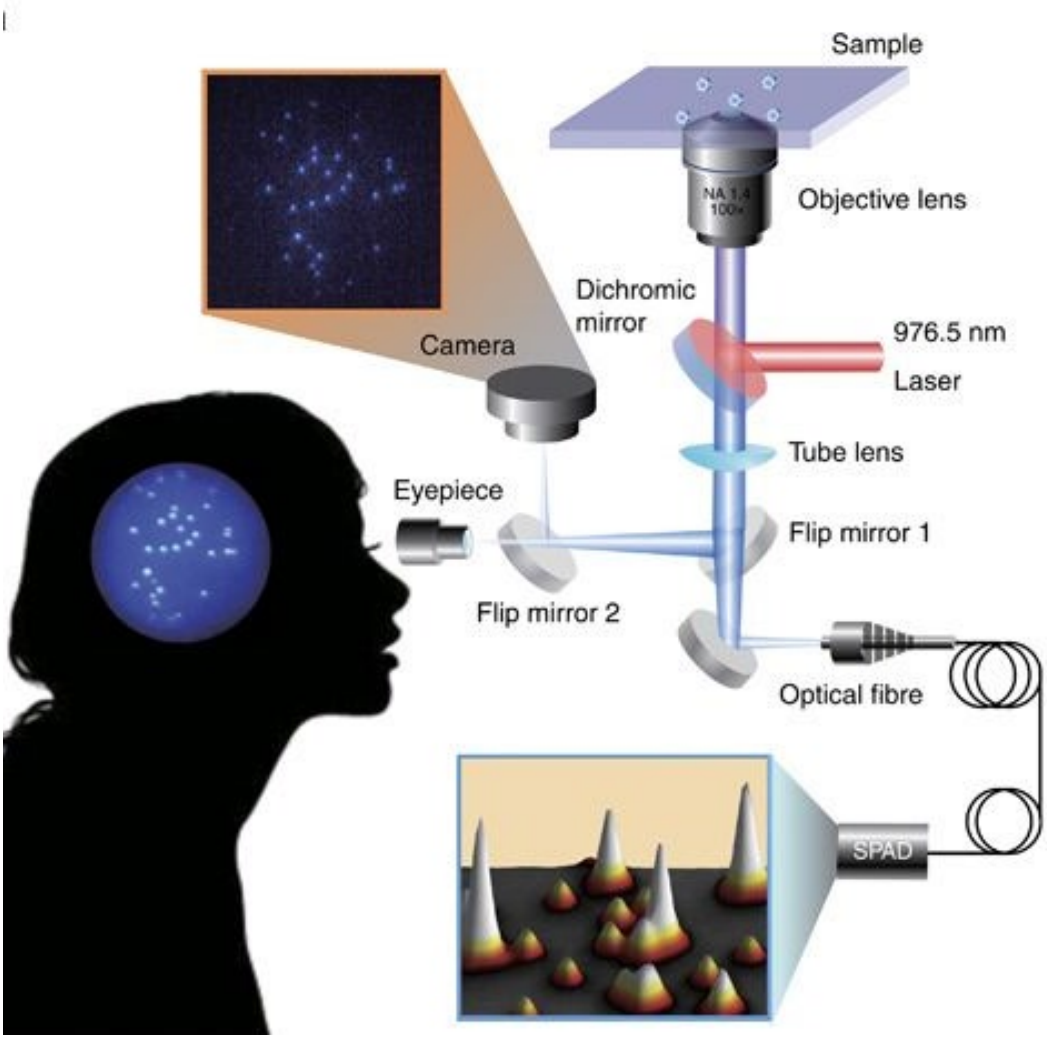

Figure 5-3. Microscopy system that compares the sensitivity of a CCD camera and our eyes (switched by a flap mirror) in the observation of single UCNPs. The photons emitted from each single UCNP are collected by an optical fibre and counted by a single photon avalanche detector (SPAD) for 100 ms, mimicking the duration time required for our brain to process images obtained from the same number of photons. Reproduce from Ref. [11]

Due to the optical diffraction limit, conventional far-field fluorescence microscopy does not have sufficient resolution to determine the number of nanoparticles when they are too close to each other. Approaches such as correlative electron microscopy [12] or the recently reported MINFLUX method [13] can be applied to improve the resolution. A high-level of uniformity in the UCNPs provides the ability for observers to identify a threshold intensity for single-UCNP detection. The emitters with a brightness higher than this threshold value will be identified as several nanoparticles within the diffraction limit

region. The threshold value measured by the system enables automatic single-nanoparticle detection in real-time by computer processing of a wide-field fluorescence image. Note that the processed computer data compensate for the non-uniform excitation field and provide an accurate single identification accuracy (100% accuracy). Remarkably, due to the background-free detection with the NIR excitation, non-blinking and non-bleaching features of the UCNPs, the human eye can also identify this threshold and recognize single UCNPs during microscopic inspection.

This system can be used to track intracellular single nanoparticle movements shown in Figure 5-4. The importance of the real-time observation of single cellular event comes from the detection of sub-cellular vesicles and protein movements and understanding their interactions in the complex cellular function. There are myriad of models [14] that propose different sub-cellular functions, including cytoskeleton re-arrangement, [15] protein dynamics, organelle movement and cooperation, [16], [17] but until now, options for the real-time observation of these models in living cells have been limited. The high brightness of the photostable UCNPs is detectable not only in a dark room but also under bright-field illumination, providing the ability to identify the position of a single nanoparticle within a living cell and establishing a powerful tool for examining intercellular re-organization and trafficking.

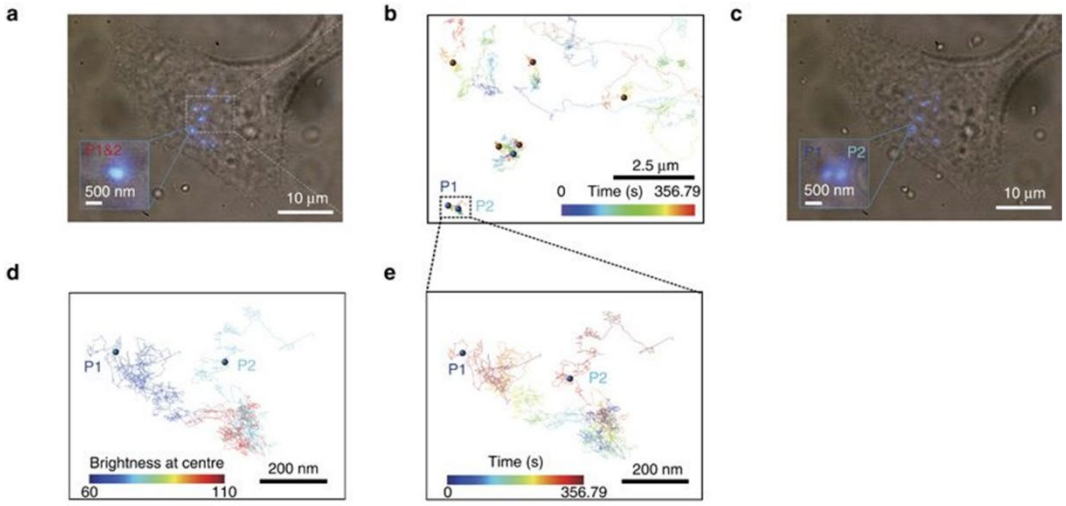

Figure 5-4. High-resolution long-term tracking of two single UCNPs confined within a diffraction-limit spot and their escape process. (a) Bright-field and epifluorescence image of a single cell taken at 0.21 s from Supplementary Video S2. The insert image is the

cluster of interest in this study, which contains two single 40 nm 4 mol% Tm3+-doped UCNPs. (b) 2D tracking of the 8.5 × 6.4 μm area for the period from 10.5 s to 367.29 s. (c) Bright-field and epifluorescence image of a single cell at 372.54 s from Supplementary Video S2. (d) Intensity map of the two nanoparticles showing the transformation from a diffraction-limit cluster (red) to two independent nanoparticles (blue for particle 1 and light blue for particle 2). (e) 2D pathways of the two tracked single nanoparticles from their confinement to their escape from their local environment over time (colour coded). Reproduced from Ref. [11]

Based on this single nanoparticle tracking system with these advantages, we further developed a single molecule immunoaggregation assay and apply it into low abundance prostate cancer biomarker detection in small volume samples.

5.3 Materials and Methods

5.3.1 Synthesis of UCNPs

NaYF4: Yb^{3+}, Tm^{3+} nanocrystals (1%Tm/60%Yb) was synthesized according to our previously reported method. In a typical experiment, 1 mmol $RECl_3 \cdot 6H_2O$ (RE = Y, Yb, Tm, 99.99%, Sigma 464317, 204870, 204668) with the desired molar ratio were added to a flask containing 6 mL OA (90%) and 15 mL ODE (90%). The mixture was heated to 160 °C under argon flow for 30 min to obtain a clear solution and then cooled down to about 50 °C, followed by the addition of 5 mL methanol (anhydrous) solution of NH_4F (4 mmol) and NaOH (2.5 mmol). After stirring for 30 min, the solution was heated to 150 °C under argon flow for 20 min to expel methanol, and then the solution was further heated to 310 °C for another 90 min. Finally, the reaction solution was cooled down to room temperature. The products were precipitated by ethanol and centrifuged (9000 rpm for 5 min), then washed 3 times with cyclohexane (anhydrous), ethanol (anhydrous) and methanol to get the nanoparticles.

To get the nanoparticles with core-shell structure, layer-by-layer epitaxial growth has been employed. The shell precursors preparation is similar with that for the core nanoparticles synthesis, until the step where the reaction solution was slowly heated to 150°C and kept for 20 min. Instead of further heating to 300 °C to trigger nanocrystal

growth, the solution was cooled down to room temperature to yield the shell precursors. For epitaxial growth, 0.15 mmol as-prepared core nanocrystals were added to a containing 6 ml OA and 6 ml ODE. The mixture was heated to 170 °C under argon for 30 min, and then further heated to 300 °C. Next, 0.25 ml as prepared shell precursors were injected into the reaction mixture and ripened at 300 °C for 4 min, followed by the same injection and ripening cycles for several times to get the nanocrystals with the desired size. Finally, the slurry was cooled down to room temperature and the formed nanocrystals were purified according to the same procedure used for the core nanocrystals.

5.3.2 Bioconjugation of UCNPs with antibodies

To convert OA capped UCNPs to cPEG (polyethylene glycol modified with a carboxy group, Mw = 3500, JenKem Technology, USA) coated ones, ligand exchange method is used. 1.5 mL of 20 mg/mL UCNPs in cyclohexane are precipitated with ethanol. After centrifuge and discarding the solution, UCNPs are redispersed in 3 mL of THF (anhydrous, Sigma) with vortex and sonication. Then 1.5 mL of 200 mg cPEG in THF solution is added. The mixed solution is stirred at room temperature for 24 h. After that, 3 mL of MiliQ water is added and mixed with shaking. Then the solution is extracted with 1 mL of hexane to remove the OA molecules. After removing the oil phase, the solution is put in vacuo overnight to evaporate organic solvents. Then the solution is dialyzed in 1 L of MiliQ water for 24 h to remove the excessive PEG molecules.

After the converting step, the cPEG-UCNPs are changed into MES buffer (pH 4.5, Sigma) using a centrifuge method at a final concentration of 1 mg/mL. Then 10 μL of cPEG-UCNPs, 100 μg of EDC and 100 μg of NHS are mixed in 90 μL MES buffer (pH 4.5). After 2 h gentle shaking, the sample is washed with the MES buffer twice (centrifuge at 14,000 rpm for 20 min). After the final centrifuge step, the precipitate is suspended with 50 μL MES buffer. The solution is mixed with 50 μL of IgG antibody (0.1 mg/mL anti-PSA monoclonal antibody produced in rabbit/anti-EphA2 monoclonal antibody produced in rabbit, Sigma) and put into a 37 °C shaker overnight. After twice washing with MES buffer (centrifuge at 14,000 rpm for 20 min), the UCNP probe is finally suspended in 100 μL of MES buffer with sonication for 5 s.

5.3.3 UCNPs Characterization

5.3.3.1 TEM size characterization

The morphology of the formed materials was characterized via transmission electron microscopy (TEM) imaging (Philips CM10 TEM with Olympus Sis Megaview G2 Digital Camera) with an operating voltage of 100 kV. The samples were prepared by placing a drop of a dilute suspension of nanocrystals onto copper grids.

5.3.3.2 Optical properties

The excitation-power-dependent emission curve of single UCNPs has been performed by a purpose-build confocal system. A 976.5 nm laser is used to excite the UCNPs, with a home build power control unit including a half wave plate and a polarizer. The emission of UCNPs is collected by a high NA objective lens (Olympus, NA = 1.4), then focused by a tube lens to an optical fibre (working as confocal aperture Airy disk = 1.01), which is linked to either a single photon avalanche detector (SPAD). The blue band emission collection is achieved by switching the filter wheel to a 475 ± 25 nm bandpass filter.

The emission intensity distribution of single UCNP was tested by the single nanoparticle imaging system. The single UCNP was selected followed by the method in Section 5.2.2 and a large amount of single UCNPs are collected of the emission intensity.

5.3.4 Immunoaggregation assay.

To test the samples with different PSA concentrations, 0.5 μL of the sample solution are added with 0.5 μL of the UCNPs probe. After mixing and incubating for 30 mins, the whole solution is added with 99 μL ethanol and spreading evenly onto one cover glass. Then the cover glass is detected with our single UCNP tracking system.

5.4 Results and Discussions

5.4.1 UCNPs Characterization

The synthesized UCNPs show highly uniform size (Figure 5-5) and emission brightness (Figure 5-6), which provides the foundation for this work in distinguishing single UCNPs and number of UCNPs in their clusters.

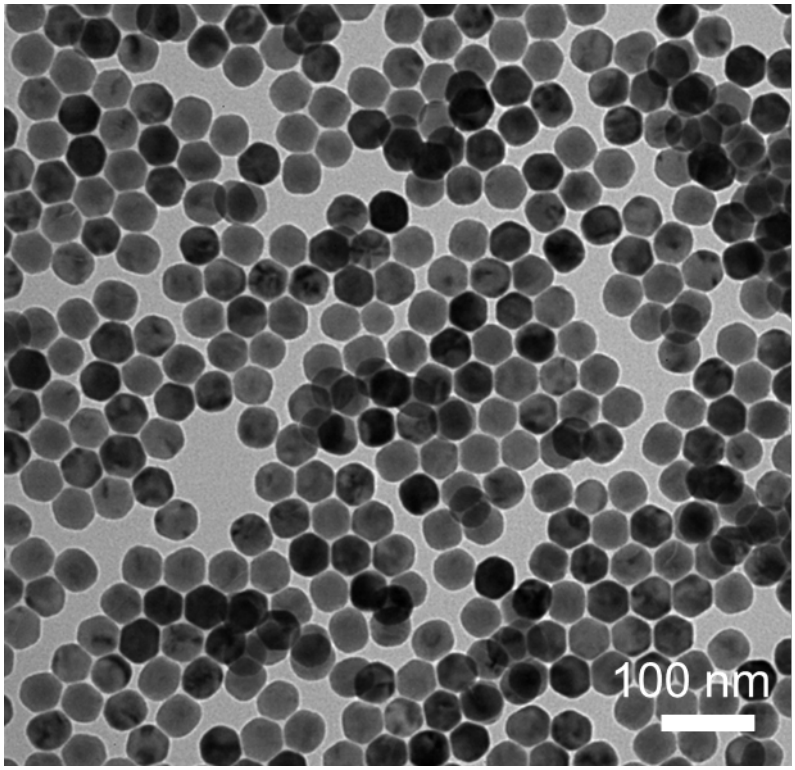

Figure 5-5. TEM photo of UCNPs.

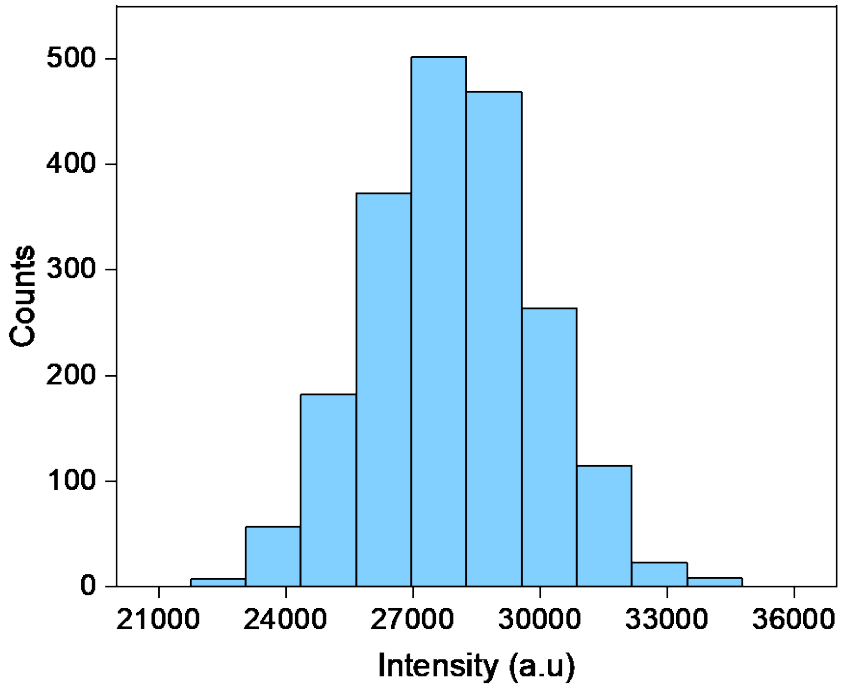

Figure 5-6. The emission intensity distribution of single UCNP.

5.4.2 Single UCNP Imaging

Wide-field illumination by a coherent laser beam usually suffers from non-uniform excitation intensity across the field with a typical Gaussian distribution pattern, which influences our intensity-based approach to judging a single nanoparticle. To compensate such an artefact, we developed an excitation pattern correction approach to correct emission images that is based on the position of nanoparticles in the non-uniform Gaussian excitation field and the power-dependency curves of UCNPs.

The process of single UCNP determination takes into account both excitation beam profile and UCNP's power dependent emission curve. The emission pattern (E_{emi}) which indicates emission intensity of a single UCNP will vary in different positions of excitation beam. Eemi can be calculated through $E_{emi} = PD \times E_{exc}$, where PD is the excitation power dependency of emission intensity of single UCNP and can be measured through single particle characterization (Figure 5-7). E_{exc} is the calculated excitation beam profile with measured spot size.

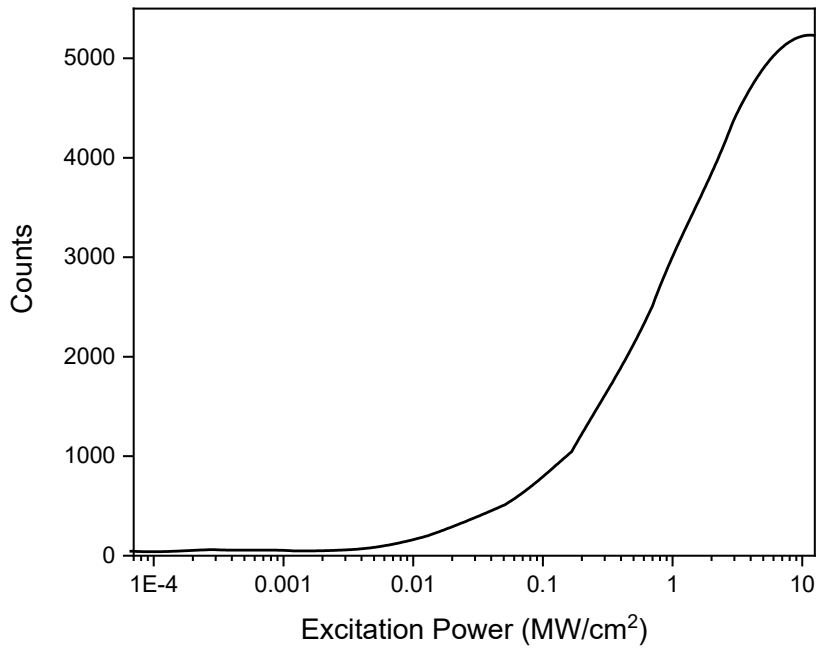

Figure 5-7. Excitation power dependent curve of single 1% mol Tm^{3+} doped UCNP.

To compensate the excitation intensity reduction due to decreased excitation intensity away from centre of Gaussian beam spot, Figure 5-8B show a 1% mol Tm^{3+} doped UCNP pattern (I_{in}). The compensation process is achieved through formula $I_{out} = I_{in} / E_{emi}$. After this intensity compensation process, single UCNP can be determined by their emission intensity. For example, single 1% mol Tm^{3+} doped UCNP should give emission value smaller than 35000. If the intensity is higher than this value, the bright spot is considerate as a non-single nanoparticle.

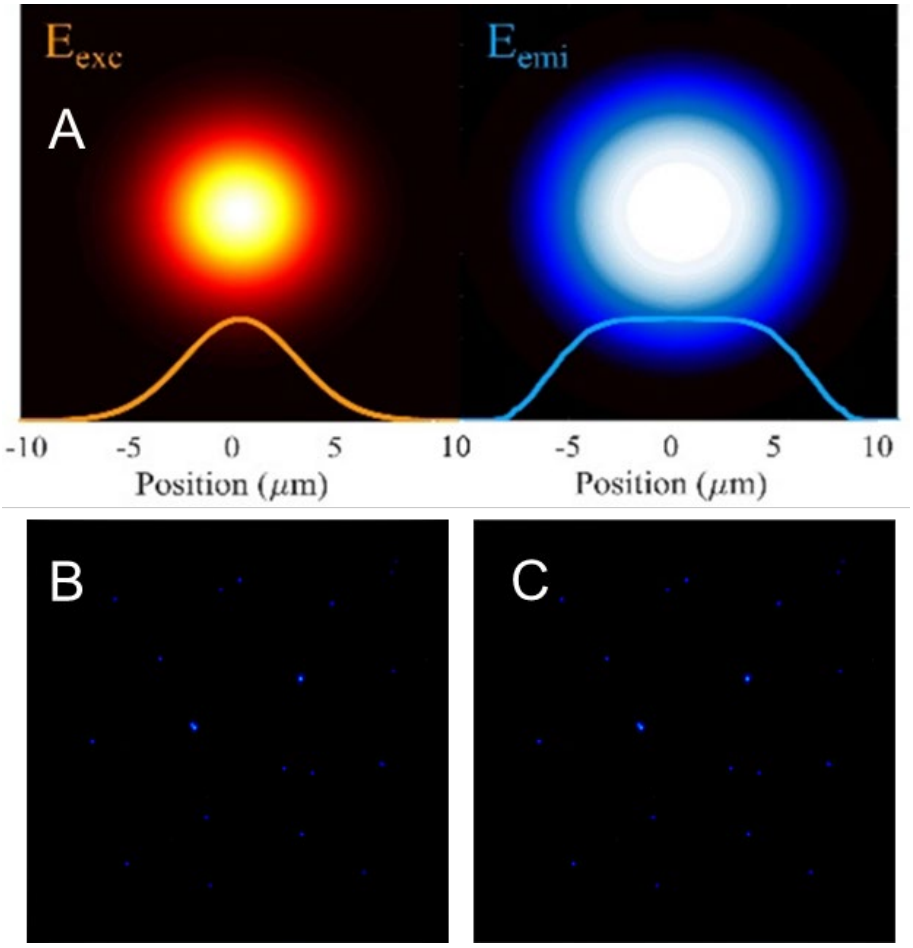

Figure 5-8. Correlation of the emission image. A. The emission intensity of a single UCNP in different positions of excitation beam. B. CCD record image after LUT correction. C. Intensity compensated image.

The number of single UCNP in the immune-aggregated cluster is determined by the emission intensity distribution of single UCNP and showed in Figure 5-9.

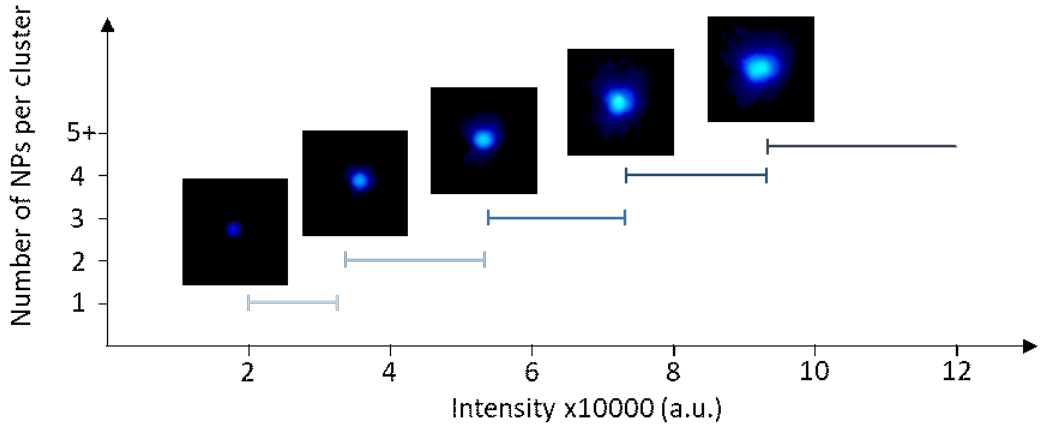

Figure 5-9. The emission intensity range of clusters containing different number of single UCNP.

5.4.3 Immunoaggregation Assay

To determine the detection limitation of this assay, several different concentration of PSA samples are tested. The single nanoparticle images were shown in Figure 5-10. As the PSA concentration increases, the number of brighter and bigger clusters that means more single UCNP inside are getting bigger. That's because PSA molecules cause the immune reaction that causes the UCNPs aggregation.

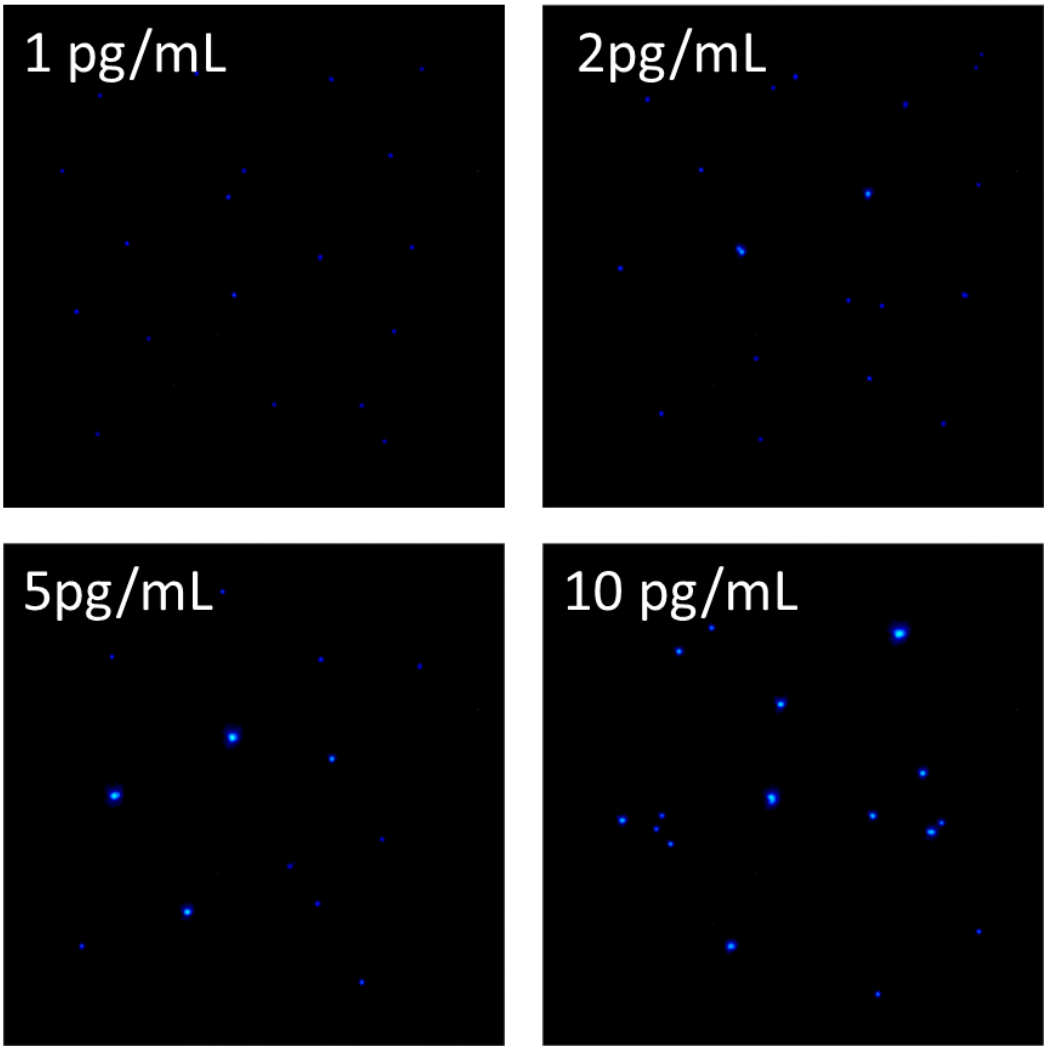

Figure 5-10. Single nanoparticle image photos of the immunoaggregation assay with different concentrations of PSA.

For every samples, around 1000 blue cluster are counted and determined how many UCNPs are inside. After Poisson distribution fitting, the distribution curves of groups testing different concentrations of PSA are shown in Figure 5-11.

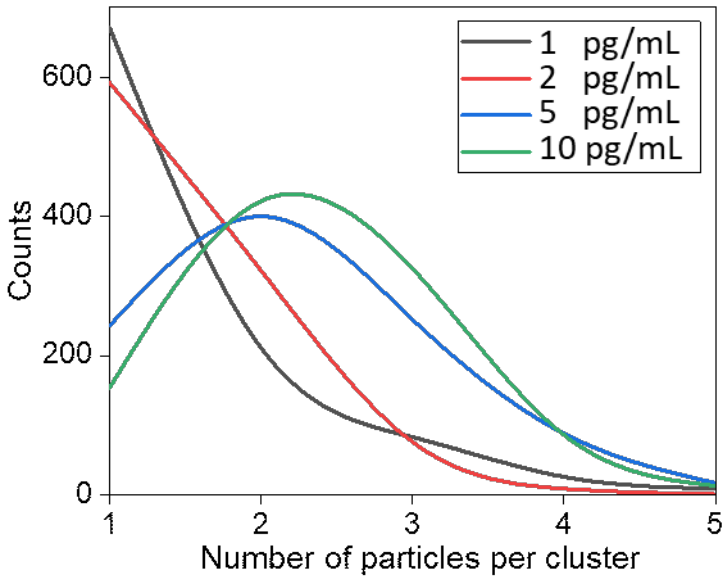

Figure 5-11. The Poisson distribution curve of the immunoaggregation assay with different PSA concentrations.

To determine the limit of detection, the Poisson parameters of every group testing different concentration of PSA and the concentrations are liner fitted. The limit of detection line is set using background add three times of noise. The Poisson parameter of the group with no PSA added is used as the background and the noise is its standard deviation. After fitting, the limit of detection is 0.60 pg/mL for PSA detection using this immunoaggregation assay.

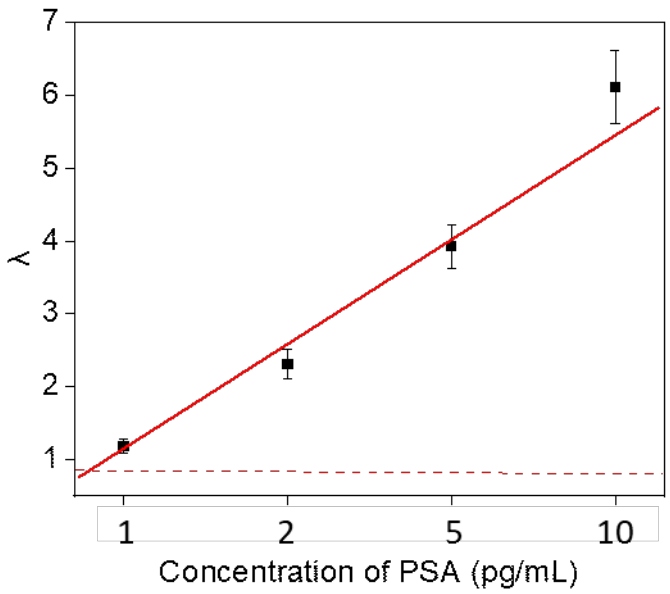

Figure 5-12. Linear regression of concentrations of PSA and Poisson parameters. The red dash line is the limit of detection level as Poisson parameter of UCNPs without PSA + 3× standard deviation.

5.5 Conclusions

Based on our designed and built single nanoparticle tacking system, we have developed a single molecule immunoaggregation assay using upconversion nanoprobe. This assay can detect less than 1 pg/mL of PSA in only 0.5 μL sample. With a limit of detection at 0.60 pg/mL and a wide dynamic range of three orders of magnitude, this assay shows a good performance in PSA detection using small volume samples.

And this assay can also be developed into a POC device as our single nanoparticle tracking system is based on simple optics and can be designed into a smaller size that we can use a smartphone to image these single nanoparticles.

Reference

[1] L. Zhu, Q. Liu, B. Yang, H. Ju, and J. Lei, "Pixel Counting of Fluorescence Spots Triggered by DNA Walkers for Ultrasensitive Quantification of Nucleic Acid," *Anal. Chem.*, vol. 90, no. 11, pp. 6357–6361, 2018.

[2] E. M. Peterson and J. M. Harris, "Identification of Individual Immobilized DNA Molecules by Their Hybridization Kinetics Using Single-Molecule Fluorescence Imaging," *Anal. Chem.*, vol. 90, no. 8, pp. 5007–5014, 2018.

[3] X. Pei, H. Yin, T. Lai, J. Zhang, F. Liu, X. Xu, and N. Li, "Multiplexed Detection of Attomoles of Nucleic Acids Using Fluorescent Nanoparticle Counting Platform," *Anal. Chem.*, vol. 90, no. 2, pp. 1376–1383, 2018.

[4] X. Li, L. Wei, L. Pan, Z. Yi, X. Wang, Z. Ye, L. Xiao, H. Li, and J. Wang, "Homogeneous Immunosorbent Assay Based on Single-Particle Enumeration Using Upconversion Nanoparticles for the Sensitive Detection of Cancer Biomarkers," *Anal. Chem.*, 2018.

[5] Z. Farka, M. J. Mickert, A. Hlaváček, P. Skládal, and H. H. Gorris, "Single Molecule Upconversion-Linked Immunosorbent Assay with Extended Dynamic Range for the Sensitive Detection of Diagnostic Biomarkers," *Anal. Chem.*, vol. 89, no. 21, pp. 11825–11830, Nov. 2017.

[6] S. H. Kim, S. Iwai, S. Araki, S. Sakakihara, R. Iino, and H. Noji, "Large-scale femtoliter droplet array for digital counting of single biomolecules," *Lab Chip*, vol. 12, no. 23, pp. 4986–4991, 2012.

[7] P. J. Sykes, S. H. Neoh, M. J. Brisco, E. Hughes, J. Condon, and A. A. Morley, "Quantitation of targets for PCR by use of limiting dilution," *Biotechniques*, vol. 13, no. 3, pp. 444–449, 1992.

[8] B. J. Hindson, K. D. Ness, D. A. Masquelier, P. Belgrader, N. J. Heredia, A. J. Makarewicz, I. J. Bright, M. Y. Lucero, A. L. Hiddessen, and T. C. Legler, "High-throughput droplet digital PCR system for absolute quantitation of DNA copy

number," *Anal. Chem.*, vol. 83, no. 22, pp. 8604–8610, 2011.

[9] Bio-Rad, "QX200™ Droplet Digital™ PCR System." [Online]. Available: http://www.bio-rad.com/en-au/product/qx200-droplet-digital-pcr-system?ID=MPOQQE4VY. [Accessed: 01-Jun-2019].

[10] D. M. Rissin, C. W. Kan, T. G. Campbell, S. C. Howes, D. R. Fournier, L. Song, T. Piech, P. P. Patel, L. Chang, and A. J. Rivnak, "Single-molecule enzyme-linked immunosorbent assay detects serum proteins at subfemtomolar concentrations," *Nat. Biotechnol.*, vol. 28, no. 6, p. 595, 2010.

[11] F. Wang, S. Wen, H. He, B. Wang, Z. Zhou, O. Shimoni, and D. Jin, "Microscopic inspection and tracking of single upconversion nanoparticles in living cells," *Light Sci. &Amp; Appl.*, vol. 7, p. 18007, Apr. 2018.

[12] A. Albanese and W. C. W. Chan, "Effect of gold nanoparticle aggregation on cell uptake and toxicity," *ACS Nano*, vol. 5, no. 7, pp. 5478–5489, 2011.

[13] F. Balzarotti, Y. Eilers, K. C. Gwosch, A. H. Gynnå, V. Westphal, F. D. Stefani, J. Elf, and S. W. Hell, "Nanometer resolution imaging and tracking of fluorescent molecules with minimal photon fluxes," *Science (80-.).*, vol. 355, no. 6325, pp. 606–612, 2017.

[14] H. Frauenfelder, G. Chen, J. Berendzen, P. W. Fenimore, H. Jansson, B. H. McMahon, I. R. Stroe, J. Swenson, and R. D. Young, "A unified model of protein dynamics," *Proc. Natl. Acad. Sci.*, vol. 106, no. 13, pp. 5129–5134, 2009.

[15] N. Fakhri, A. D. Wessel, C. Willms, M. Pasquali, D. R. Klopfenstein, F. C. MacKintosh, and C. F. Schmidt, "High-resolution mapping of intracellular fluctuations using carbon nanotubes," *Science (80-.).*, vol. 344, no. 6187, p. 1031 LP-1035, May 2014.

[16] A. M. Valm, S. Cohen, W. R. Legant, J. Melunis, U. Hershberg, E. Wait, A. R. Cohen, M. W. Davidson, E. Betzig, and J. Lippincott-Schwartz, "Applying systems-level spectral imaging and analysis to reveal the organelle interactome,"

Nature, vol. 546, no. 7656, p. 162, 2017.

[17] B.-B. Chu, Y.-C. Liao, W. Qi, C. Xie, X. Du, J. Wang, H. Yang, H.-H. Miao, B.-L. Li, and B.-L. Song, "Cholesterol transport through lysosome-peroxisome membrane contacts," *Cell*, vol. 161, no. 2, pp. 291–306, 2015.

Chapter 6 Conclusions and Perspectives

6.1 Conclusion

In this thesis, we focused on exploring new cancer in-vitro diagnosis assays using UCNPs. To this end, my PhD study was designed into two main parallel streams to develop new surface functionalization strategies (Chapter 2 & 3) and UCNPs based quantitative IVD assays (Chapter 4 & 5), respectively.

The main research achievements and outcomes through my PhD study are summarised as below:

(1) The comprehensive literature review in Chapter 1 on the conventional cancer IVD platforms and new nanomaterials based IVD assays has been structured and composed.

(2) Chapter 2 is about a new surface modification strategy for UCNPs. Two single-chain variable fragments with highly binding affinity to UCNPs surface have been selected using phage display technology. They showed significant positive binding signals in the ELISA tests. Moreover, the gene sequencing results indicated that these two fragments have the designed structure and can be produced through protein engineering.

(3) Chapter 3, in the format of a published paper, reports a facile and high-yield bioconjugation strategy for UCNPs based on a bispecific antibody (BsAb), free of chemical reaction steps. One end of the BsAb is designed to recognize methoxy polyethylene glycol (mPEG) coated UCNPs, and the other end of the BsAb is to recognize the cancer antigen biomarker. Through simple vortexing, BsAb-UCNP nanoprobes form within 30 min and show higher (up to 54%) association to the target than the traditional UCNP nanoprobes in the ELISA-like assay. We further demonstrate its successful binding to the cancer cells with high efficiency and specificity for background-free fluorescence imaging under near-infrared excitation.

(4) Chapter 4, also in the format of a published paper, reports a new quantitative lateral flow strip using highly doped UCNPs and smartphone. We design a compact device to create a focused illumination spot with high irradiance, which activates a range of

highly doped 50 nm upconversion nanoparticles (UCNPs) to produce orders of magnitude more brighter emissions. The device employs a very low-cost laser diode, simplified excitation, and collection optics, and permits a mobile phone camera to record the results. Using highly erbium ions (Er^{3+}) and thulium ions (Tm^{3+}) doped UCNPs as two independent reporters on two-color lateral flow strips, new records of limit of detection (LOD), 89 pg/mL and 400 pg/mL, have been achieved for the ultra-sensitive detection of PSA and EphA2 biomarkers, respectively without crosstalk.

(5) Chapter 5 is about another UCNPs based quantitative IVD assay for ultra-small volume samples. This chapter first summarizes my contributed one co-authored paper reporting a single nanoparticle tracking system. Based on this single nanoparticle tracking system, we report a nanoparticle aggregation immunoassay for detecting the low abundance of cancer biomarkers in the sub-microliter sample. After mixing 0.5 μL of prostate specific antigen (PSA) sample with polyclone antibodies modified UCNP probes and spreading the solution on a cover glass, we used a wide-field microscope with a 980 nm laser light source to image every single UCNP and aggregated immunocomplexes consisting of PSA and UCNPs. We calculate the number of UCNPs in each immunocomplex using fluorescence intensity. The distribution of single UCNP and immunocomplexes consisting of different numbers of UCNPs fits the Poisson distribution and is related to the concentration of PSA. Our digital immune-aggregation assay reaches a limit of detection of 0.6 pg/mL PSA in 0.5 μL of sample and covers a dynamic range of three orders of magnitude.

6.2 Perspectives

Though my PhD thesis has achieved quite a lot in the exploration new UCNPs surface functionalization strategies for stable and specific nanoprobe and new quantitative IVD assays based on UCNPs for highly sensitive rapid detection and quantification of cancer biomarkers, with new opportunities opening up we realize the research becomes highly multidisciplinary with much work needing to be done towards the transformational phase of addressing the end-users' applications.

Phage display can be further applied for other kinds of nanomaterials to select the anti-nanomaterial antibodies. With the help of the bispecific antibody, it will be easier for nanomaterials bioapplications, such as sensing, imaging, drug delivery, and therapy.

The importance and urgent requirements of cancer screening and monitoring make most conventional cancer diagnostic assays and platforms, that are carried out in centralized or hospital-based laboratories by using expensive equipment that requires highly trained personnel to operate, seem to be powerless. This brings POC diagnostics, simplified and miniaturized test that reduces the overall cost of materials, equipment, and personnel, more and more popular.

Most NPs, like UCNPs, make the IVD assays highly sensitive and specific. However, more works need to be done to further develop these assays to a higher level for POC applications. A POC diagnostic device must ideally be cost-effective, rapid, functional without excessive prior-processing of samples, highly sensitive to enable detection of cancer at an early stage, and specific to prevent over-diagnosis, misdiagnosis, or missed-diagnosis. The device must facilitate “self-use” or use by a general practitioner or nurse in a local practice. Results must be returned promptly to initiate treatment as soon as possible, which ultimately leads to the enhancement of the patient’s wellbeing.

Currently reported NPs based assays are mainly based on reading fluorescence intensity using photon detector or scientific CCD camera that is too large and too expensive. Fortunately, the quality of the camera and the speed of CPU, built in smartphones, will continue to be improved and support more sophisticated image analysis and data processing, which shows a huge potential to drive the field of POCT to a brighter future. Our strip sensor has demonstrated this, and now we are still working on transfer our single nanoparticle tracking system to a smartphone-based device.